

Kinetic Solitary Electrostatic Structures in Collisionless Plasma: Phase-Space Holes

I H Hutchinson

*Plasma Science and Fusion Center,
Massachusetts Institute of Technology,
Cambridge, MA 02139,
USA*

The physics of isolated plasma potential structures sustained by a deficit of phase-space density on trapped orbits, commonly known as electron or ion holes, is reviewed. The principles of their equilibria are explained and illustrated, and contrasted with solitons. A literature review mostly prior to 2016 highlights the key historical developments of the field. Progress since, especially in hole acceleration, stability, and multi-dimensional effects, is summarized in more detail.

CONTENTS

	Acknowledgments	51	
I. Introduction	1	References	51
II. Principles and formulation	4		
A. Governing Equations	4		
B. Non-dimensionalization	5		
C. Constancy on orbits	5		
D. Steady One-Dimensional Equilibria	5		
E. Illustrative BGK equilibria	7		
III. One dimensional soliton and hole equilibria	8		
A. Prototypical Solitons	8		
B. Pseudo-potential solitary structure analysis	9		
C. Ion Acoustic Solitons	10		
D. Electron acoustic solitons	10		
E. Soliton – Hole Comparison	11		
IV. Historical Background	12		
A. Initial theory and simulation 1957-1970	12		
B. Experiment, Simulation, and Analytic Consolidation 1970-1993	13		
C. Ubiquitous holes in space, multidimensional simulation, stability, 1994-2008	15		
D. Lab and Space holes, renewed theory, 2008-	21		
V. Time Dependence and Hole Kinematics	25		
A. Landau Damping and Resonant Interactions	25		
B. Kinematics of Holes as Composite Bodies	26		
C. Oscillatory Instability of Electron Hole Velocity	28		
D. Hole-Soliton Coupling and Slow Electron Holes	28		
VI. Asymmetric Electron and Ion Holes	31		
A. Theory of hole asymmetry and acceleration	31		
B. Recent ion hole observations	34		
VII. Transverse Instability Theory	36		
A. Jetting as the instability mechanism	36		
B. Instability calculation including magnetic field	37		
C. Strong magnetic field approximation	40		
D. Ion response effect on transverse instability	42		
E. Generalized multi-mode transverse instability	42		
VIII. Multi-dimensional holes	44		
A. Equilibria	44		
B. Gyro orbit effects and Scattering	46		
C. Magnetic field perturbations	49		
IX. Prospects	50		

I. INTRODUCTION

The aim of this review is to introduce and survey the physics of long-lived nonlinear electrostatic plasma structures in which the electric potentials are supported self-consistently by non-thermal particle velocity distributions. It is now realized that these phenomena occur very widely, often as the end state of kinetic instabilities. They are coherent rather than turbulent, and persist for long durations relative to typical instability timescales.

Modern satellite measurements observe solitary potential structures almost everywhere in space plasmas; and scattering from them may sometimes cause particle energization and precipitation. Because of their short spatial extent, their often rapid motion past an observing satellite produces an electric field pulse of wide bandwidth in the frequency domain. Pulsed nonlinear low density laboratory experiments can also generate them.

There is a wide theoretical variety of such phenomena, which would soon overwhelm the compass of any single review. Therefore to limit the scope, I have adopted boundaries to the domain of interest that are indicated in the paper's title.

“Kinetic” limits the scope to phenomena that need a comprehensive plasma description beyond the widely-used fluid or Maxwellian approximations. Complicated velocity distributions of the particles, having depleted regions of phase-space (so called holes) are intrinsic to the present topic. Fluid solitons such as ion acoustic solitons that are describable by purely fluid nonlinear equations have an enormous literature and various book-length reviews already (see e.g. Lamb, 1980, Dodd *et al.*, 1982 and more recently Drazin and Johnson, 1989, Infeld and Rowlands, 2000). An elementary discussion aiming to clarify these omitted phenomena from a kinetic perspec-

tive is included for comparison with holes, but the soliton literature is not reviewed.

“Solitary” means, nevertheless, that the focus is on aperiodic structures, not extended periodic waves. When periodic plasma waves have substantial amplitudes, important nonlinear effects occur, such as particle trapping and wave-wave coupling. There is an extensive literature concerning periodic nonlinear waves that is not addressed here. It is now increasingly appreciated, however, that many important coherent non-linear plasma phenomena can only readily be understood in the space domain z , not the Fourier domain \mathbf{k} . More simply put, our present concern is potential structures that vary only over a limited spatial extent and connect to external regions that are essentially uniform. These localized objects can be considered to be isolated positive or negative potential humps, which will be referred to as electron or ion holes and are our main focus, but the expression arguably applies also to isolated double layers, referring to transitions between two different externally uniform potentials. They are a subsidiary interest and will be mentioned but not comprehensively reviewed.

“Electrostatic” phenomena predominate in both theory and observation. However, a magnetic field \mathbf{B} is often important for the existence and stability of the holes, and while most analyses regard the magnetic field as a uniform background, the presence of moving holes can also induce measurable local perturbations to \mathbf{B} , which will briefly be addressed.

Many plasmas are to an excellent approximation “Collisionless”, which is essential for the non-thermal structures to persist. The equation governing the particles is then Vlasov’s equation, which expresses the invariance of the velocity distribution $f(\mathbf{v})$ along particle orbits.

Calling the phenomena “Structures” alludes to them being of a persistent shape and size that varies only slowly relative to their particle transit times. (However the literature also widely uses instead the term solitary “wave”, hence the acronym ESW for electrostatic solitary waves, though the alternative phrase “Time Domain Structure” TDS is arguably more precise.) In the rest frame of the solitary structure, there are then generally considered to be three ordered timescales: the transit or bounce time of the particles, which is much shorter than the structure’s evolution or acceleration time, which is much shorter than the particle collision time (on which the structure decays collisionally). Time variations of the potential that are as fast as the particle transit or bounce frequency cannot be ignored when analyzing the *stability* of holes, but the *equilibria* are generally taken to be almost steady on the transit time, which means kinetic plus potential energy is an approximate constant of the motion, and in a one-dimensional situation the equilibrium distribution is a function only of energy in the rest frame of the structure.

By way of orientation, Figure 1 illustrates the parti-

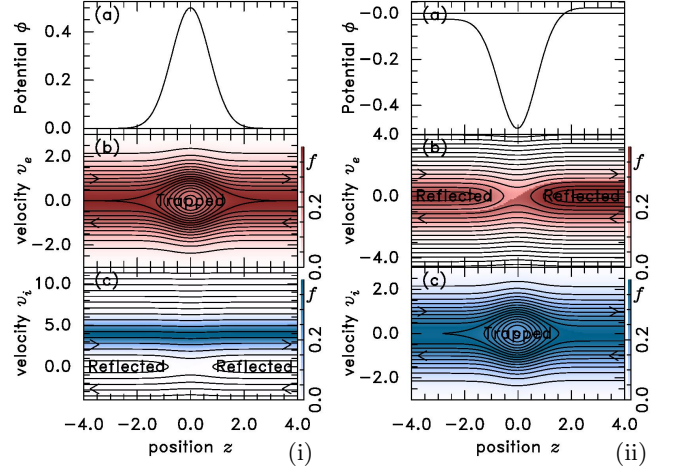


FIG. 1 Illustrative one dimensional electron hole (i), and ion hole (ii), showing (a) the assumed potential, (b) the electron phase space, and (c) the ion phase space. The electron and ion velocities are normalized respectively to their thermal velocities $\sqrt{T/m_e}$ and $\sqrt{T/m_i}$. On the contours of constant energy the distribution function $f(v)$ has a constant value indicated by the color. Particle orbits coincide with the contours. In (i) the external ion Maxwellian has a mean velocity shift of 4. In (ii) there is no ion shift but a small electron shift, plus an asymmetry in ϕ between $z \rightarrow \pm\infty$.

cle orbits in one-dimensional phase-space (the z, v plane) that arise from a prescribed steady potential $\phi(z)$. In Fig. 1(i) producing a positive potential requires $f_e(v)$ in the trapped region to have a depression relative to its distant value at $v = 0$. The acceleration induced by the gradients of the potential cause the trapped orbits to circulate clockwise around a stagnation point, forming a phase-space vortex. That depressed phase-space density vortex is the electron “hole”. Meanwhile, in this illustration, the mean ion velocity is larger ($4v_{ti}$) in the rest frame of the hole than its thermal speed $v_{ti} = \sqrt{T/m_i}$. Therefore negligible numbers of ions are on reflected orbits, but the density of ions at $z = 0$ is slightly enhanced near $z = 0$ by the orbit expansion. When the ion shift is large enough that the populated ion orbits are effectively straight horizontal lines, a hole equilibrium would be well approximated by regarding the ions as uniform neutralizing background. In Fig. 1(ii), by contrast, the ions are taken as unshifted in the hole frame, sustaining the negative potential by their trapped phase-space-density depression. In this more complicated illustrative case, the external electron distribution is slightly shifted, by $-0.3v_{te}$, giving rise to important asymmetric electron reflection from the negative potential peak, and accompanying discontinuities in $f_e(v)$. Such reflection generally induces a potential difference across the hole, with important imbalanced forces causing acceleration, which will be discussed later in detail.

To illustrate the long-lasting persistence of holes, Fig. 2 plots normalized ϕ , n_e , and color contours of $f_e(x, v)$

from a fully self-consistent particle in cell (PIC) simulation of a pre-formed pure electron hole with 600,000 computational particles per cell. A tiny amplitude decay rate of only approximately $5 \times 10^{-5} \omega_{pe}$ occurs. It is attributable to the numerical collisionality arising from particle discreteness noise. Electron holes can persist stably with negligible evolution other than slow spatial drift for immense durations in sufficiently quiescent plasmas.

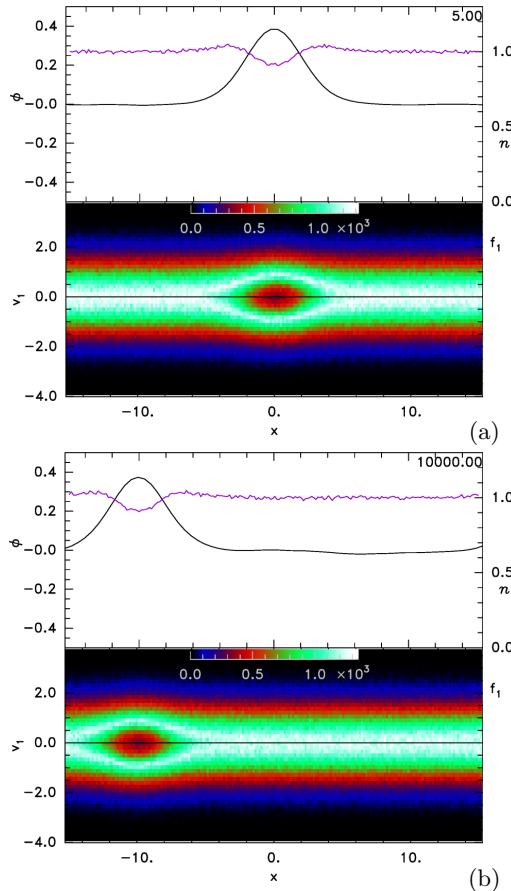


FIG. 2 Two states of a 1-D particle in cell simulation showing negligible amplitude decay of a pre-formed electron hole: initially (a), after time $10,000\omega_{pe}^{-1}$ (b). Upper frame: potential and density; lower frame: contours of phase-space density.

A guide to the contents of the article is as follows. Section II sets forth the key equations governing these localized Vlasov-Poisson structures, and explains the scaling of space and time to give the appropriate dimensionless variables in which it is most convenient to work. Elementary examples of self-consistent one-dimensional electron holes are discussed, illustrating the physical principles that allow steady solitary structures to exist. These principles were a major emphasis of a tutorial review by the author Hutchinson (2017), originally presented in 2016. So introductory development is curtailed in the present review and the reader should consult that tutorial paper for a more comprehensive introduction to the principles of the field, and its prospects at that time. For

the same reason, characteristic formation mechanisms of electron holes, discussed in Hutchinson (2017), are omitted here, but some videos of simulations of hole formation may be found at <https://www.youtube.com/@ihhutchinson/playlists> and links in the Supplementary Material.

Section III shows how the pseudo-potential approach is used to calculate solitary structures when the charge density as a function of potential is known. Fluid solitons are compared with electron and ion holes, and the important distinctions are explained.

The limited length of the earlier tutorial obviated a thorough critical review of prior literature. Therefore Section IV seeks to expand substantially upon the historical perspective from the field's beginnings in the 1950s. It aims to cite the most influential papers, note why they were influential, and also sometimes to provide a critical assessment, from today's perspective, of their strengths and weaknesses. This approach risks not only inadvertent omissions, but also apparent disrespect toward my predecessors in the field, because it is not profitable to attempt to cite every paper that bears on electron and ion hole theory. So let me apologize up front for any unwelcome omissions or remarks concerning the pioneering work of many creative authors that opened up the topic; and simply plead that I am deeply conscious of their contributions, and have attempted to state as fairly and respectfully as I can my understanding of what the contributions are.

The subsequent sections cover largely conceptual developments in electron and ion hole physics since 2016, and are organized topically rather than historically. The idea of hole *kinematics*, principally momentum conservation, Section V, has seen great development since then. It addresses the behavior of a hole as a robust compound entity that is able to accelerate in response to imbalance of forces, while retaining approximately constant potential shape in its rest frame. The forces treated within the kinematic discussion can also induce asymmetry in the hole potential, most notably a potential drop across the hole, as discussed in Section VI. The kinematic perspective underlies a rigorous development of hole stability (Section VII) to motions along the direction of the predominant electric field and particle motion: generally parallel to the magnetic field. In addition to uniform one-dimensional acceleration, holes can often be unstable to parallel shifts that vary sinusoidally in the plane perpendicular to the magnetic field. This phenomenon kinks the hole, and is called the “transverse instability”. Recent stability analysis has revealed its true underlying mechanisms. Holes are observed usually to be localized in the transverse directions as well as the parallel direction. The strength of the background magnetic field is critical in determining stability and instability. Often, holes initially well approximated as one-dimensional break up by the transverse instability into multidimensional struc-

tures that are usually oblate, but sometimes even prolate. Their resulting localized equilibria, once the break up is complete, require multidimensional equilibrium calculations which are the topic of Section VIII.

It is extremely difficult to observe electron holes in laboratory experiments. The main problem is that electron holes have characteristic extent of a few Debye lengths, and in moderate density lab plasmas, the Debye length is uncomfortably short (typically a few tens of micrometers). Diagnostics to measure the plasma potential with sufficient spatial resolution, which so far are limited to electric Langmuir type probes, have only rarely been possible. Another problem is the great difficulty of producing truly collisionless plasmas either because of limitations of finite connection lengths, or high Coulomb or neutral collision frequency even in toroidal configurations. Nevertheless a handful of laboratory observations will briefly be described in the historical review.

By contrast, space plasma measurements occur in deeply collisionless plasmas with Debye lengths from tens to thousands of meters. And satellites routinely encounter electron and ion holes. In the mid 1990s diagnostic sampling speeds began to be sufficient to resolve in time (and thereby space) the electric fields of holes, along a single track through the hole. With the availability of data now from coordinated multi-satellite missions, near-simultaneous multiple-point measurements within a single hole have become possible. This enables direct diagnosis of the three dimensional extent of holes, and provides unambiguous and precise measurements of their velocity. At the same time (but with much slower time resolution) many satellites obtain comprehensive measurements of the background ion and electron velocity distribution functions. These new measurements provide rich opportunities to confront the theories of electron and ion holes and to use them to help interpret the physics of the solar wind, the Earth's magnetosphere, and many other heliospherical plasma regions.

It would be inappropriate in this paper to review extensively the diagnostic instrumental techniques themselves, whether on Earth or in space, but substantial effort has been made in the relevant sections to relate the theoretical developments to observations that bear on them. We are beginning to see very encouraging signs of agreement between theory and experiment in critical tests of our understanding of plasma holes.

Another important contribution, since the earliest years, to understanding electron holes and indeed a host of other non-linear phenomena, has come from kinetic plasma simulation. One dimensional particle in cell and continuum Vlasov simulations have long given the clearest picture of how electron holes arise as the natural result of nonlinear trapping in two-stream instabilities, followed by the merging of smaller holes into fewer or even just one deeper or longer hole. Multidimensional simulations around the year 2000 were very influential in showing

the importance and observing the threshold of the transverse instability, although it was not until much more recently that rigorous analytical calculations have shown good quantitative agreement with simulation in the frequencies, wavelengths, and growth rates, and thereby identified the driving mechanism of these instabilities. Numerical simulation *techniques* are not reviewed here, but the results of simulations and their comparison with the phenomena will be discussed within the previously outlined sections.

II. PRINCIPLES AND FORMULATION

A. Governing Equations

The Vlasov equation governs the particle velocity distribution $f(\mathbf{v})$ in collisionless plasmas. In three dimensions it is written

$$\frac{\partial f}{\partial t} + \mathbf{v} \cdot \frac{\partial f}{\partial \mathbf{x}} + \frac{q}{m} (\mathbf{E} + \mathbf{v} \wedge \mathbf{B}) \cdot \frac{\partial f}{\partial \mathbf{v}} = 0, \quad (1)$$

and can be considered Boltzmann's equation including the Lorentz acceleration arising from electromagnetic fields acting on particle charge q and mass m , but with the collision term on the right hand side set to zero. A recent book about the Vlasov equation Bertrand, Sarto, and Ghizzo (2019) provides a comprehensive introduction and reviews linear and nonlinear treatments. It also includes some discussion of phase-space holes. Since \mathbf{v} is the time rate of change of position \mathbf{x} and the acceleration $\frac{q}{m}(\mathbf{E} + \mathbf{v} \wedge \mathbf{B})$ is the time rate of change of velocity \mathbf{v} , the left hand side is the total convective derivative of f along a particle's six-dimensional phase-space (\mathbf{x}, \mathbf{v}) orbit; and Vlasov's equation states that f remains constant along phase-space orbits.

We shall adopt the usual convention in plasma physics to take cartesian coordinates in which the background magnetic field \mathbf{B} is in the z direction. Particles then move freely along z but are constrained to circular Larmor orbits in the transverse directions x and y . In strong enough magnetic fields, or when the plasma is uniform in the transverse directions, the variation can be taken as one-dimensional along z . Therefore in a uniform background magnetic field we will consider z to be the spatial coordinate of the one-dimensional Vlasov equation

$$\frac{\partial f}{\partial t} + v \frac{\partial f}{\partial z} - \frac{q}{m} \frac{d\phi}{dz} \frac{\partial f}{\partial v} = 0, \quad (2)$$

where the electric force is expressed in terms of the electrostatic potential ϕ and there is no component of the magnetic force along z . The one-dimensional distribution $f(v) = f_{\parallel}(v_{\parallel}) \equiv \int f(\mathbf{v}) d^2 \mathbf{v}_{\perp}$ is then implied.

The potential is governed by Poisson's equation

$$\nabla \cdot \mathbf{E} = -\nabla^2 \phi = \frac{\rho}{\epsilon_0} = \frac{1}{\epsilon_0} \sum_{species} qn, \quad (3)$$

where ρ is the total charge density determined by the sum over charge species of their charge densities qn . The particle densities n are the integrals over all velocities of the respective species velocity distributions:

$$n = \int f(\mathbf{v}) d^3 \mathbf{v}. \quad (4)$$

The one-dimensional approximation reduces equations (3) and (4) to scalar differential and integral expressions. Equations (1), (3) and (4) or their one-dimensional forms constitute the time dependent kinetic mathematical description of the collisionless plasma, and must be solved self-consistently.

No plasma in nature *exactly* obeys the Vlasov equation. At sufficiently fine scales in velocity or position, collisional or other non-ideal effects become significant. Their influence is normally represented by replacing the right hand side of equation 1 with a non-zero “collision term”. Nevertheless, a pure Vlasov treatment is an excellent approximation for almost all the purposes of this review. A phase-space density modulation usually progresses with time, governed by the Vlasov equation, to finer and finer scales by “phase-mixing”, until dissipative effects (represented by the collision term which we will not discuss) take over. This process undergirds Landau damping, for example, which is taught in most plasma textbooks. The nonlinear aspects ignoring collisions have been analyzed in great mathematical detail, most famously by Villani. A moderately approachable tutorial for his ideas is Villani (2014). Landau damping questions in the present context will be revisited briefly in section V.A.

B. Non-dimensionalization

A characteristic energy, effectively temperature measured in energy units (so as to avoid repetitive factors of Boltzmann’s constant), is taken as T_0 (the same regardless of species). If we measure potential in units of T_0 then its dimensionless form $\hat{\phi}$ is such that $\phi = \hat{\phi} T_0/e$ where $-e$ is the charge on an electron. The velocity is normalized to the thermal speed; so $v = \hat{v} \sqrt{T_0/m} = \hat{v} v_t$. The characteristic length over which potential varies in a plasma is the Debye length, λ_D , such that $\lambda_D^2 = \epsilon_0 T_0 / n_{e\infty} e^2$, using the distant background electron density $n_{e\infty}$. This is the natural length normalization unit: $\mathbf{x} = \hat{\mathbf{x}} \lambda_D$. Substituting these into equation (1) it becomes for each particle species

$$\frac{\partial f}{\partial \hat{t}} + \hat{\mathbf{v}} \cdot \frac{\partial f}{\partial \hat{\mathbf{x}}} + \frac{q}{e} \left[-\hat{\nabla} \hat{\phi} + \hat{\mathbf{v}} \wedge \hat{\boldsymbol{\Omega}} \right] \cdot \frac{\partial f}{\partial \hat{\mathbf{v}}} = 0, \quad (5)$$

where $\hat{t} = t \sqrt{T_0/m} / \lambda_D$ is the normalized time and $\hat{\boldsymbol{\Omega}} = (e\mathbf{B}/m) \lambda_D / \sqrt{T_0/m}$ is the normalized cyclotron frequency (vector). This time scaling is written $t =$

$\hat{t} \lambda_D / v_t = \hat{t} / \omega_p$, where ω_p is the plasma frequency: $\omega_p^2 = (T_0/m) / \lambda_D^2 = n_{e\infty} e^2 / \epsilon_0 m$. It is important to note that the time scaling is *different* for different species because by these definitions $\omega_{pi}^2 = \omega_{pe}^2 m_e / m_i$, even though the length scaling is the same.

The dimensionless particle density \hat{n} is normalized to the (uniform) background density n_∞ giving $n = \hat{n} n_\infty$. The normalized distribution function \hat{f} is then such that $\hat{n} = \int f d^3 \mathbf{v} / n_\infty = \int \hat{f} d^3 \hat{\mathbf{v}} = \int \hat{f} d^3 \mathbf{v} / (T_0/m)^{3/2}$, so that $\hat{f}(\hat{\mathbf{v}}) = [(T_0/m)^{3/2} / n_\infty] f(\mathbf{v})$ for each species. The one-dimensional distribution has instead $\hat{f}(v) = [(T_0/m)^{1/2} / n_\infty] f(v)$. Poisson’s equation (3) then becomes

$$-\hat{\nabla}^2 \hat{\phi} = \sum_{species} \left(\frac{n_\infty q}{n_{e\infty} e} \hat{n} \right). \quad (6)$$

Evidently for electrons $n_\infty q / n_{e\infty} e = -1$. For a single ion species, distant quasineutrality implies that $n_\infty q / n_{e\infty} e = 1$ (regardless of ion charge magnitude $Z = q/e$). We can therefore regard these ratios as the normalized charge \hat{q} equal to ± 1 . We shall not worry in our treatment about the possibility that a dependence of q on Z (absent in \hat{q}) remains in the normalized Vlasov equation (5), but it ought to be accommodated when necessary.

To avoid encumbering the notation, the hats on dimensionless quantities are henceforth dropped and it is understood that we are working in scaled units, unless otherwise indicated.

C. Constancy on orbits

Usually Vlasov’s differential equation need not be solved explicitly. Instead, its property of ensuring f is constant along orbits enables us, if ϕ is known for all prior time and space, to obtain $f(\mathbf{v})$ at any position and time by solving for the phase-space orbit and following it backwards in time until some boundary condition or initial condition is encountered that prescribes the value of f on it. And this approach is almost universal in electron and ion hole theory. However, the loop of equations consisting of f being given by Vlasov using $\phi(\mathbf{x}, t)$, ϕ given by Poisson using $n(\mathbf{x})$, n being given by f , will not be satisfied for arbitrarily chosen ϕ and f conditions. A process is required to determine a self-consistent set of parameters for which the equations are all satisfied.

D. Steady One-Dimensional Equilibria

For the rest of this section we limit ourselves to one-dimensional discussion of structures that are steady in their rest frame. An immediate consequence of steadiness is that particle energy $\mathcal{E}(z, v) = \frac{1}{2} v^2 + q\phi(z)$ (dimensionless units) is constant along orbits, which then means

$f(z, v)$ is a function only of \mathcal{E} and (possibly) sign of v (written σ_v), not of z and v separately. As a shorthand, we will sometimes write the distribution function with an energy argument as $f(\mathcal{E})$ meaning $f(z, \sigma_v \sqrt{2[\mathcal{E} - q\phi(z)]})$. It follows that the density $n(z) = \int f dv$ is a function of potential $n(z) = n(\phi(z))$, and Poisson's equation takes on the special form $-\frac{d^2\phi}{dz^2} = \rho(\phi)$, where $\rho = \sum qn(\phi)$. The standard technique to solve such a differential equation where the inhomogeneous term is a function only of the dependent (not the independent) variable, is to multiply by a factor $\frac{d\phi}{dz}$ and integrate, giving $-\frac{1}{2}(d\phi/dz)^2 = \int \rho d\phi + C$. The right hand side of this equation is often called the pseudo-potential, written V . The integral of the inverse of square root of this equation gives the implicit solution

$$z(\phi) = \int \frac{d\phi}{\sqrt{-2V}} + \text{const.} \quad (7)$$

This is the obvious way to proceed if the $n(\phi)$ are known, which they are if $f(\mathcal{E})$ is prescribed. It is also applicable to fluid plasma equations where only densities $n(\phi)$ are considered, as will be discussed in the next section.

To determine self-consistent steady kinetic equilibria, however, there are two alternative ways proceed. We can either assume that $f(\mathcal{E})$ is prescribed and find the self-consistent $\phi(z)$, which is the inverse of the $z(\phi)$ just discussed, equation (7); or we can assume that the potential variation $\phi(z)$ is prescribed and find the $f(\mathcal{E})$ (satisfying the Vlasov and Poisson equations) that is required for self-consistency.

These two alternatives were introduced by Bernstein, Greene, and Kruskal (1957), who called them the “differential equation” and “integral equation” approaches, referring to the type of equation that needs to be solved. In the subsequent literature the first is often called the pseudo-potential, classical-potential, or Sagdeev approach, and the second the BGK approach. The insight Bernstein *et al.* brought was that although the distribution f of passing particles (with orbits extending to distant boundaries) is determined by boundary conditions and constancy on orbits, the distribution on trapped orbits (that cannot be tracked back to a boundary) is determined by initial conditions of hole formation, and can for equilibrium purposes be considered to be a free choice. Moreover, the required self-consistent choice can be found for an essentially arbitrarily prescribed potential $\phi(z)$ sequentially (over a progressive series of potential maxima and minima). It requires that Poisson's equation be satisfied by a combination of the known passing distribution $f(\mathcal{E})$ for $\mathcal{E} \geq 0$ plus initially unknown distributions of trapped particles ($\mathcal{E} < 0$) that can be found by sequentially solving integral equations. The result is called a BGK wave or mode.

Specifically, for a positive solitary potential structure $\phi(z)$, such as is illustrated in Fig. 1(i), of maximum height

$\phi = \psi$, prescribed in a distant uniform background having $\phi = 0$, the density of the passing (untrapped) electrons is $n_p(\phi) = \int_{\mathcal{E} > 0} f(\mathcal{E}) dv$, where f is known from boundary conditions, while the trapped electron density is $n_t(\phi) = \int_{-\phi < \mathcal{E} < 0} f(\mathcal{E}) dv$ where f is unknown. The ion density $n(\phi)$ is entirely prescribed by boundary conditions since no ion orbits are trapped. And the divergence term $d^2\phi/dz^2$ is prescribed (and a function of ϕ). Consequently Poisson's equation $-\frac{d^2\phi}{dz^2} = q_e(n_p + n_t - n_i)$ determines the required value of the trapped density $n_t(\phi)$. It will be correctly obtained if and only if the trapped f satisfies an integral equation:

$$n_t(\phi) = \int_{-\phi < \mathcal{E} < 0} f dv = 2 \int_{-\phi}^0 f(\mathcal{E}) \frac{d\mathcal{E}}{\sqrt{2(\mathcal{E} + \phi)}}, \quad (8)$$

accounting for both signs of v and trapped symmetry. This is a form of Abel's integral equation, whose well known solution for $-\psi < \mathcal{E} < 0$ is

$$f(\mathcal{E}) = f(0) + \frac{1}{\sqrt{2}\pi} \int_0^{-\mathcal{E}} \frac{dn_t}{d\phi} \frac{d\phi}{\sqrt{-\mathcal{E} - \phi}}. \quad (9)$$

Obviously, the same argument applies for negative potential structures, that is ion holes, exchanging the identities of electrons and ions and the resulting charge signs. For an extended BGK spatial profile of potential maxima and minima, the treatment alternates between determining reflected electrons and reflected ions.

The two different starting points for obtaining self-consistent hole equilibria — the differential aka pseudo-potential, vs. the integral aka BGK approaches — have different practical and mathematical weaknesses and strengths. But both require an extra constraint to avoid singularities in trapped $df/dv|_{\mathcal{E}=0}$ at the trapping boundary $\mathcal{E} = 0$. Such mathematical singularities are physically implausible, except as an approximation of uncertain applicability. The differential approach can easily specify an $f(v)$ without such singularities, but then finds that, when f 's relative shape at $-\psi < \mathcal{E} < 0$ is fixed (which is commonly assumed), the amplitude ψ is set by the slope $df/dv|_{\mathcal{E}=0}$ chosen, for fixed passing and repelled-species distributions. Conversely, the integral approach will encounter singularities in the solved-for trapped $df/dv|_{\mathcal{E}=0}$ unless the potential near $\phi = 0$ ($\phi(z)$ as $|z| \rightarrow \infty$) has the form of an exponential decay with characteristic length equal to the background plasma (generalized) Debye shielding length λ such that

$$\frac{1}{\lambda^2} = \left. \frac{dn_e}{d\phi} \right|_0 + \left. \frac{dn_i}{d\phi} \right|_0. \quad (10)$$

These constraints are effectively the same, as is further explained, for example, in references (Hutchinson and Zhou, 2016) section II and (Hutchinson, 2023b) section III. However, this fact is subtle and is not widely recognized; and some authors fallaciously maintain that only

the pseudo-potential approach is appropriate (see e.g. Hutchinson (2023a); Schamel and Chakrabarti (2023)). Equation 10, though necessary, is not always sufficient to avoid singularity.

Unfortunately the situation is confused still more by an erroneous assertion about ion holes (Schamel and Bujarbarua, 1980), that they cannot exist unless the species temperature ratio $T_e/T_i = \theta \gtrsim 3.5$. This assertion has been widely cited and repeated ((Buchanan and Doring, 1993; Bujarbarua and Schamel, 1981; Eliasson *et al.*, 2006; Grießmeier and Schamel, 2002; Hudson *et al.*, 1983; Johnsen *et al.*, 1987; Péceli *et al.*, 1984; Schamel, 1982b; Schamel *et al.*, 2018; Wang *et al.*, 2021)), despite published theoretical counter-examples such as (Chen *et al.*, 2004). The correct form arising from the requirement that λ^2 be positive is that $\theta < 3.5$ when the value of $dn_i/d\phi$ takes its most negative value, which for a shifted passing Maxwellian is $-0.285 (\simeq -1/3.5)$ at a shift velocity of 2.13. But in any case that shift places the hole velocity far out in the wing of the background distribution, where the phase-space density is only one tenth of its Maxwellian peak, and the amplitude of any ion hole would be severely limited. It does not apply at all to more typical holes in the bulk of the ion distribution. In short, no absolute temperature ratio requirement applies to ion (or electron) holes.

E. Illustrative BGK equilibria

The integral equation BGK approach has been extensively discussed in the literature; for expanded introductions see for example (Bernstein *et al.*, 1957; Hutchinson, 2017; Krasovsky *et al.*, 2003); we here give a few general examples of this approach to electron holes (ignoring ion response) to illustrate its key features and restrictions. One simple and convenient mathematical potential shape is to take

$$\phi(z) = \psi \operatorname{sech}^l(z/l\lambda). \quad (11)$$

The contribution of $d^2\phi/dz^2$ to the required trapped particle distribution 9 can then be found analytically (Hutchinson, 2023b). Examples of distribution functions are shown in figure 3 for an unshifted Maxwellian background distribution and negligible repelled particle response, i.e. $\lambda = 1$. For $l = 2$ the slope df_t/dv is zero at $\mathcal{E} = 0$, while the more typical $l = 4$ gives a profile that is a negative temperature Maxwellian. It turns out that values of l greater than 4 produce a weak slope singularity despite having the correct Debye shielding asymptotic potential decay. For all potentials of this type, the required trapped distribution falls monotonically at low v_ψ .

As is clear from the figure, the lower the value of l , the narrower the potential profile, and the deeper the hole

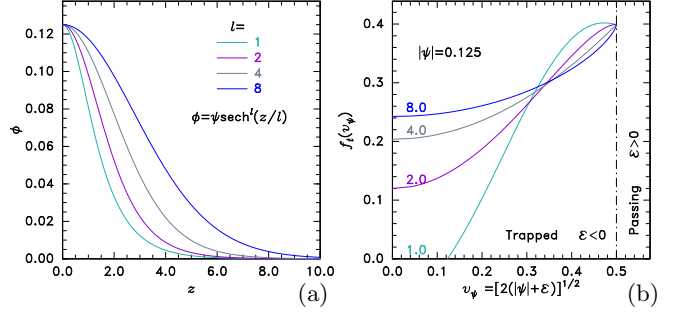


FIG. 3 Illustrative examples for (a) potential profiles $\phi = \psi \operatorname{sech}^l(z/l)$ of (b) the trapped distributions as a function of dimensionless velocity v_ψ at the potential peak. Lines labeled with the value of l .

in the distribution is required to be. An important limitation of allowable hole amplitude ψ for any prescribed shape like this is that the distribution cannot physically be negative, yet nothing in the mathematics prevents finding a solution with such a trapped $f(\mathcal{E})$; one must simply avoid prescribing a ψ that causes it. The illustrated case $l = 1$ for $|\psi| = 0.125$ violates this requirement, and is disallowed. Quite generally the width in z of a hole must exceed a minimum that is proportional to $\psi^{1/4}$ (Hutchinson, 2017).

To explore a fuller range of possible hole shapes, a potential form that has more adjustable parameters is needed. One way to implement that, while still observing the asymptotic constraints at $z \rightarrow \infty, \phi \rightarrow 0$, is to use an inner form which is a Taylor expansion of $\sqrt{\phi(z)}$ about the peak $z = 0$ thus: $\sqrt{\phi} = \sqrt{\psi}(1 + c_2 z^2 + c_4 z^4 + c_6 z^6)$; and then matching it at some join position z_j and potential ϕ_j to the asymptotic form required. The reason for expanding $\sqrt{\phi}$ rather than ϕ itself, is that, as detailed in the Supplementary Material, it is possible not merely to avoid singularities in f' but actually to prescribe its trapped value at and near $\mathcal{E} = 0$ by requiring the variation for $z > z_j$ to be such that

$$\frac{\sqrt{\phi_j}}{1 + a\sqrt{\phi_j}} \exp(\pm(z - z_j)/2\lambda) = \frac{\sqrt{\phi}}{1 + a\sqrt{\phi}}, \quad (12)$$

where a is a constant depending on the prescribed $f'(0)$ value. The other adjustable specified parameters (in addition to ψ) used here are c_2 and ϕ_j . The equations that result from requiring ϕ , $d\phi/dz$ and $d^2\phi/dz^2$ to be continuous at the join can be solved to find c_4 , c_6 , and z_j , giving a fully specified $\phi(z)$ function. The Abel integral equation then is solved (numerically) to find f . Figure 4 shows example results varying the potential curvature at the peak, keeping the join potential ϕ_j fixed (as indicated by the cross), and setting $f'(0) = 0$ (to lowest relevant order). The entire distributions are plotted: at left versus velocity v_ψ measured at the peak of the potential (the deepest part of the potential energy well), and at right versus energy. The passing distribution is chosen as a

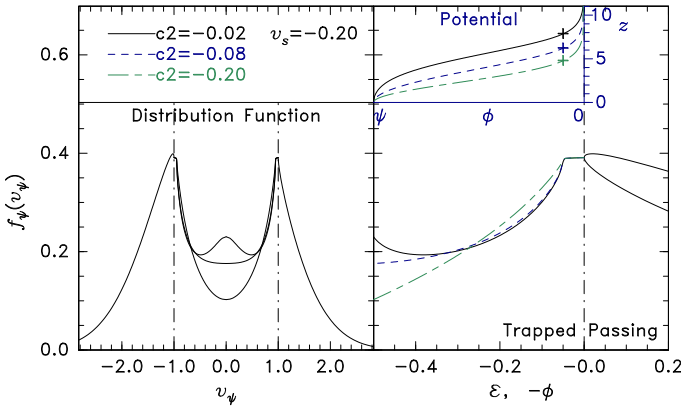


FIG. 4 Examples of the adjustable asymptotically matched potential profile and the resulting trapped distribution shapes.

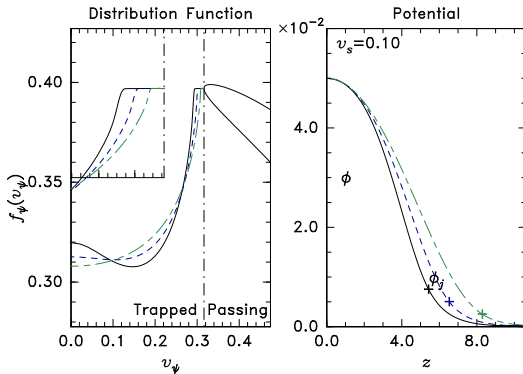


FIG. 5 Variation of the join potential ϕ_j and the resulting shape for fixed central potential curvature $c_2 = -0.05$.

Maxwellian shifted by $v_s = -0.2$, to illustrate asymmetry. Low curvature ($c_2 = -0.02$) causes a non-monotonic $f(v_\psi)$ having a rise at low $|v_\psi|$. As $|c_2|$ is increased, it disappears and the hole bottom becomes deeper. Note the flat trapped region near $\mathcal{E} = 0$, and the different $f(\mathcal{E})$ curves for the two velocity signs of passing particles $\mathcal{E} > 0$. The potential is plotted on its side on the same energy scale to indicate the correspondence between ϕ (at some position z) and the marginal trapped orbit energy that contributes to the density integral. This case has $|\psi| = 0.5$ but without encountering negative trapped $f(v)$ limitation, because the hole z -width is large enough.

Figure 5 explores several values of ϕ_j at fixed $c_2 = -0.05$, giving a detailed insert of the flat and join regions of $f(v_\psi)$, and showing the potential shape trends, for $\psi = 0.05$. Requiring a small derivative f' at the trapped/passing boundary $\mathcal{E} \rightarrow 0$, as these examples do, is physically appropriate for more complicated situations (to be discussed later) where stochastic trapping and de-trapping of orbits occurs. Newly trapped orbits will generally sustain phase space density approximately equal to the adjacent passing value, down to a trapping depth determined by the orbit energy diffusion. That depth

might be represented approximately by energy $-\phi_j$. Actually the passing distribution, when asymmetric, also possesses divergent v -derivative at $\mathcal{E} = 0$ and non-zero ϕ . A modification of the passing velocity distribution has been proposed (Korn and Schamel, 1996) to remove this singularity. However, orbit diffusion will probably be less important for passing orbits because they are being constantly renewed by influx from distant $|z|$ regions, so it is justifiable to pay more attention to avoiding the trapped distribution slope singularity, or even constraining its finite value. Of course, all these mathematical representations are just analytic conveniences and approximations. Actual physical holes may have fine-scale distribution variation arising from phase mixing but will have coarse-grained variation in v and z that is smooth.

III. ONE DIMENSIONAL SOLITON AND HOLE EQUILIBRIA

The main purpose of this section is to identify the characteristics of one-dimensional fluid solitons that distinguish them from kinetic structures such as electron and ion holes. This helps us to understand kinetically how electrostatic structures work, and gives practical guidance on identifying structures observed in nature. In keeping with our overall approach, we treat a soliton in its own rest frame right from the start.

In the process we will exemplify the pseudo-potential approach to calculating solitary structure equilibria, but with highly simplified particle distributions and consequent density behavior.

A. Prototypical Solitons

In a positive solitary potential structure like figure 1(i), the potential curvature $\phi'' = d^2\phi/dz^2$ at its peak is negative. But in the wings of the structure, approaching $\phi = 0$, ϕ'' must be positive, so as to bring the potential derivative to zero, matching the uniform external background. More generally for a single positive or negative peak potential ψ , the signs of ϕ'' must be opposite ψ at $\phi = \psi$, and the same as ψ at $\phi = 0$.

Obviously Poisson's equation $-d^2\phi/dz^2 = \rho$ (scaled units) requires equivalent statements about the charge density ρ : that it has the same sign as ψ at its peak and the opposite sign in the wings. Also the charge density must be zero in the background, i.e. at $\phi = 0$, in order for the potential there to be uniform. Therefore the charge density must be a nonlinear function of potential: starting at zero when $\phi = 0$, initially having sign opposite to ψ , that is $\psi d\rho/d\phi|_0 < 0$, then reversing and becoming the same sign as ψ at the potential peak. At least one of the components of the plasma must therefore have substantial curvature in its density dependence $n(\phi)$.

A *single-velocity-stream* (S) component moving in a static potential has velocity satisfying the conservation of energy $\mathcal{E}_S = v^2/2 + q\phi = \text{constant}$. Provided $q\phi/\mathcal{E}_S < 1$, no reflection occurs and the fluid continuity equation then immediately yields

$$n_S(\phi) = \frac{n_{S\infty}}{\sqrt{1 - q\phi/\mathcal{E}_S}}, \quad (13)$$

where n_∞ denotes the density at $\phi = 0$, which is $z = \infty$. Notice that the slope $dn_S/d\phi$ has the sign of $q\phi$, so it could not by itself be responsible for the correct ϕ'' sign in the potential wings near $\phi = 0$. Also, $|dn_S/d\phi|$ becomes large as ϕ approaches \mathcal{E}_S/q . Bear in mind that the stream energy \mathcal{E}_S can be considered to set the speed of the structure in the frame in which the stream is stationary.

By contrast, a *broad distribution of velocities* (B), approximately centered on zero, has density that depends on potential with opposite slope sign. Qualitatively, when $q\phi$ is positive (repelling particles) low energy particles are reflected before reaching potential ϕ ; their absence reduces $n_B(\phi)$ below $n_{B\infty}$. When $q\phi$ is negative (attracting particles), then provided that the distribution on trapped (negative \mathcal{E}) orbits remains fully populated, the density increases with ϕ as the distribution broadens through acceleration. The standard model of such a distribution is the Maxwellian, which when unshifted from $v = 0$ gives the Boltzmann density distribution:

$$n_B(\phi) = n_{B\infty} \exp(-q\phi/T). \quad (14)$$

This dependence can also be regarded as the solution of the steady isothermal fluid momentum equation. Shifted Maxwellians or alternative shapes change this expression, but the general principle remains that provided the trapped orbits remain populated such that $f(\mathcal{E}) \gtrsim f(0)$, and the distribution peak is shifted less than approximately its width, thus remaining substantial at $\mathcal{E} = 0$, the slope $dn/d\phi$ has the sign of $-q\phi$: opposite that for an unreflected single stream.

Fluid solitons work by balancing these two types of density behavior against one another. Reduced to their simplest prototype, fluid solitons have a stream component S , and a broad component B , plus possibly an extra neutralizing uniform charge component C , which might represent ions for a soliton moving at approximately electron thermal speeds (so fast that ions cannot respond), or a background of (approximately immobile) charged dust for “dust ion acoustic” solitons (see e.g. Mamun and Shukla (2005)). These two or three components give rise to a charge density that depends only on ϕ :

$$\rho(\phi) = \frac{q_S n_{S\infty}}{\sqrt{1 - q_S \phi/\mathcal{E}_S}} + q_B n_{B\infty} \exp(-q_B \phi/T_B) + q_C n_C, \quad (15)$$

where $q_S n_{S\infty} + q_B n_{B\infty} + q_C n_C = 0$ to satisfy distant

neutrality. Its derivative is

$$\frac{d\rho}{d\phi} = \frac{1}{2} \frac{n_{S\infty} q_S^2}{\mathcal{E}_S (1 - q_S \phi/\mathcal{E}_S)^{3/2}} - \frac{n_{B\infty} q_B^2 \exp(-q_B \phi/T_B)}{T_B}, \quad (16)$$

which at $\phi = 0$ is $\frac{d\rho}{d\phi} = \frac{1}{2} n_{S\infty} q_S^2 / \mathcal{E}_S - n_{B\infty} q_B^2 / T_B$; so the required distant condition $d\rho/d\phi|_0 < 0$ is satisfied only if

$$\mathcal{E}_S > |n_{S\infty} q_S / n_{B\infty} q_B| T_B / 2. \quad (17)$$

B. Pseudo-potential solitary structure analysis

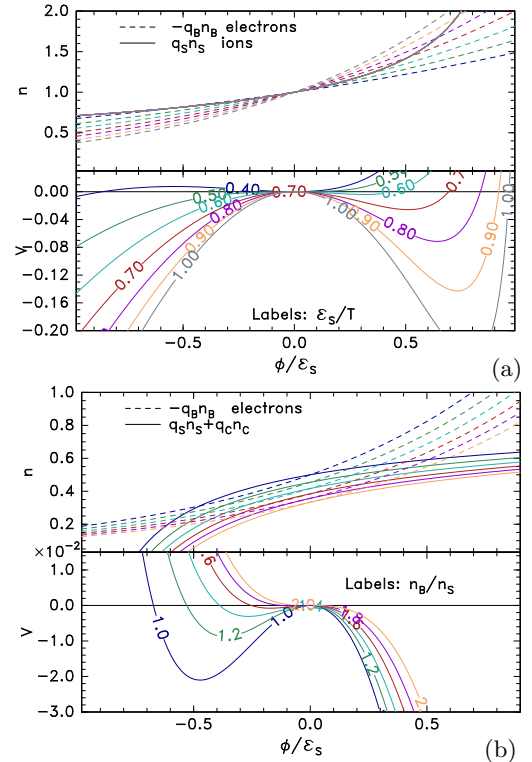


FIG. 6 Examples of particle densities $n(\phi)$ and the resulting pseudo-potential $V(\phi)$ for (a) ion acoustic solitons for a range of soliton speeds relative to the (ion) stream $\mathcal{E}_S = v^2/2$, (b) electron acoustic solitons for a range of ratios of broad to stream densities n_B/n_S (for the case $\mathcal{E}_S = T_B$).

Pseudo-potential analysis can be applied to any one-dimensional equilibrium where the charge density is a known function of potential, whether solitons or holes. Then, because in Poisson’s equation the charge is a function of the dependent variable, ϕ , but not of the independent variable, z , a first integral can be found by mul-

tilying by $d\phi/dz$ and integrating to get

$$\begin{aligned} \frac{1}{2} \left(\frac{d\phi}{dz} \right)^2 &= -V(\phi) = - \int_0^\phi \rho d\phi \\ &= 2\mathcal{E}_S n_{S\infty} \left[\sqrt{1 - \frac{q_S \phi}{\mathcal{E}_S}} - 1 \right] \\ &+ T_B n_{B\infty} \left[\exp \left(-\frac{q_B \phi}{T_B} \right) - 1 \right] - q_C n_C \phi. \end{aligned} \quad (18)$$

Because of analogies that will not be explained here, the quantity $V(\phi)$ is called the pseudo-potential, classical potential, or Sagdeev potential¹, regardless of the exact form of $\rho(\phi)$. It is illustrated together with the densities that give rise to it, in figure 6. The pseudo-potential must be negative throughout the potential range $0 - \psi$ and satisfy the conditions $V(0) = 0$, $dV/d\phi|_{\phi=0} = 0$ and $V(\psi) = 0$. The conditions at $\phi = 0$ are satisfied by the chosen integration constant in eq. (18) and distant neutrality $\rho(0) = 0$. The third condition, $d\phi/dz = 0$ (i.e. $V = 0$) at the potential peak $\phi = \psi$, for our simple fluid soliton gives an equation relating the stream energy \mathcal{E}_S (equivalent to speed of the soliton with respect to the stream) and ψ

$$1 - \frac{q_S \psi}{\mathcal{E}_S} = \left\{ 1 - \frac{T_B n_{B\infty}}{2\mathcal{E}_S n_{S\infty}} \left[\exp \left(-\frac{q_B \psi}{T_B} \right) - 1 \right] + \frac{n_C q_C \psi}{n_{S\infty} 2\mathcal{E}_S} \right\}^2 \quad (19)$$

Whose solution is

$$\mathcal{E}_S = \frac{\frac{1}{4} T_B \frac{n_{B\infty}}{n_{S\infty}} \left\{ \exp \left(-\frac{q_B \psi}{T_B} \right) - 1 - \frac{n_C q_C \psi}{n_{B\infty} T_B} \right\}^2}{\exp \left(-\frac{q_B \psi}{T_B} \right) - 1 + \frac{q_B \psi}{T_B}}, \quad (20)$$

using $n_C q_C + n_{S\infty} q_S = -n_{B\infty} q_B$.

C. Ion Acoustic Solitons

Ion acoustic solitons are so called because they operate under the same assumptions as linear sinusoidal ion acoustic waves. They take the stream to be ions and the broad distribution to be electrons. They do not require n_C and have (most simply) $q_S = -q_B = 1$ and $n_{S\infty} = n_{B\infty} = 1$. Figure 6(a) shows the form of their densities and pseudo-potentials. Equation 20 is then exactly the classic result of Sagdeev (1966) eq (39). It is plotted in Figure 7(a). These cold ion, Maxwellian electron, equations possess no solution with $\psi < 0$ because for negative ϕ and $\mathcal{E}_S > T_B/2$, the equation $d\rho/d\phi = 0$ has no solution, meaning $d\rho/d\phi$ cannot

¹ The expression Sagdeev potential recognizes his extensive early contributions, using this technique, to fluid ion acoustic soliton theory that we are guided by in this subsection.

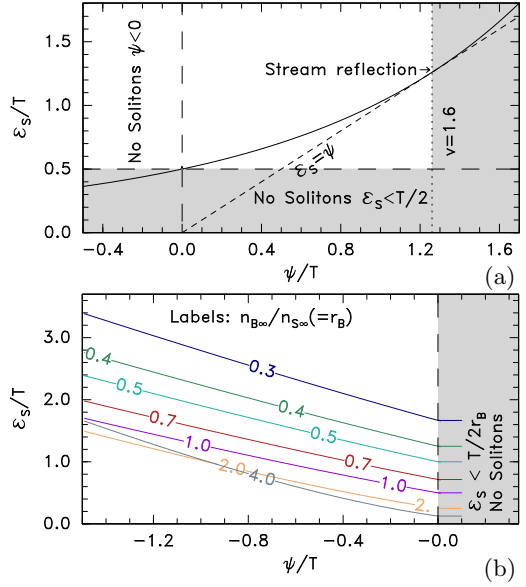


FIG. 7 Relation between stream energy and amplitude of (a) simple ion acoustic solitons, (b) simple electron acoustic solitons for various values of $n_{B\infty}/n_{S\infty}$.

change sign. So these solitons are always positive. Also, at $\mathcal{E}_S = 1.26T_B$, $v_h \simeq 1.59\sqrt{T_B/m_S}$, the potential ψ reaches the same value as the energy, thus beginning to reflect the stream and breaking the assumptions governing the stream density. Solitons with higher speed and non-zero stream width cannot exist. More complicated electron distributions, non-Maxwellian or even sums of multiple Maxwellians of different temperatures or velocity shifts alter the function $n_B(\phi)$. It can then sometimes be possible for negative potential (“rarefactive”) ion acoustic solitons to exist (Cairns *et al.*, 1995).

D. Electron acoustic solitons

Electron acoustic solitons, relate by analogy to a much more unusual type of sinusoidal wave referred to as the electron acoustic mode (see Gary and Tokar (1985)), which arises from the electron response in a distribution having hot and cold electron components. Reduced to the simplest prototype, one can assume a cold stream S and broad distribution B that are both electrons ($q_S = q_B = -1$), but of different densities. Ions are a constant (in the simplest case) charge neutralizing background C . Then the slope is $d\rho/d\phi|_0 = (e^2/T_B)[n_{S\infty}/2\mathcal{E}_S - n_{B\infty}/T_B]$, which to be negative requires $\mathcal{E}_S > (n_{S\infty}/n_{B\infty})T_B/2$. Figure 6(b) shows the resulting density and pseudo-potential shapes, for different ratios of stream to broad distribution densities.

Equation 20 becomes

$$\mathcal{E}_S = \frac{\frac{1}{4}T_B n_{B\infty}/n_{S\infty} \left\{ \exp\left(\frac{e\psi}{T_B}\right) - 1 - \frac{e\psi}{T_B} \frac{(n_{S\infty} + n_{B\infty})}{n_{B\infty}} \right\}^2}{\exp\left(\frac{e\psi}{T_B}\right) - 1 - \frac{e\psi}{T_B}}. \quad (21)$$

However, not all solutions of this equation give rise to solitons, because a soliton must have a continuous variation of $\rho(\phi)$ over the range $0 \leq |\phi| \leq |\psi|$. Consider the second derivative of ρ :

$$\frac{d^2\rho}{d\phi^2} = \frac{3}{4} \frac{n_{S\infty} q_S^3}{\mathcal{E}_S^2 (1 - q_S \phi / \mathcal{E}_S)^{5/2}} + \frac{n_{B\infty} q_B^3 \exp(-q_B \phi / T_B)}{T_B^2}. \quad (22)$$

It is always negative for electron acoustic solitons when n_S is positive² because $q_S = q_B = -1$. Consequently if $d\rho/d\phi|_0 < 0$ (as it must be for positive ψ) then at increasingly positive values of ϕ , $d\rho/d\phi$ decreases, instead of increasing. It therefore does not become positive to allow ρ continuously to become positive and $V(\phi)$ to return to zero as is clear in figure 6(b). This demonstrates that there can be no positive-potential purely electron acoustic solitons for any electron distribution constructed from unreflected streams of positive density (n_S) and Boltzmann-like trapped density contribution. This remains true if the streams have finite pressure. Figure 7(b) shows the resulting relationship between \mathcal{E}_S and ψ for a range of $n_{B\infty}/n_{S\infty}$.

E. Soliton – Hole Comparison

The illustrative assumptions about the fluid behavior can of course be generalized by introducing finite pressure (that is velocity spread, or temperature) of the stream, or introducing multiple streams of different velocities or temperatures giving rise to more complicated charge functions $\rho(\phi)$ (see for example Lakhina *et al.*, 2018). However, notice that for any set of prescribed external velocity distributions f_e, f_i , represented here by $\mathcal{E}_S, q_S n_{S\infty}, q_B n_{B\infty}, n_C, T_B$, our simple fluid solitons have a single solution for amplitude ψ . This discrete solution is a major characteristic of all fluid solitons, which is not shared by electron or ion holes. Holes can have continuous ranges of amplitudes and speeds depending on the degree of trapped particle reduction, even for fixed passing particle distributions. The discrete solutions for solitons arise because of the assumption of a fixed form for the trapped particle distribution. In our simple case we

assumed effectively that it follows the Maxwellian dependence $f(\mathcal{E}) \propto \exp(-\mathcal{E}/T_0)$ where T_0 is the background (i.e. untrapped) particle temperature. This assumption is mathematically convenient but poorly justified physically because it implies an enhancement of the distribution function on trapped orbits.

A more physically plausible assumption might be that the trapped $f(v)$ is a flat plateau (for negative \mathcal{E}) at its value where $\mathcal{E} = 0$. That is what would arise for a potential structure that gradually grew up from zero in a time long compared with the typical transit time of the attracted particles (Gurevich, 1968) because newly trapped particles always sample the external distribution at zero energy. Such a flat trapped distribution gives a mathematically more complicated density function, but still gives discrete solutions for ψ versus the untrapped distribution's parameters. In our illustrative case those parameters were \mathcal{E}_S and $n_{B\infty}/n_{S\infty}$ but treated within a plasma frame in which the distributions are fixed, they can be considered to dictate the soliton's speed relative to the background plasma .

Electron and ion hole equilibria can still be found using the pseudo-potential differential equation approach, but they do not assume some fixed relationship between the trapped ($\mathcal{E} < 0$) distribution $f(\mathcal{E})$ and the background untrapped ($\mathcal{E} > 0$) $f(\mathcal{E})$. Instead they suppose that the trapped distribution is a variable function that controls the hole amplitude ψ and shape $\phi(z)$ through its contribution to the charge density. Consequently there is generally no fixed relationship between amplitude ψ and hole velocity v_h .

A characteristic of the flat plateau trapped distribution is that, unlike an unshifted Maxwellian, its derivative is discontinuous at $\mathcal{E} = 0$. The mathematical result, which is effectively inherent to holes, but not always to solitons, is that the expansion of the density for small ϕ possesses half-integer powers. As an important example, the total density of a “Schamel distribution” electron hole having trapped dependence $f(\mathcal{E}) = f(0) \exp(-\beta \mathcal{E})$, for an attracted species with a (single) shifted Maxwellian untrapped distribution has the expansion

$$n_e = 1 - \frac{1}{2} Z'_r(U) \phi - \frac{4}{3} b \phi^{3/2} + \frac{1}{16} Z''_r(U) \phi^2 + O(\phi^{5/2}), \quad (23)$$

where $U = v_s/\sqrt{2}$ measures the shift velocity v_s (scaled to $\sqrt{T/m}$) of the Maxwellian, $b = \exp(-U^2)(1 - \beta - 2U^2)/\sqrt{\pi}$, and Z_r is the real part of the plasma dispersion function³. The $\phi^{3/2}$ term is the first non-zero half-integer power. Derivative discontinuity is absent when $\beta = 1$ and $U = 0$ (unshifted Maxwellian), but the flat trapped

² A negative density stream of finite spread might be used to represent a depression within the Maxwellian distribution function. Allowing such an electron stream invalidates this proof that ψ cannot be positive. So does allowing an ion stream with significant potential response, but arguably that should anyway be called an “ion acoustic”, not an “electron acoustic” soliton.

³ The ϕ^2 coefficient was stated incorrectly in (Hutchinson, 2017) and the present form corrects that error, and conforms with prior literature.

distribution has $\beta = 0$, and so has $b \neq 0$ even for $U = 0$. The Schamel distribution has the attractive features of continuous $f(v)$ and non-singular f'_t at $\mathcal{E} = 0$.⁴

It can be shown (Schamel, 1972, 1973) that for small ϕ the density dependence (23) corresponds to a nonlinear wave equation governing the potential

$$\frac{\partial \phi}{\partial t} + (1 + b\phi^{1/2} + \phi) \frac{\partial \phi}{\partial z} + \frac{1}{2} \frac{\partial^3 \phi}{\partial z^3} = 0. \quad (24)$$

When $b = 0$ (and the 1 term is removed by a coordinate transformation) this is the Korteweg-de Vries (KdV) equation (Korteweg and de Vries, 1895) which is the standard of much soliton analysis, historically including shallow water waves and the simplified ion acoustic soliton. That soliton has shape (see Sagdeev, 1966 eq. 40) $\phi = \psi \operatorname{sech}^2([2\pi\psi/3]^{1/2}z)$. The full equation (24) with $b \neq 0$ is sometimes called the modified KdV equation. It gives rise instead (ignoring the ϕ term in the bracket) to the potential shape (Schamel, 1986) $\phi = \psi \operatorname{sech}^4([b\sqrt{\psi}/15]^{1/2}z)$. This solution shape is a popular example for kinetic electron holes. Actually, the soliton literature historically spoke of “the Modified KdV equation” as having nonlinearity factor (i.e. the bracketed term in eq. 24) being ϕ^2 , which gives rise to solitary potentials $\phi \propto \operatorname{sech}(x/\ell)$. A general nonlinearity factor ϕ^n has also been considered by Dodd *et al.* (1982). So 24 should really be called “a” modified KdV equation.

The ion acoustic soliton’s amplitude is fixed by the (repelled distribution’s) stream energy in the hole frame, \mathcal{E}_S , giving $\psi = (3/2)[1 - 1/(2\mathcal{E}_S)]$, and its small-amplitude width is proportional to $\psi^{-1/2}$. By contrast, because the electron hole’s trapped distribution (b) can vary, its amplitude can vary even with fixed untrapped distribution(s).

What is more, since nothing forces the trapped distribution to have the dependence $f(\mathcal{E}) = f(0) \exp(-\beta\mathcal{E})$, we are at liberty to choose almost any different shape (not just sech^4) for an electron hole, and still avoid derivative singularity at $\mathcal{E} \rightarrow 0$ provided the distant potential decay has the correct shielding length λ .

In summary: The key difference between solitons and kinetic electron and ion holes is that solitons have particle densities in the presence of the potential structure that are entirely determined by the background particle distributions, while holes allow the trapped particle distribution to vary independent of the background. Solitons are usually treated using fluid approximations, which often makes their mathematics more tractable, but that is not essential. The central charge density sustaining a soliton generally arises from streaming repelled particles being slowed and thereby densified by the potential,

rather than from the deficit of trapped attracted particles in a hole. The soliton’s speed relative to the background stream(s) crucially controls the densification. The absence of independent variability of the trapped density causes solitons to have a discrete amplitude ψ for given background distributions in the soliton’s frame. Changing soliton velocity v_s , in a frame of reference in which the background distributions are fixed, changes the background it sees in its own reference frame. Therefore a unique functional dependence between ψ and v_s arises. Generally $|\psi|$ increases with $|v_s|$ when v_s is measured relative to a narrow particle stream. Also, the soliton width generally has a discrete inverse relationship approximately proportional to $\psi^{-1/2}$. Holes have no such discrete relationships, and can have a continuous range of amplitudes in a fixed background at fixed velocity, as well as continuous ranges of velocities and widths.

IV. HISTORICAL BACKGROUND

This section surveys the historical development of kinetic electrostatic structures from their beginnings to approximately 2016. Figure 8 attempts to summarize in a single timeline that past history, which we will now seek to fill out with more detailed explanation and citation.

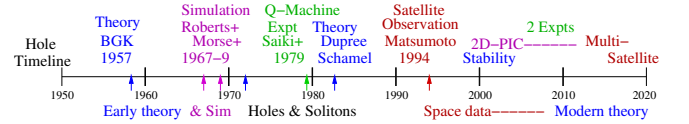


FIG. 8 Phase-space hole research. Colors indicate theory (blue), simulation (magenta), laboratory experiment (green), and space satellite observation (red). A few key milestones are indicated with arrows.

A. Initial theory and simulation 1957-1970

The work of Bernstein *et al.* (1957) can be considered the historic foundation of the field of kinetic electrostatic plasma structures. But in those days, even before experiments had persuaded doubting plasma physicists that Landau damping was real, there were many other nonlinear plasma wave aspects being pursued ahead of the rather abstract possibility of solitary BGK structures. The first subsequent paper to demonstrate that they were naturally formed was a very early one-dimensional continuum Vlasov simulation by Roberts and Berk (1967), of an electron two stream instability growing, trapping electrons, forming a train of electron holes, and undergoing a pairwise hole merging event to create bigger holes. More detail of the trapping process for a single hole was given the same year in Berk and Roberts (1967), and more detail of the hole merging in Berk, Nielsen, and Roberts

⁴ Recent papers (Schamel, 2015; Schamel *et al.*, 2018, 2020) introduce generalizations of the Maxwellian trapped distribution shape that have discontinuities and slope singularities at $\mathcal{E} = 0$.

(1970). Fig. 9 illustrates the merging process.

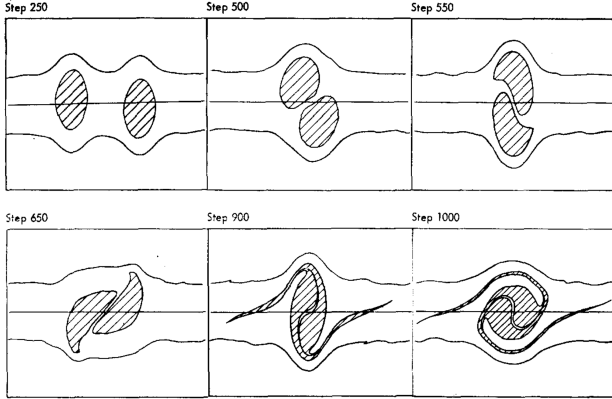


FIG. 9 Early Vlasov simulation of hole merging in phase-space (z, v). Reprinted from (Berk *et al.*, 1970) with the permission of AIP publishing. The phase-space density is zero in the shaded region and unity elsewhere.

Morse and Nielson (1969) observed the same sorts of phenomena, but with a particle in cell code, and with the important addition of two and three dimensional simulations that, unlike the one dimensional case, did *not* observe hole formation, thus calling into question the applicability of the one-dimensional approximation to unmagnetized plasmas. Analytic BGK theory of a “shock” that now would be called a double layer, was also published by Montgomery and Joyce (1969).

B. Experiment, Simulation, and Analytic Consolidation 1970-1993

The year 1972 saw the publication of a seminal paper by Schamel (1972), in which he introduced the idea of supposing that the velocity distribution of trapped particles be represented by a Maxwellian $f(v) \propto \exp(-\beta v^2/2)$ of (possibly) negative inverse temperature β . This ansatz, used with the pseudo-potential solution method, is frequently called the Schamel hole. The work addresses non-linear periodic waves of arbitrary wavelength, including infinite, which represents the solitary case, and introduces the notion of a Nonlinear Dispersion Relation (NDR). For solitary potentials with cold ions, the NDR expresses the fact that for fixed β there is a unique relationship between hole speed relative to the ions and the peak hole potential ψ . For modest $|\beta| \lesssim 1$ this is a small modification of the relationship for ion acoustic solitons given earlier by Vedenov, Velikhov, and Sagdeev (1961). The paper also shows that trapping effects when $\beta \neq 1$ can be represented approximately by a single “modified Korteweg-de Vries” partial differential equation with an extra non-linear term equal to $\sqrt{\phi}$ times a coefficient $b = (1 - \beta)/\sqrt{\pi}$ proportional to the difference of electron distribution in the trapped region from the external

Maxwellian. This equation gives rise to wave solutions called “snoidal” or “cnoidal” with narrower peaks than troughs, and in the infinite wavelength limit to solitons of the shape $\phi(z) = \psi \operatorname{sech}^4(z/\lambda)$, rather than the more familiar $\psi \operatorname{sech}^2(z/\lambda)$ form arising from the standard soliton KdV equation.

In 1972 also, Davidson (1972) published a helpful wide-ranging book about nonlinear plasma theory, which briefly addresses solitons and particle trapping but not significantly our current emphasis, holes. Sakanaka (1972) reported continuum Vlasov simulations of ion-beam plasma interactions giving rise to a shock and simultaneously an ion “vortex” or ion hole, though not a solitary hole. During the ensuing years of the 1970s decade, several important theoretical papers concerning double layers appeared, culminating in a review by Block (1978), which summarizes the double layer field. But a critical result giving the first unambiguous laboratory observations of an electron hole appeared in two 1979 papers: Saeki, Michelsen, Pecseli, and Rasmussen (1979), and Lynov, Michelsen, Pecseli, Rasmussen, Saeki, and Turikov (1979). They discuss the same experimental data, obtained in a long magnetized plasma filled wave-guide (Q-machine), but the second gives expanded modelling in the form of PIC simulations; and Lynov, Michelsen, Pecseli, and Rasmussen (1980) expand it further. Under some circumstances the experimental data and simulation showed merging of two electron holes into one.

Presumably inspired by this experiment, Schamel (1979) immediately published a theoretical analysis of the electron hole and Gould-Trivelpiece soliton that were observed in it, accounting for the important finite transverse extent imposed by the waveguide. The effect is to require an extra term $-\frac{\partial^2 r \phi}{r \partial r^2} = k_\perp^2 \phi(0, z)$ with k_\perp fixed by the waveguide, in addition to $-\frac{\partial^2 \phi}{\partial z^2}$, in Poisson’s equation. Ignoring any ion response, which is a good approximation for the experiment, and approximating the hole amplitude ψ as small, it is shown that for an electron hole to exist, the trapped inverse temperature β must be sufficiently negative; the potential form is then $\phi = \psi \operatorname{sech}^4(z/\ell)$ with $\ell = (15/b\sqrt{\psi})^{1/2}$. The alert reader will observe that b and $\sqrt{\psi}$ must therefore be inversely proportional to one another in order to satisfy the constraint that the asymptotic potential form is $\phi \propto \exp(-z/\lambda)$, where λ is the plasma screening length (the Debye length modified by k_\perp , independent of hole properties). For a hole moving relative to the Maxwellian background electrons at speed v_h , the value of b is $b = (1 - \beta - v_h^2) \exp(-v_h^2/2)/\sqrt{\pi}$. Small ψ (the limit under discussion using a Taylor expansion of the densities) then implies large positive b which requires large negative β , regardless of moderate values of v_h^2 . It is unfortunate therefore that Schamel’s paper assumes β is fixed and of limited size (-3), and concludes incor-

rectly that in the limit of vanishing amplitude ($\psi \rightarrow 0$) and perpendicular wave-number ($k_\perp \rightarrow 0$) the hole must move at speed $v_h^2 = 1.71(T_e/m_e)$. This conclusion ignores the normal situation that in the limit, $b\sqrt{\psi}$ is finite for an electron hole, not zero; and a self-consistent $\beta \propto 1/\sqrt{\psi}$ exists to permit any v_h such that $\exp(-v_h^2/2)$ is not vanishingly small. Nevertheless, this experiment and the analysis and simulation it inspired remain important milestones in the physics of kinetic electrostatic structures.

Another important theory paper in 1979 was Schwarzmeier, Lewis, Abraham-Shrauner, and Symon (1979). In it the instability of adjacent peaks in an initially periodic non-linear BGK wave was simulated and analytically calculated. The results agree rather well; and represent the first stage of the merging of adjacent electron holes at the potential peaks into larger amplitude and eventually solitary holes. This process had been seen in lower resolution in the simulations of (Roberts and Berk, 1967) and (Morse and Nielson, 1969). But the work of Schwarzmeier *et al.*, together with its refinement by Ling and Abraham-Shrauner (1981), is notable in being the first (and for a long time the only persuasive) application of the mathematical methods of Lewis and Symon (1979) to the problem of determining the general unstable eigenmode of a BGK equilibrium.

Analytic *ion* hole equilibria based on the Schamel approach were addressed by Schamel and Bujarbarua (1980). The ion hole equations are highly similar to those for the electron hole, and a paper with additional details treating both followed soon after: Bujarbarua and Schamel (1981); then Schamel (1982a) covered much the same ground, with additional explanatory diagrams and mathematical details, and added discussion of double layers.

In 1982 Schamel (1982b) also addressed the stability of a solitary electron hole using the general mathematical apparatus of Lewis and Symon (1979). His truncated series expansion of the Vlasov solutions, using a so-called fluid approximation was of questionable accuracy, but also he assumed erroneously that the most dangerous (unstable) mode was a symmetric potential perturbation, which subsequent simulations and theory have shown to be incorrect.

Pécseli, Armstrong, and Trulsen (1981) in 1981 reported the “first experimental observations” of an ion hole. In effect it was of the type simulated by Sakanaka (1972). More extended interpretation of this research in a beam-plasma device is presented in Pécseli, Trulsen, and Armstrong (1984), together with PIC simulations.

The paper of (Dupree, 1982) arose primarily from attempts to understand the PIC simulations of his students Berman, Tetreault, Dupree, and Boutros-Ghali (1982) which showed (for a mass ratio $m_i/m_e = 4$) non-linear growth of current-driven electrostatic ion instabilities *below* the linear growth threshold. He had long been

interested in the phase-space density granulations that occur in non-linear plasma turbulence, which he called “clumps”: locally coherent positive or negative phase-space density perturbations. But in (Dupree, 1982) he begins by criticizing his prior clump theory and pointing out that holes (density depressions) have the ability to trap particles self-consistently by their fields, which density enhancements do not. The paper argues that Maxwellian (Schamel) holes are states of maximal entropy, and shows how to calculate the effective mass, charge, and energy of a hole, illustrating it with analytic calculations for a “step function” trapped distribution $f(v)$, which proves to be not much different from a Maxwellian hole. It was followed by Dupree (1983) which addressed in detail the evolution of a one-dimensional hole when it grows in amplitude or accelerates, behaving as an (almost) rigid body that obeys Newton’s second law. The mathematical detail in its 255 equations makes the paper rather forbidding. But it systematically derives the mass, momentum, and energy changes arising from acceleration and growth, under shallow hole approximations, and shows some foundational concepts concerning what might be termed a hole’s kinematics (i) the effective mass of a hole is negative, (ii) if a hole moves into a phase-space region with higher background $f(v)$, then its depth (and consequently its potential amplitude) increases because the trapped $f(v)$ remains constant. (iii) electron reflection from an ion hole in a current carrying plasma can cause an acceleration into a higher $f_i(v)$ and hence such growth.

Temerin, Cerny, Lotko, and Mozer (1982) is the first reported observation in space of double layers and “solitary waves” (bipolar excursions of parallel electric field). Its data was compared with simulation and analytic theory by Hudson, Lotko, Roth, and Witt (1983).

Turikov (1984) introduced a different type of theoretical electron hole, whose equilibrium can apparently move at any speed v_h (even considerably greater than thermal speed) relative to the passing electrons. He used an integral equation method with prescribed potential shape, whose length δ was regarded as adjustable; but he prescribed also that the trapped distribution $f(z, v)$ is exactly zero at the hole center ($z = 0, v = 0$). There is then a monotonic increasing relationship between spatial width δ and speed v_h . Allowing δ to vary in this way does not give rise to Debye shielding asymptotic potential decay, and therefore induces a slope singularity (which is negative for $|v_h| \gtrsim 1.3$): $df/dv \rightarrow -\infty$ at $\mathcal{E} \rightarrow 0$. The trapped $f(v)$ is then non-monotonic, consisting of a peak at slightly negative \mathcal{E} , but a lower value (even ~ 0) at the trapping boundary $\mathcal{E} = 0$, as illustrated in Fig. (10). Although this theoretical structure has a hollow phase-space vortex of trapped particles, it is not a hole in the background phase-space. Instead, the net positive charge at the hole spatial center is produced by the acceleration of the (predominant) passing electrons, reducing their

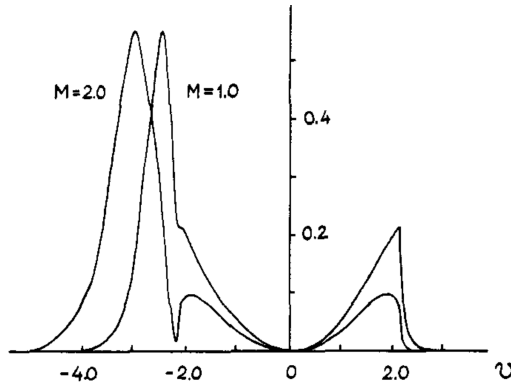


FIG. 10 The distribution function $f(v)$ of Turikov's fast, deep holes. From (Turikov, 1984) copyright IOP Publishing. Reproduced with permission. All rights reserved. Amplitude $\psi = 5$. M is his notation for normalized hole velocity v_h .

density as they move through the attracting potential; while the negative charge required in the hole wings is provided by the trapped peak in f . The lower value at its edge $\mathcal{E} = 0$, matching to the passing distribution, is permitted by the slope singularity. Turikov's simulations show that these equilibria are unstable for $|v_h| \gtrsim 2$ on a timescale $\sim 10/\omega_{pe}$, so they are then extremely transitory.

In 1986 Schamel (1986) presented a review recapitulating the electron hole experiments and his own theory of electron and ion holes. Dupree's negative hole mass is mentioned; and remarks made on the methods and difficulty of stability analysis of holes. Double layers are also substantially reviewed, together with experiments and simulations.

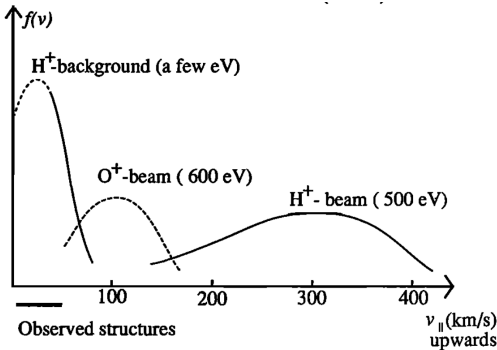


FIG. 11 The schematic model of the plasma environment in which slow ion holes (velocities indicated by the horizontal bar) were observed by Viking. From (Koskinen *et al.*, 1990).

The Viking satellite launched in 1986 clearly identified negative potential solitary structures (which were most likely ion holes) in the magnetosphere as reported by Boström, Gustafsson, Holback, Holmgren, Koskinen, and Kintner (1988). Probes 80m apart measured density or electric field, seeing up to $\sim 50\%$ density drops that prop-

agated along the magnetic field from one probe to the other, hence determining the velocity. Simultaneously, bipolar electric field excursions were observed, consistent with passing through the gradients of a solitary potential valley: the hole. More detailed interpretation, Koskinen, Lundin, and Holback (1990), of the plasma environment of the polar regions in which they were observed, which had a substantial energetic upward-propagating mostly proton beam, indicated that they were propagating at approximately the speed of the bulk ions (not the beam), as illustrated in Fig. (11).

The work of Ghizzo, Izrar, Bertrand, Fijalkow, Feix, and Shoucri (1988) addressed the stability of a periodic train of electron holes to hole merging. Their linearized analysis assumed an eigenstructure not unlike that of Schwarzmeier *et al.* (1979), and they also performed high-resolution Vlasov simulations, observing the initial "macroparticle" behavior of individual holes, but concluding that the eventual state after long enough time was virtually always a single large merged hole.

Collantes and Turikov (1988) analyze the linear stability of a single electron hole, first for wavelengths short compared with the hole extent, by using $f(v)$ at the hole center in a supposed uniform infinite plasma analysis. They find that there is no unstable mode with short enough wavelength to satisfy this approximation, unless the hole is of the unusual high velocity v_h type introduced by Turikov (1984). Then second, they use the methods of Lewis and Symon (1979), to identify a set of perturbation eigenfunctions of extent comparable to the hole. For a $\text{sech}^4(\alpha z)$ equilibrium they select a symmetric $\text{sech}^3(\alpha z)$ perturbation shape. For the Vlasov solution they use an expansion like Schamel (1982b), which is justified only for short transit time particles, but they carry it to higher order derivatives. They find instability with growth rate of order unity. Previous and subsequent simulations show no such instabilities in single isolated holes of typical length. This disagreement is not explained but is probably attributable to unsatisfactory approximations.

Raadu and Rasmussen (1988) and the review of Raadu (1989) represent the state then of double layer theory; and (in the latter) simulation, experiment, and applications in space and astrophysical plasmas. Double layer research saw continuous theoretical and observational development thereafter. But remarkably, the subsequent period saw very little new development of the theory of electron and ion holes, until a new impetus arose.

C. Ubiquitous holes in space, multidimensional simulation, stability, 1994-2008

Arguably the high-sample-rate (up to 12kHz (Matsumoto *et al.*, 1994b)) observations from the Geotail satellite published by Matsumoto, Kojima,

Miyatake, Omura, Okada, Nagano, and Tsutsui (1994a) opened a new era by identifying “Broadband Electrostatic Noise” (BEN), with the presence of solitary holes. Simulations by Omura *et al.* (1994, 1996) published alongside the observations suggested electron holes generated by electron streaming as being the most likely explanation. Demonstrating the solitary nature of BEN, which had been observed for decades in many missions using spectral instruments, notably in the “Plasma Sheet Boundary Layer” PSBL of the Earth’s magnetotail, indicated that holes occur elsewhere than in the polar regions. A wide ranging review in 2000 by Lakhina, Tsurutani, Kojima, and Matsumoto (2000) gives helpful explanations of the near-Earth plasma regions mentioned in this section, and discusses where broadband fluctuations, including electron holes, occur. It also surveys many theoretical ideas concerning the associated mechanisms.

Geotail instruments also identified holes in the Earth’s bow shock (Matsumoto *et al.*, 1997). Solitary holes in the data from the Galileo satellite in the magnetotail when crossing a magnetic flux rope, were observed by Mottez, Perraut, Roux, and Louarn (1997). The Polar satellite observed large amplitude electric fields in the PSBL at intermediate distances, reported by Cattell, Wygant, Dombeck, Mozer, Temerin, and Russell (1998), including electron holes analyzed by Franz, Kintner, and Pickett (1998). The auroral region plasma observations from the FAST satellite, Ergun *et al.* (1998a,b), showed holes

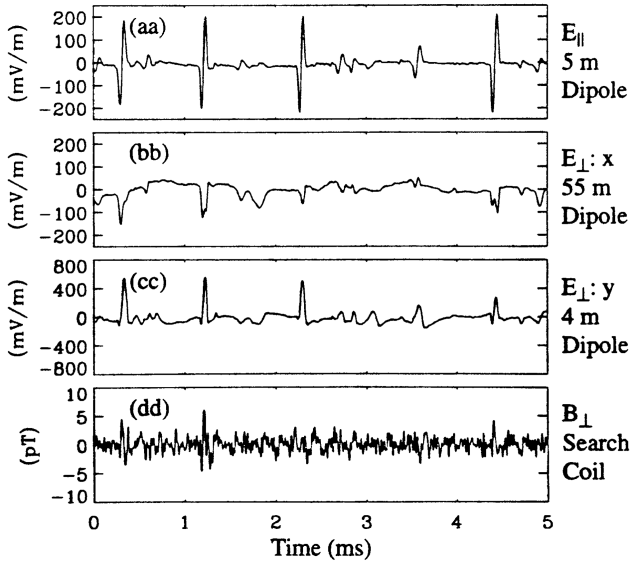


FIG. 12 Electric and magnetic field pulses observed from electron holes. Reprinted with permission from (Ergun *et al.*, 1998b) copyright (1998) by the American Physical Society.

whose finite transverse extent was indicated by unipolar transverse electric field E_{\perp} and magnetic field B_{\perp} pulses, at the same time as bipolar parallel electric E_{\parallel} pulses, as illustrated in Fig. 12. Further details are in Ergun *et al.*

(1999).

Pulsed electric fields indicating electron holes were seen in the (120kHz!) data of the WIND satellite at the Earth’s bow shock, by Bale, Kellogg, Larsen, Lin, Goetz, and Lepping (1998), and near the L1 Lagrange point (the free solar wind, albeit with unusual potential shapes,) as reported by Mangeney, Salem, Lacombe, Bougeret, Perche, Manning, Kellogg, Goetz, Monson, and Bosqued (1999). (However more recent bow shock observations(Kamaletdinov *et al.*, 2022; Wang *et al.*, 2020), to be discussed later, call into question the presumed positive polarity of the structures’ potentials, and implicate instead ion holes.) Thus, in just a few years it had become clear that with the right instruments — rapidly-sampled electric probes — electrostatic solitary structures could be seen on occasions almost everywhere one looks in space.

Meanwhile, Saeki and Genma (1998) ran 1-D PIC simulations that included the response of ions with $m_i = 100m_e$, $T_e = 40T_i$. They started with an artificially grown hole, stationary with respect to the particle distributions, having peak potential $\psi = 1.2$. With immobile ions thereafter the hole persists quiescent but with small symmetric oscillations for at least 160 (ω_{pe}^{-1}). However, turning on the ion response, the hole immediately elongates and by time 40 has split into two holes propagating in opposite directions, ending up approximately 100 (λ_{De}) apart at time 160. These separating holes are accompanied by an ion compressional pulse to which the electron response seems coupled. These are called coupled hole solitons (CHS), they are trailed by ion acoustic wave wakes. A theoretical equilibrium analysis of the resulting CHS determines a maximum hole amplitude ψ for given speed and hole phase-space area, with which the simulation observations appear to agree. Some large initial potentials split up into more than two CHS structures.

A surge of simulation was triggered by the satellite measurements. And the growing power of then-current high-performance computers enabled multidimensional simulations with respectable resolution to be run for long times extending deep into the non-linear stages of instabilities.

Miyake, Omura, Matsumoto, and Kojima (1998) investigated bump-on-tail instabilities, in a two-dimensional PIC simulation of limited extent, exploring notably the effect of background magnetic field strength which we express as the cyclotron frequency Ω (normalized to ω_{pe}) on electron holes. They found that at $\Omega = 0.2$ holes formed but quite quickly decayed away while at $\Omega = 1$, they were sustained much longer, to times approaching $900\omega_{pe}^{-1}$. At intermediate $\Omega = 0.4$ they showed the decay rate was sensitive to discrete particle simulation noise. Writing the bounce frequency of electrons in the holes ω_b (which depends on hole depth), these three strengths correspond to $\Omega/\omega_b = 1, 5$, and 2 respectively.

Oppenheim, Newman, and Goldman (1999) and (Goldman *et al.*, 1999) performed 2-D two-stream instability simulations with much larger domains, so the long time behavior of truly isolated holes could be discerned. With strong magnetic field $\Omega = 5$, well defined holes extended in the transverse direction were formed by time 448, but eventually (by time 1920) they were broken up by rather slow growing instabilities, accompanied by long parallel wavelength streaks of small transverse extent ($k_{\parallel} \ll k_{\perp}$) that were identified as lying on the “Whistler” branch of the cold plasma dispersion relation. Greater clarity was obtained by starting the simulation in a 1-D mode suppressing transverse potential variation; then after a time of “many thousands”, when 1-D holes had developed, switching to 2-D mode to observe the transverse instability grow from negligible amplitude, to break up the holes in the next few thousand (ω_{pe}^{-1}). Exploration of magnetic field strength showed little difference for $\Omega > 5$ but at $\Omega = 0$ holes do not form, and for $\Omega < 1$ they form but quite quickly break up by transverse instability, yet without generating whistler waves.

The relationship between hole amplitude (ψ) and hole parallel length was investigated by Muschietti, Roth, Ergun, and Carlson (1999). They derived the minimum possible hole length δ for a given ψ of holes with assumed Gaussian potential shapes. It is constrained by the non-negativity of the trapped phase-space density, as explained in (Hutchinson, 2017), leading to $\delta_{min} \sim \psi^{1/4}$. They compared FAST observations with the theoretical dependence and found good agreement within (substantial) uncertainty. These facts are evidence against an alternative theory that the phenomena might be ion acoustic solitons, because solitons have the opposite dependence of length on amplitude. They also reported the beginnings of two-dimensional simulation of pre-formed electron holes.

Muschietti, Roth, Carlson, and Ergun (2000) pursued further the 2-D simulation of the transverse instability using prepared analytic electron hole equilibria starting uniform in the transverse direction and observing the growth of their kinks. The magnetic field strength and perpendicular electron temperature were varied while keeping ψ and the hole length fixed. This fixes the bounce frequency for deeply trapped electrons, ω_b . They found that when $\Omega/\omega_b > 1$ kink damping, rather than growth, occurred. This stability criterion is in qualitative agreement with rigorous theory to be discussed later. Muschietti *et al.* speculated that the mechanism of the instability was “electron focusing” on the concave side of the kink. That idea was disproved much more recently when the true mechanism was discovered.

An observational statistical analysis of lasting importance was that of Polar satellite data by Franz, Kintner, Seyler, Pickett, and Scudder (2000). Over a range of magnetic field strengths $0.04 < \Omega < 4$, they found a systematic relationship involving the ratio of the peak

perpendicular and parallel electric fields E_{\perp}/E_{\parallel} for each hole. The statistical average over 1003 holes was found to be well approximated by the equation

$$\left\langle \frac{E_{\perp}^2}{E_{\parallel}^2} \right\rangle^{-1/2} = \left(1 + \frac{\omega_{pe}^2}{\Omega_e^2} \right)^{1/2}. \quad (25)$$

Simple mindedly, for a single potential structure of peak height ψ with perpendicular and parallel scale sizes L_{\perp} and L_{\parallel} the order of magnitude of the perpendicular and parallel electric fields are proportional to ψ/L . So the authors proposed that $E_{\parallel}/E_{\perp} \simeq L_{\perp}/L_{\parallel}$ and that this field ratio was therefore a measure of the aspect ratio, that is the oblateness in 3-D, of the holes. This experimental scaling is widely referred to in subsequent work. It amounts to the intuitively plausible requirement that the transverse dimensions of an electron hole cannot be smaller than roughly the electron gyro-radius. Franz *et al.* also offered a speculative theoretical basis for the scaling, drawing on gyrokinetic equations. We shall say more about the experimental measure and the theory later. Bale *et al.* (2002) observed electron holes in data from WIND, during bow shock crossings, displaying positive correlation of length with amplitude and satisfying the width/amplitude constraint $\delta > \delta_{min} \propto \psi^{1/4}$. Their electric fields were predominantly in the parallel direction, indicating substantially oblate holes, as expected from eq. (25) since Ω was small $\sim 1/80$.

Addressing the related questions of transverse instability and transverse hole extent, Miyake, Omura, and Matsumoto (2000) performed 2-D PIC simulations of initially symmetric two-Maxwellian-stream electron distributions, at $\Omega = 1$. A comparison was made between simulations with immobile ions and mobile ions of mass $m_i = 100m_e$ having ion temperature high enough to damp ion acoustic waves. Using immobile ions, the unstable electron waves quickly organize themselves by merging into a single hole extended across the entire transverse domain. With mobile ions, by contrast, the initial organization is into a few unaligned individual potential peaks of aspect ratio approximately unity, which then align themselves into a hole of greater transverse extent but with imperfections or gaps. Subsequently the mobile ion case shows signatures of perpendicularly propagating “Lower Hybrid” waves that cause a slow decay of the hole amplitude.

Fully 3-D PIC simulations were performed by Singh, Loo, and Wells (2001), having 36 electrons per Debye cube λ_{De}^3 : impressive for the day, but subject to significant particle discreteness noise. The plasma was initialized with Maxwellian electrons plus a beam of density 10%, velocity $v_b = 4$ (relative to electron Maxwellian), and temperature $T_b < T_e$. The magnetic field strength Ω was varied. A qualitatively rather similar picture emerged of electron holes forming, breaking up and re-forming in the first few hundred ω_{pe}^{-1} . For $\Omega > 2$, longer

lived holes were observed. The authors used a mass ratio $m_i/m_e = 1836$, and later in time, they observed broken-up holes of approximately spherical shape associated with shorter wavelength oblique waves they called “Lower Hybrid”, as well as longer parallel wavelength “whistlers” at high Ω . Further discussion of these simulations is in Singh (2003).

Schamel (2000) recapitulates electron and ion hole theory based on the pseudopotential approach, but includes treatment of periodic as well as solitary potentials. The treatment is unified mathematically; and the small amplitude limit and relation to Van Kampen modes is addressed.

Revisiting mathematical kinetic analysis of the transverse instability (without reference to the much earlier (Schamel, 1982b)), Vetoulis and Oppenheim (2001) attempted to address the coupling of an electron hole to a wave via bounce resonance. However, their expansion of the potential perturbation in a Fourier series of sinusoidal waves led them to approximate the hole influence as a perturbation on the wave, rather than supposing (more plausibly) that the wave was a small perturbation on the hole oscillation. They concluded that $\partial f/\partial \mathcal{E} > 0$ at bounce resonance was necessary for instability. Although this is the familiar criterion for sinusoidal wave growth in a uniform plasma, it turns out, as we shall see later, that it does not apply to holes.

Newman, Goldman, Spector, and Perez (2001b) simulated in two dimensions a waterbag electron hole at high $\Omega > \omega_p$. They imposed an initial uniform kink displacement in the parallel direction ξ , with transverse dependence $\propto \exp(ik_y y)$ as a model of the transverse instability’s eigenstructure. The hole experiences a vibration, illustrated in Fig. 13 showing the time evolution of the phase space surface at fixed y . In view of the $\exp i(k_y y - \omega t)$ dependence this figure could also be construed visually as the kink’s y -dependence with the t -axis corresponding to $(k_y/\omega)y$. An analytic treatment derives the predicted real part of the frequency of the oscillation, which agrees very well with the simulation. They proposed a coupling between the hole and the wave as the mechanism to explain the growth of oscillations and accompanying whistler waves that were observed in a larger domain able to accommodate them. This work, though highly simplified, identified several important features of the transverse instability.

A somewhat similar approach, accounting only for parallel electron motion, was taken by Berthomier, Muschietti, Bonnell, Roth, and Carlson (2002), in which the resonant energy transfer from a sinusoidal whistler wave to the trapped particles of an electron hole and the energy transfer by Landau damping to passing electrons both contribute terms proportional to $+df/d\mathcal{E}|_{\text{resonant}}$ to the growth rate. Again, this approach effectively ignores the motion of the hole, and makes coupling to whistler waves the primary mechanism. Instability with growth

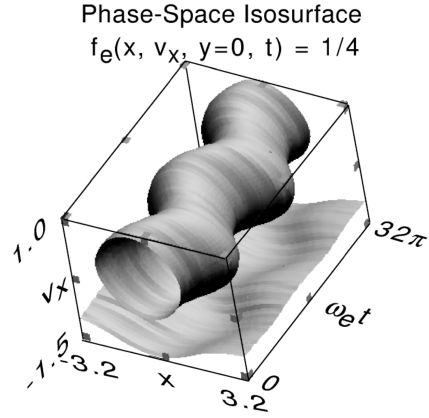


FIG. 13 Vibrating electron hole kink. The bounding surfaces of the non-zero- $f(v)$ waterbag are shown. Reprinted with permission from (Newman *et al.*, 2001b) copyright (2001) by the American Physical society.

rate of order a percent of the wave frequency, was found over most of the domain $0 \leq k_\perp \lesssim 1$ and $0.1 \lesssim \omega \lesssim 1$. This mechanism is further explored for three-dimensional holes by Berthomier *et al.* (2008).

Jovanović and Schamel (2002) is a more comprehensive assault on the linearized transverse instability in a magnetized hole, solving Vlasov’s equation by integration over prior time accounting for the full helical motion of the electrons in the unperturbed potential. Expansion in perpendicular cyclotron harmonics naturally arises. Different approximations of sometimes questionable applicability are adopted for handling different resonances and non-resonant and passing particles analytically. It concludes that bounce resonance “yields the destabilization of the hole”. At low frequency ($\omega \simeq \omega_b$), large growth rates and hole breakup might occur, while at high frequency when $\Omega \pm \omega \sim \omega_b$ “the instability manifests in the emission of linear waves”. No purely growing instabilities ($\Re(\omega) = 0$) are found. These predictions are now known not to be in agreement with simulation.

Roth, Muschietti, Carlson, Mozer, and Ergun (2002) presents FAST satellite data that shows electron holes of limited transverse extent, but strongly elongated in the parallel direction. This shape is indicated by separated positive and negative parallel electric field spikes, between which there is unipolar substantial perpendicular electric field. See Fig. 14(a). A model of these elongated holes [Fig. 14(b)], shows that they require non-monotonic trapped velocity distributions. And the authors analyze the interaction of multiple such holes, solving single particle orbits in prescribed fields. They also present a multidimensional PIC treatment of interacting holes, in which the smaller hole is absorbed (“cannibalized”) by the larger.

Axisymmetric three-dimensional electron hole equilibria, but without parallel elongation, were analyzed by Chen and Parks (2002), and revisited by Chen,

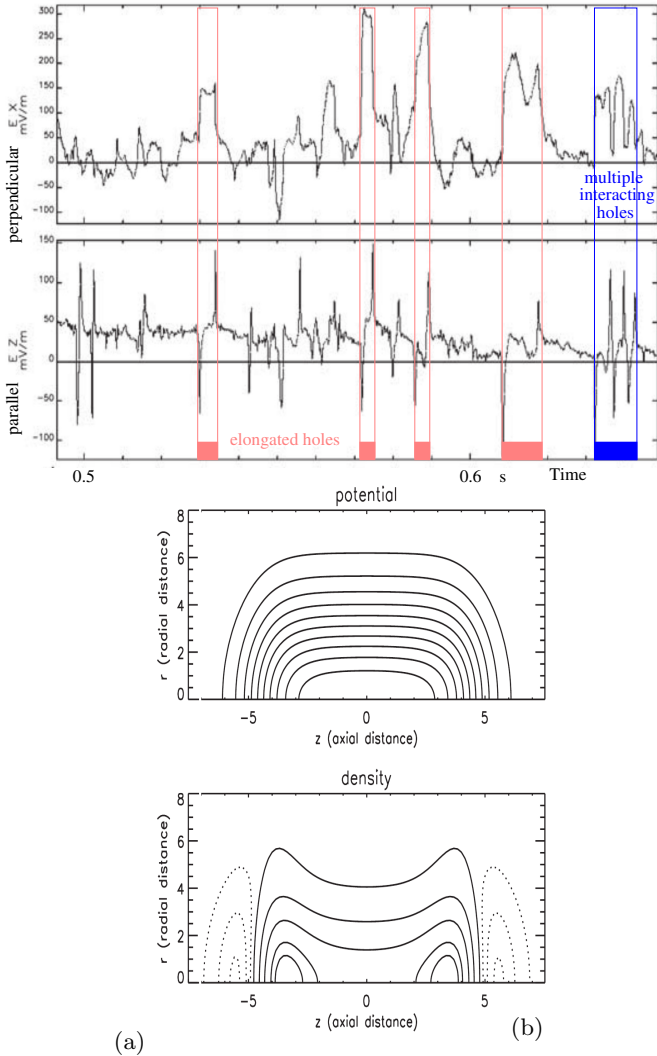


FIG. 14 (a) Perpendicular and parallel electric field as a function of time, observed by the FAST satellite (time relative to 1996/12/29 19:36:24), indicating holes of modest transverse extent but substantially elongated in the parallel direction (pink boxes). In the blue box, multiple such holes seem to be interacting. (b) Model contours of an elongated hole potential and electron density. After (Roth *et al.*, 2002).

Thouless, and Tang (2004). They used the integral equation method and derived analytic forms for the required trapped distribution with assumed potential shapes Gaussian in the parallel and perpendicular directions. They derived lower limits on the parallel and perpendicular extent as a function of hole amplitude and ion to electron temperature ratio. The limits arise from the requirement that the distribution must be non-negative. Chen, Pickett, Kintner, Franz, and Gurnett (2005) develop the treatment more fully, and show favorable comparison with Polar spacecraft observations. Franz, Kintner, Pickett, and Chen (2005) present those observations in more detail and argue that only electron holes (not electron-acoustic solitons) are consistent with them.

In Krasovsky, Matsumoto, and Omura (2004a), theoretically analyzing multidimensional electron holes, it is argued that, whatever the spatial form, substantial velocity anisotropy of the particle distribution is essential for holes to exist. This argument was given more rigorous form by Ng and Bhattacharjee (2005) who qualify it by showing that if the background distribution has dependence on angular momentum (conserved in a spherically symmetric hole) then in principle spherically symmetric solutions exist. The background distributions at infinity are however pathological (see (Hutchinson, 2017) endnote 68), so the practical conclusion remains the same.

Friedland, Peinetti, Bertsche, Fajans, and Wurtele (2004) report an unusual type of electron hole in a pure electron plasma trap. The holes are directly excited by applying a resonant wave perturbation whose frequency is chirped on a time-scale slow compared with the electron bounce/transit time. The velocity resonance then moves from the outer wing of the background electron distribution into its bulk. As it does so, it drags a “bucket” of weakly populated trapped particle orbits into a much more strongly populated region, forming an electron hole. Theory, simulation, and laboratory measurements are reported to be consistent.

Meanwhile simulations were growing in size, speed, and sophistication, and illustrating a great variety of complex behavior. Goldman, Newman, and Ergun (2003) performed a one dimensional simulation with equal temperature ions and electrons ($m_i/m_e = 400$) in a long $640\lambda_{De}$ box with open (rather than periodic) boundaries, starting with electron drift (relative to ions) of $v_d = v_{te}$, but initializing with a local charge-neutral density depression. A double layer rapidly forms; and accelerates a beam of electrons into the background, giving rise to two-stream instability, electron hole formation, and merging. In the opposite direction, on a longer timescale, an ion beam gives rise to trains of ion and electron holes. Similar trains of ion holes had been observed by Børve, Pécseli, and Trulsen (2001) in 2.5 dimensional hybrid PIC simulations of ion beam-plasma interactions with Boltzmann electrons. The ion holes were not fully solitary structures in either study, but were clearly ion phase-space vortices with central phase-space depletion.

Drake, Swisdak, Cattell, Shay, Rogers, and Zeiler (2003) performed three-dimensional PIC simulations ($m_i/m_e = 100$) of magnetic reconnection with a guide field ($\Omega = 2.5\omega_{pe}$). They observed large current densities, well beyond the Buneman stability limit, parallel electron beams, and consequent electron holes along the x-line and magnetic separatrix. The holes and their electron scattering were implicated in anomalously high effective resistivity.

Eliasson and Shukla (2004a) simulate electrons and ions of large mass ratio ($m_i/m_e = 29500$) using a (one-dimensional) Fourier Vlasov code. They start with a Schamel type pure electron hole (uniform ion density)

at zero velocity with respect to ions, and observe that after dwelling stationary for a time $\sim 120\omega_{pe}^{-1}$, the electron hole suddenly moves away with a velocity $\sim 0.55v_{te}$, leaving behind a stationary negative potential peak associated with the ions that have been repelled during the dwell period. This is the clearest early demonstration of “self-acceleration” of a stationary electron hole by repulsion from an ion density depression. They also observe merging of two holes of the same type when they collide. Eliasson and Shukla (2004b) consider ion holes with and without trapped Langmuir waves providing extra ponderomotive force on the ions, and simulate collisions of counter-propagating ion holes.

A different way to generate electron holes was simulated by Califano and Lontano (2005), who applied a large amplitude forcing field to one end of their one-dimensional Vlasov-Maxwell (not just electrostatic) code. The Langmuir wave packet generated was chosen to have frequency $\omega_0 = 1.1$ and by “wave breaking” was observed to induce electron holes that traveled much faster than the group velocity of the packet.

A more extensive two-dimensional electromagnetic PIC study of warm two stream electron distributions was undertaken by Umeda, Omura, Miyake, Matsumoto, and Ashour-Abdalla (2006), but with immobile ions. They specified the initial thermal velocity spread of the beams, v_t , normalized to the beams’ drift velocity $\pm v_d$, varying the ratio $v_t/v_d = 0.25 - 0.5$, and the magnetic field strength $\Omega = 0.5 - 10(\omega_{pe})$. In the nonlinear state, the passing electron temperature T_e , hole potential ψ , and bounce frequency ω_b were estimated from the simulation. The crucial new finding, illustrated in Fig. 15, was that when $v_t/v_d = 0.5$, giving hole potentials $\psi/T_e \lesssim 1$, the final state was a long-lasting (up to $t=10000$) one-dimensional hole (uniform in the transverse direction) when $\Omega \gtrsim 1$, while for $\Omega = 0.5$ the hole was broken up transversely with only slowly decaying ψ (reaching zero at time 5000), in approximate agreement with the magnetic field strength criterion $\Omega \gtrsim \omega_b$ for transverse stability. By contrast, for $v_t/v_d = 0.35$ (colder streams) the holes are higher in amplitude (ψ/T_e up to 4), and give rise to whistler waves that break up the holes transversely by $t=1000$ even for $\Omega = 2$, as had been observed for example by Oppenheim *et al.* (1999) with similar beam parameters. They conclude that the whistler breakup effects do not occur when “the potential energy of the holes is smaller than the electron thermal energy”. Later simulations with much longer domains and including ion dynamics by Umeda (2008), indicate somewhat enhanced susceptibility to low frequency wave excitation which causes the holes to decay faster: on a timescale of a few thousand. Lu, Lembege, Tao, and Wang (2008) revisit two-dimensional two-stream instability including ions $m_i/m_e = 1836$ traveling at the velocity of one of the electron streams, but only with $v_t/v_d = 0.25, 0.22$: the high potential energy case. They observe the whistler

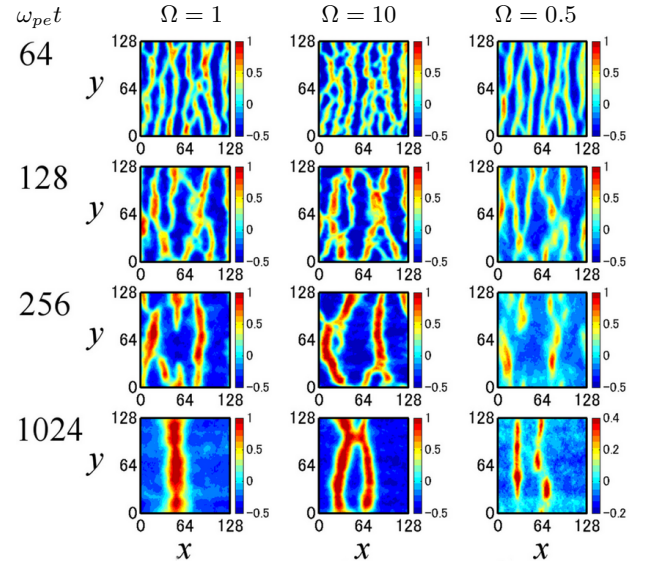


FIG. 15 Hole evolution in warm two-stream instability PIC 2-D simulations for three magnetic field strengths $\Omega = 1, 10, 0.5$ at four times $t = 64, 128, 256, 1024$, for the low-potential-energy case $v_t/v_d = 0.5$. Whistler waves are not significantly excited. The parallel direction is x . From (Umeda *et al.*, 2006).

waves, and with immobile ions ($m_i/m_e = \infty$) the wave amplitude is much greater. Artificially low $m_i/m_e = 100$ permits lower hybrid waves to be excited quite early in the simulations.

Newman *et al.* (2007) performed one- and two-dimensional continuum Vlasov simulations of a double layer, showing how the resulting two-stream electron distribution on the higher-potential side gives rise to electron holes propagating away from the layer and merging as they go. The two-dimensional hole shapes are visually similar to those in Figure 15, and the effects of different degrees of magnetization were also explored. The double-layer acceleration results in continuous production of holes in this open-boundary simulation.

In analytic theory, Goldman, Newman, and Mangeney (2007) performed analysis aimed at trying to deduce information about the passing particle velocity distribution shape based on the observed spatial length of the hole’s potential, for small amplitude sech^4 holes.

In further observational analysis, Pickett *et al.* (2004) made a search, at Earth-distance $4.5-6.5R_E$, for solitary structures observed by more than one of the satellites of the Cluster mission. Unfortunately no persuasive correlated examples were discovered. This is perhaps not entirely surprising since distances of at least 80km separated the individual craft, but it places an upper bound on the lengths over which the electron (or ion) holes preserve their shape. Later, pursuing correlated holes, Pickett *et al.* (2008) reported a single example of a solitary structure seeming to appear at two satellites. The satel-

lites were at Earth-distance $11.8R_e$ and spaced by 30km parallel and 40km perpendicular to the magnetic field. The observations' time difference was 22ms; so if they really were of the same hole, one deduces parallel speed of 1300km/s, and a very flat oblate shape.

The electron hole Cluster data analyzed statistically by Cattell *et al.* (2005) indicated correlation between the presence of holes and relatively narrow electron beams. The beams were predicted by reconnection simulations: an important indication that electron holes are part of the complicated processes involved in reconnection. It was found in Cluster data by Pickett *et al.* (2005) that solitary waves occur throughout the Earth's magnetosheath from Bow Shock to Magnetopause. They infer that holes are being generated throughout that region, perhaps as a result of two-stream instability.

D. Lab and Space holes, renewed theory, 2008-

The first new laboratory observations of electron holes since 1979 arose in reconnection experiments and were reported by Fox, Porkolab, Egedal, Katz, and Le (2008) and Fox *et al.* (2012). The holes were detected by small (60 μ m dia) electric probes sampled at up to 5GHz. Two probes spaced 4.6mm apart along the magnetic field observed a delay of order 1.2ns in the arrival time, which enabled the hole parallel speed and direction (in the positive electron acceleration direction) to be deduced. The holes were determined to be roughly spherical and showed negligible arrival time delay when the probes were spaced instead in the perpendicular direction. Unusual features included long hole lengths of $\sim 60\lambda_{De}$ and fast speeds up to $2v_{te}$. Possible local enhancement of electron temperature might decrease these normalized estimates, but in any case they are not theoretically impossible in substantially distorted electron distributions.

In 2010, laboratory electron holes (as well as wave packets and irregular fluctuations) were observed by Lefebvre, Chen, Gekelman, Kintner, Pickett, Pribyl, Vincena, Chiang, and Judy (2010). They were generated by an electron beam injected into LAPD, a large magnetized basic plasma device, and were detected with small arrays of electric probes of diameter 10 μ m, sampled at speeds well above the local plasma frequency (0.3-0.7GHz). The observed coherent propagation from one probe to another provided speed and size measurements. The mechanism of hole formation was rather uncertain, because they were observed in an electron velocity distribution having beam particles of energy ~ 60 eV, greatly broadened by earlier instabilities. The cold background plasma with $T_e \sim 0.2$ eV made up the remaining $\sim 75\%$ of the density. Hole amplitudes of $\sim 0.1 - 0.25$ V were observed, extending upward to 0.75V at high magnetic field $\Omega/\omega_{pe} \simeq 4$.

Andersson, Ergun, Tao, Roux, Lecontel, Angelopoulos, Bonnell, McFadden, Larson, Eriksson, Johansson, Cully,

Newman, Goldman, Glassmeier, and Baumjohann (2009) observed a new phenomenon, parallel magnetic field enhancement inside electron holes, during a "bursty bulk flow" event measured by a THEMIS satellite at $\sim 10R_E$. Prior perpendicular magnetic perturbations (e.g. (Ergun *et al.*, 1998a,b, 1999)) had been attributed to Lorentz transformation of perpendicular electric fields in moving holes. But parallel B -fields cannot arise by that mechanism. Instead B_{\parallel} perturbations, always enhancements, can arise from electron $\mathbf{E} \wedge \mathbf{B}$ drift current in holes of limited transverse extent. The hole velocities ($\sim 10^8$ m/s c.f. $v_{te} \sim 0.4 \times 10^8$ m/s) were deduced from the relative magnitudes of perpendicular \mathbf{B} and \mathbf{E} taking B_{\perp} to arise by Lorentz transformation. The resulting hole lengths were typically $L_{\parallel} \simeq 20 - 30\lambda_{De}$, somewhat greater than the deduced L_{\perp} . In these hot plasmas, $T_e \sim 8$ keV, potentials were $\sim 0.5T_e$. The authors note that long, fast ($v_h > v_{te}$) holes like these were characteristic of the laboratory reconnection observations of Fox *et al.* (2008).

Tao *et al.* (2011) followed up with detailed theory of electromagnetic electron holes. They addressed the key question of whether it is justifiable to include the electron $\mathbf{E} \wedge \mathbf{B}$ drift, but ignore the corresponding ion drift, which in a steady uniform plasma is exactly the same and would cancel the current. Using two dimensional test particle orbit calculations they determine the ratio of the actual current density to the presumed $\mathbf{E} \wedge \mathbf{B}$ drift current as a function of the ratio of transit time to cyclotron period $\delta t\Omega/2\pi$. The (plotted) current ratio is approximately unity above $\delta t\Omega/2\pi \simeq 0.4$, but declines steeply below, becoming < 0.15 at $\delta t\Omega/2\pi < 0.15$. Electrons in the THEMIS observations have $\delta t\Omega/2\pi \simeq 1$, validating their current; ions have cyclotron frequencies ~ 1000 times smaller, making their current negligible. The authors also derive a more accurate estimate of the hole velocity v_h by including the drift current effects, and use it to analyze in more detail the same data as Andersson *et al.* (2009). They find $\sim 20\%$ lower length and speed estimates; and invoke the two-dimensional electromagnetic simulations of Du *et al.* (2011) in support of their model.

Massive two-dimensional PIC simulations of reconnection at physical mass ratio, in boxes large enough to avoid strong boundary condition influence, were performed by Lapenta *et al.* (2010, 2011). It was found that "bipolar structures" in the parallel electric field (electron holes, see Fig. 16) were generated for all values of the guide field, and not just when the guide field is strong as was the case in (Drake *et al.*, 2003). This new result accorded better with the Cluster observations (Cattell *et al.*, 2005). A notable reconnection event encountered by Cluster and analyzed by Viberg, Khotyaintsev, Vaivads, André, and Pickett (2013) identified electrostatic solitary structures "localized to the separatrix regions", broadly consistent with the simulations. Goldman, Newman, Lapenta, Andersson, Gosling, Eriksson, Markidis, Eastwood, and Er-

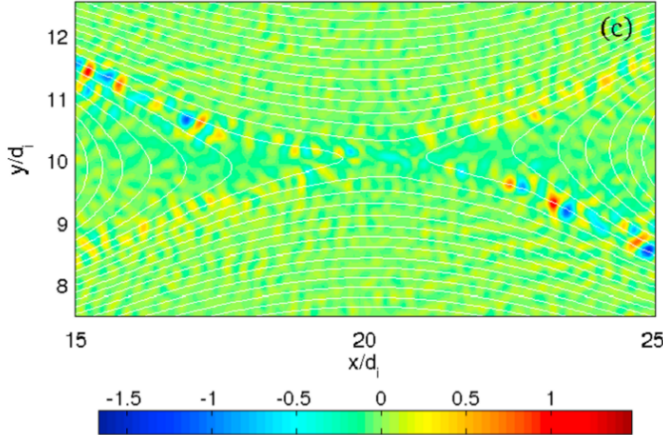


FIG. 16 Parallel electric field contours in a reconnecting magnetic field. Electrons are strongly accelerated inward along the top left and bottom right separatrix, giving rise to electron holes that appear as blue and red bipolar E_{\parallel} regions. After (Lapenta *et al.*, 2011).

gun (2014) followed up with simulation and analysis that shows the electron holes emitting quasi-parallel ($k_{\perp} \ll k_{\parallel}$) whistlers by a Cerenkov process. The whistlers grow till they cause the holes to decay, and can then persist further than the holes.

Lesur, Diamond, and Kosuga (2014) perform one-dimensional Vlasov and PIC simulations of high resolution showing persuasively that the supposed sub-critical ion acoustic instability growth obtained by Berman *et al.* (1982), which Dupree (1982) developed his ion hole growth mechanism to explain, does not really happen. Lesur was able to reproduce Berman's result by using the small number of PIC particles he used; but using much greater numbers, and hence reduced noise, or using the continuum Vlasov code, the effect was suppressed. Dupree's hole growth phenomenon remains a possible real effect, but it does not produce subcritical Buneman instability and hole appearance.

Malaspina, Newman, Willson, Goetz, Kellogg, and Kerstin (2013) made a statistical study of electron holes in the free solar wind, and discovered that 47% of them occur within 6000km of a current sheet, whereas only 17% randomly chosen times are within the same range. Holes that were even closer tended to have higher amplitudes. They conclude that mechanisms producing electron holes are active near current sheets (where reconnection is likely occurring) in the solar wind. And Malaspina, Andersson, Ergun, Wygant, Bonnell, Kletzing, Reeves, Skoug, and Larsen (2014); Malaspina, Wygant, Ergun, Reeves, Skoug, and Larsen (2015) observed in data from the Van Allen Probes double-layers generating electron holes all associated with "dipolarizations" of the magnetic field and other plasma boundaries within the magnetosphere.

Vasko, Agapitov, Mozer, Artemyev, and Jovanovic

(2015) report magnetic perturbations associated with electron holes measured by the Van Allen Probes in the outer radiation belt. The key novelty is that, unlike the prior observations (Andersson *et al.*, 2009) and theory (Tao *et al.*, 2011) of $\mathbf{E} \wedge \mathbf{B}$ electron current, the parallel field B_{\parallel} is *depressed* rather than being enhanced within the holes. They propose that this sign reversal might be explained by diamagnetic current, associated with a trapped electron population that is extremely hot (e.g. $T_{\perp} \simeq 0.3$ or 6keV), anisotropic ($T_{\perp}/T_{\parallel} > 2$), and dense ($n_t \sim 65\%$ of unperturbed), even though the cold background is only a few eV. If this interpretation is correct, these would be extremely exotic electron hole parameters. Mozer, Agapitov, Artemyev, Drake, Krasnorskikh, Lejosne, and Vasko (2015) reported a month later on "Time Domain Structures" (TDS) observed by Van Allen Probes in the outer radiation belt. These are also of various intense and exotic types, arising shortly after plasma injections into the belt. They appear to be responsible for production of anisotropic velocity distributions strongly enhanced at small pitch angles (i.e. *parallel* to B).

A previously under-appreciated environment in which electron holes are to be expected is in the wake of unmagnetized bodies such as the Moon, as plasma such as the solar wind, flows past. Solitary electrostatic structures were observed by satellite Galileo in the wake of Jupiter's moon Europa, Kurth *et al.* (2001); and near to the (Earth's) Moon, Hashimoto *et al.* (2010). Pickett, Kurth, Gurnett, Huff, Faden, Averkamp, Pisa, and Jones (2015) surveyed ESW observations by Cassini in the vicinity of Saturn, and noted holes clustered in the wake of its moon Enceladus, although impacts from its dust plume somewhat polluted the measurements. Moreover the Moon wake had long been modelled analytically ((Gurevich *et al.*, 1969; Gurevich and Pitaevsky, 1975)), and by simulations ((Birch and Chapman, 2001; Farrell *et al.*, 1998)) at low mass ratio ($m_i/m_e = 20$, inadequate to separate the species) that hinted at hole formation. In 2015 however, physical mass ratio simulations by Haakonsen, Hutchinson, and Zhou (2015), and analysis by Hutchinson, Haakonsen, and Zhou (2015) showed theoretically how electron holes are spawned and grow in the wake. The underlying instability mechanism is the inflow along transverse magnetic field lines of electrons and ions into the density-depleted, negatively charged, wake. In combination with the steady downstream convection of the fieldlines and particles, a dimple (or "notch") arises in the electron velocity distribution within the wake, found from the solution to the Vlasov equation (Hutchinson, 2012). The dimple is Penrose unstable and nonlinearly forms small holes. Those holes grow as they are convected downstream into the rising wake density by a mechanism analogous to that of Dupree (Dupree, 1983). The simulations observe this hole amplitude growth, especially for holes that are prevented by ion interactions

from being repelled out of the wake. The grown holes disrupt the ions even before the ion distribution itself becomes unstable.

In view of the substantial accumulated data of the ARTEMIS mission's two satellites orbiting the (Earth's) Moon out to about 10 Moon radii, Hutchinson and Malaspina (2018) undertook to compare the theoretical predictions of wake electron hole production with observations inside the Moon wake when it is in the solar wind. Analytic solution of the Vlasov equation characterizes the counter-streaming electron (and ion) distributions filling in the wake along the magnetic field. They are linearly unstable. PIC simulations were also performed that model the rising density of the wake, as illustrated in figure 17(a). The lower frame shows color

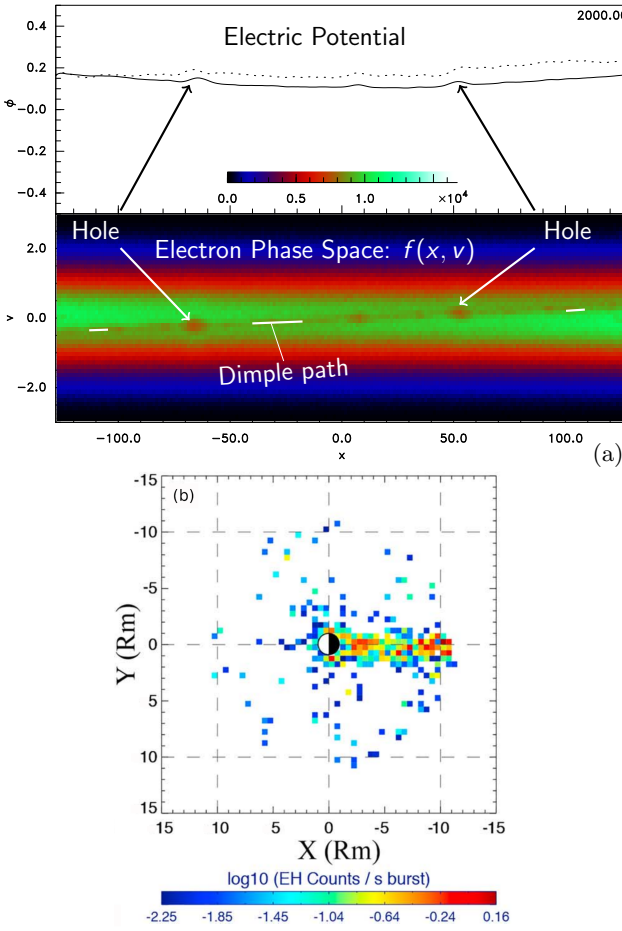


FIG. 17 (a) Simulation of electron holes induced in a wake. (b) Observations of hole occurrence near the moon. The wake streams away from the sun toward negative X. From Hutchinson and Malaspina (2018).

contours in phase space of a fully developed nonlinear state in which the dimple appears as a depressed phase-space density $f_e(x, v)$ diagonal line in which are embedded electron holes nonlinearly emerging from its instability. Those holes are observed to propagate out of the

(open boundary) simulation along the track of the dimple, which is also the phase space orbit of electrons. The potential across the modelled wake is depressed in the center, which is responsible for the hole acceleration.

It proved not to be possible to determine in the satellite data the hole velocities, because of sampling speed limitations, but hole existence was reliably determined. The statistical data is shown as a two-dimensional histogram projected onto the ecliptic plane in figure 17(b). The Moon wake streams away from the sun toward negative X, and in it are by far the majority of the observed electron holes. The 161 single holes observed outside the wake in the $10 R_m$ disk traversed are typical of elsewhere in the solar wind where they are often associated with current sheets. These are only $\sim 4\%$ of the total observed, the rest are clustered along the wake. The detailed profile of the hole observations within the wake shows that the hole density is somewhat hollow, peaking off the wake axis. It is concluded that holes are formed within the wake, and propagate outward, confirming the theoretical predictions. But must also break up on a length scale less than the wake width, since few holes are observed to propagate outside the wake.

Since the Moon's orbit around the earth takes it from the solar wind across the bow shock and into the magnetosphere, the ARTEMIS data also documents how electron hole occurrence varies correspondingly. Malaspina

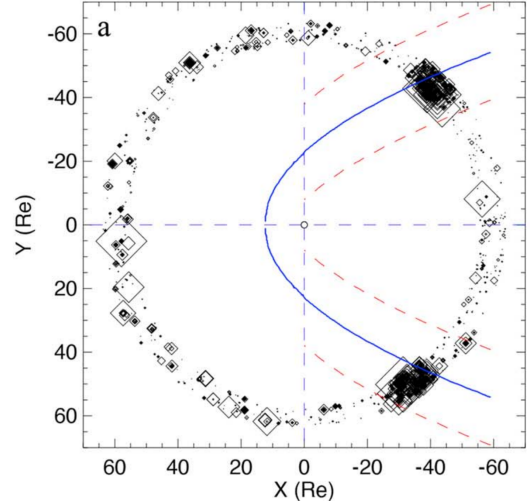


FIG. 18 Occurrence of electron holes near the moon as it moves from the solar wind across the Earth's bow shock (blue parabola) into the magnetosphere. Symbol area denotes potential amplitude. From Malaspina and Hutchinson (2019)

and Hutchinson (2019) report the Artemis data of figure 18, showing all the holes detected. As we already know from figure 17 almost all of them are in the Moon's wake when it lies in the solar wind, to the left of approximately the blue parabolic curve. However, the statistics show that only a very small fraction of those that occur when the Moon is in the Magnetosphere, to the right of

the curve, are observed to lie in the wake. Instead they are essentially isotropically distributed around the Moon. Since there is little systematic steady plasma flow there and no appreciable wake, a different mechanism is their cause. Also note the intense electron hole occurrence in the vicinity of the bow shock and magnetopause (between the two red dashed lines). It is concluded that at least four different processes cause the holes observed in the data. When the moon is in the solar wind the holes are caused by (i) its wake, and (ii) current sheets in the solar wind. The magnetospheric mechanisms can be grouped as (iii) magnetotail processes and (iv) processes at the interface of magnetosphere and solar wind.

Norgren, André, Vaivads, and Khotyaintsev (2015b) were successful in finding multi-spacecraft detection of electron holes in Cluster data obtained seven years earlier. The holes were observed in the PSBL where the Debye length was $\lambda_{De} \sim 2\text{km}$; and the hole parallel lengths were typically $2 - 4\lambda_{De}$. The two spacecraft were separated by $\sim 30\text{km}$ parallel and $\sim 20\text{km}$ perpendicular to the magnetic field. Time delays of 50-70ms for the holes to pass between them were observed; and identification of the corresponding holes was made persuasive by the preserved shapes of trains of multiple holes of different amplitudes. The hole amplitudes were $\sim 0.1T_e$ and speeds in the ion frame were approximately 2% of the electron thermal speed. That would place their velocity within the ion distribution spread if $T_i \simeq T_e$. These are then *slow* electron holes. Their generation mechanism could not be definitively identified. However, Norgren, André, Graham, Khotyaintsev, and Vaivads (2015a) analyze different electric field data from Cluster together with measured velocity distributions to explore the sorts of instabilities that might give rise to the observed electron holes. They use two Maxwellian electron components and one ion component. Although their fits to the observed $f_e(v)$ do not result in instability, they show that a narrowing of electron beam spread can give instability, and suggest that effect might represent the distribution prior to the effects of instability spreading the beam. Graham, Khotyaintsev, Vaivads, and André (2016) present more systematic statistical analysis of hole parameters as a function of background plasma parameters, for the magnetopause data from Cluster. In summary, they find a wide range of hole speeds (relative to ions) from $\sim v_{ti}$ up to $\sim v_{te}$. There is strong linear correlation of hole length with λ_{De} : the peak to peak (E_{\parallel}) length is $\simeq 9\lambda_{De}$. Maximum potentials are small $\sim 0.01T_e$, and easily satisfy the existence requirement (Chen *et al.* (2004)) of non-negative trapped distribution. An extensive review of the Cluster mission observations of solitary electrostatic structures has been published by Pickett (2021).

Throughout this prior history of electron hole research a remarkable missing element was direct experimental measurement of the trapped phase-space deficit responsible for sustaining the potential. The reasons are that

laboratory experiments have not had velocity distribution measurements (at all) and the impressive satellite measurements of the velocity distributions have not had sufficient time (and hence space) resolution to distinguish spatially between inside and outside the hole. The MMS particle distribution instruments give fast single energy, angularly resolved, measurements every 0.195ms, which is shorter than the hole transit time. The energy is scanned sequentially in time to produce the entire distribution. Mozer, Agapitov, Giles, and Vasko (2018) used MMS data from four satellites transiting 20 similar holes to reconstruct a statistically “superposed epoch” approximation to the distribution function with sufficient resolution, for the first time. The result is shown in figure 19

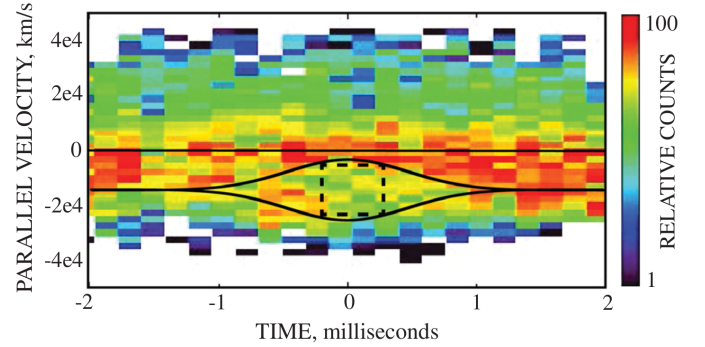


FIG. 19 Reconstructed “superposed epoch” phase space contour plot of the velocity distribution in an electron hole set observed in the magnetosphere. Reprinted with permission from Mozer *et al.* (2018) copyright the American Physical Society (2018).

in which the horizontal (time) axis corresponds to parallel position (z). It is therefore equivalent to a phase-space contour plot of $f(x, v)$. The trapping region lies within the square box, in which there is a detectable decrease of phase-space density relative to the surrounding region. Although the statistical significance is somewhat disappointing, this result required a tour de force of analysis.

The MMS Electron Drift Instrument (EDI) data for a different train of holes was analyzed by Norgren *et al.* (2022). It measures the difference in electron flux between two relatively narrow collimated directions at comparable positive and negative velocities, obtaining 1000 samples per second: (just) sufficient to resolve the satellite’s passage through the holes. This measurement’s value is that it can be used to analyze single holes and demonstrate the flux decrease expected from the reduced trapped phase-space density. The correlation between hole presence and flux decrease is very good; although the (one dimensional) model predictions of the flux decrease are roughly a factor of two less than those observed, perhaps because of multi-dimensional effects. Nevertheless this data contributes importantly to confirming trapped electron deficit experimentally.

V. TIME DEPENDENCE AND HOLE KINEMATICS

We now move to a discussion, organized topically, of progress since approximately 2016. The perspective adopted is primarily a theoretical one, aimed at reporting and clarifying the understanding of different physical mechanisms responsible for electron and ion hole behavior. There have been many important contributions too from satellite observation and these will be brought out within the relevant topics. The present section concentrates on ways in which holes respond to the background plasma, limiting the discussion to essentially one-dimensional effects.

A. Landau Damping and Resonant Interactions

For a steady self-consistent electron hole equilibrium, obviously collisions eventually become important and cause it to decay on the collision timescale. Simulations usually have some equivalent degree of dissipation arising from particle discreteness or higher order effective viscosity for example. Our treatment continues to neglect collisions and ignore the dissipation timescale.

However, the question sometimes arises whether soliton or hole equilibria experience Landau damping when there is a slope on one of the background distribution functions at the velocity of the potential structure. After all, Landau damping is an important collisionless dissipation mechanism. The one-dimensional answer is that in most situations electron hole equilibria do *not* experience Landau damping; but something else can happen.

One way to understand this answer qualitatively is to realize that a BGK soliton or hole is like (and sometimes actually is Carril *et al.* (2023)) the final nonlinear stage of a coherent kinetic wave, in which Landau damping (or growth) has stopped in a perfectly collisionless plasma because of non-linear particle trapping (see e.g. Swanson (1989) chapter 8, and early theory such as O’Neil (1965)).

Long ago, it was shown that nonlinear steady undamped periodic or solitary waves can be constructed arbitrarily close to uniform equilibria, by choice of the trapped distribution. Buchanan and Dorning (1993); Holloway and Dorning (1991); Korn and Schamel (1996). Later observations by Montgomery *et al.* (2001) of a signature of electron acoustic wave contributions to stimulated Raman scattering, which was unexpected on the basis of strong linearized Landau damping, motivated the further question as to how undamped periodic waves can grow, driven (by modulated ponderomotive forces) out of an initially uniform plasma background. Krapchev and Ram (1980) had addressed the “adiabatic” evolution under the conservation of phase-space action, finding a dispersion relation of what is sometimes called the “thumb” shape, which corresponds to the hypothetical “undamped wave” of Stix (1962). The dispersion curve has, in ad-

dition to the Langmuir wave, a lower frequency branch that today would be called an electron acoustic wave.

Simulations driven by an applied sinusoidal field, to model the SRS situation of Montgomery *et al.*, found non-linear waves that persisted approximately undamped well after the driver was turned off. They were dubbed Kinetic Electrostatic Electron Nonlinear or KEEN waves, and are comprehensively reported by Johnston *et al.* (2009), and recapitulated more recently in Bertrand *et al.* (2019) chapter 5.7-8.

Waves of the KEEN type have been shown sometimes to experience what is called the Negative Mass Instability (NMI) (Dodin *et al.*, 2013; Hara *et al.*, 2015). It is a type of Trapped Particle Instability (Kruer *et al.*, 1969) arising from the positive derivative of the trapped velocity distribution with energy (action), and consists of bunching of trapped electrons locally on their phase space orbits within the trapped vortex. Brunner and Valeo (2004) proposed that NMI is responsible for the burstiness of SRS. (Dodin and Fisch, 2014) suggest that the NMI plays a vital role in the *formation* of persistent waves. But countless simulations show fully formed steady electron holes with no NMI.

Valentini *et al.* (2012), surveyed the applicability of Landau damping and discussed the suppression of Landau damping to give undamped waves. But a related published comment Schamel (2013) disputed how to understand the important phenomena. Controversy and misunderstanding still persist.

A different perspective is to recognize that Landau damping arises inherently from the initial conditions, which is why Landau used a Laplace transform (not a Fourier transform) in his original derivation (Landau, 1946). Those initial conditions are that there is an initial wave potential in which the initial particle distribution is perhaps linearly but not non-linearly consistent with it. The (initial) Landau damping occurs in the process of acquiring the required non-linear consistency, and when or if that is acquired the damping stops. But hole or soliton equilibrium conditions are already non-linearly self consistent. So the Landau linearized analysis, leading to damping at a rate proportional to the resonant $|df/dv|$, does not apply. In summary then, linear Landau damping does not apply to electron and ion hole equilibria.

An important alternative phenomenon that can happen, however, is that the solitary potential structure can accelerate. One way this occurs is as a consequence of imbalanced reflection of the repelled species (when a non-zero slope exists on the background distribution). This phenomenon is (like Landau damping) caused by resonant particles (moving at or near the structure velocity). There are also other ways a hole can experience an instability that feeds on its own structure and particle energy, regardless of repelled species reflection. Moreover any transverse variation of the potential can give rise to particle orbits in which parallel energy is not conserved even

in a steady rest frame, and as a result particles can trap or detrap from the structure, and/or experience stochastic orbits. Furthermore if there are background field fluctuations, caused by other waves or moving electrostatic structures, these also can cause stochastic diffusion of the particle orbits in phase space. In general, orbit perturbations are liable to cause orbit detrapping and, for holes at least, gradual decay of the density deficit that is responsible for sustaining the potential.

In succeeding sections we shall see that much of the recent theoretical progress in electron and ion hole physics consists of developing a rigorous understanding of the effects of acceleration, instability, and stochastic orbits, which are the important collisionless mechanisms causing holes to (grow or) decay, and thereby determining their lifetimes.

B. Kinematics of Holes as Composite Bodies

The wake simulations of Haakonsen *et al.* (2015) showed electron holes spawned by the dimple instability arising from electron parallel cross-wake influx, usually then propagating out of the wake along the phase-space orbits of electrons. However, a few holes did not propagate out, instead remaining within it and being convected into downstream increasing density regions, all the while growing to large amplitude and eventually disrupting even the ion streams. The pressing theoretical question was why these few behaved differently in their response to the background parallel electric field environment. This turns out to be answered by detailed consideration of the kinematics of the electron holes, that is, of their momentum and energy conservation. Dupree, long before, had pioneered these considerations, discovering some important results. However, his treatment omitted a vital component of the momentum conservation of the repelled species (ions for electron holes), by making a small-potential expansion that omitted the lowest-order non-zero term. Hutchinson and Zhou (2016) and (Zhou and Hutchinson, 2016) therefore derived the momentum conservation expressions for electrons and ions associated with an electron hole either accelerating or growing in amplitude, without small-potential approximations and showed that they agreed with particle in cell simulations, as will now be outlined.

The key to electrostatic hole momentum conservation is the recognition that the electric field itself of a one-dimensional solitary potential structure exerts zero total force on the plasma. This is so because the Maxwell stress of the (z -component) electric field $E^2/2$ is zero at distant positions z_1 and z_2 on either side of the hole ($z_1 < 0 < z_2$). A simple demonstration is to write the force density exerted as $\rho E = \frac{dE}{dz}E = \frac{d}{dz}E^2/2$, and integrate from z_1 to z_2 , to obtain the total force $-\int_{z_1}^{z_2} \rho d\phi = [E^2/2]_{z_1}^{z_2}$ which is zero for $|z_{1,2}| \gg 1$. No-

tice that the so-called quasi-potential, introduced earlier, $\int \rho d\phi$, is in fact minus the Maxwell stress (as noted by (Andrews and Allen, 1971)). Zero total field force implies that the total particle momentum must be conserved. In a *steady* potential structure, no net particle momentum changes occur. Passing particles flow out of the region $z_1 < z < z_2$ carrying the same momentum they brought in; trapped particles bounce within the hole and no average momentum change occurs. However, when there is some time rate of change of the potential, even within the initial rest frame of the hole, then orbit energy is no longer conserved, particle “energization” effects occur, and more importantly for our present discussion, momentum exchange occurs which we will call “jetting” because the hole acts somewhat like a jet engine. When a hole accelerates, individual passing particles no longer carry out the same momentum they carried in, and trapped particles experience non-zero average acceleration, yet the total particle momentum must still be conserved.

The derivation of the momentum change of particles of a particular energy proceeds using the approximation that the transit time δt of the orbit across the hole is short compared with the timescale of potential change. For a hole of speed U and acceleration \dot{U} , the particle acceleration time is of order v/\dot{U} , and the approximation is that $\delta t\dot{U}/v$ is small. The total time derivative of passing particle momentum is then found to be (Hutchinson and Zhou, 2016)

$$\dot{P}_p = m\dot{U} \int_{z_1}^{z_2} \int \left[-2 + 3\frac{v_1}{v} - \left(\frac{v_1}{v}\right)^3 \right] f_1(v_1) dv_1 dz, \quad (26)$$

where v_1 is the external velocity (at z_1) and f_1 the external distribution, and $v = \sqrt{v_1^2 - 2q\phi(z)}$ is the velocity at z where potential is ϕ (approximated by short transit time as unaffected by \dot{U}). [We retain the mass m in this expression so as here to regard time as measured in the same units for electrons and ions. In our standard dimensionless notation, one can consider this to be a time scaling factor for \dot{U} , different for the different species.] The momentum derivative of trapped particles is simply the total trapped mass times the hole acceleration:

$$\dot{P}_t = m\dot{U} \int_{z_1}^{z_2} \int_{-v_0}^{v_0} f_t(v) dv dz, \quad (27)$$

where $v_0 = \sqrt{2|\phi(z)|}$ is the velocity of a particle of zero energy, which is the upper bound of trapped particles. These expressions make no approximation with respect to hole potential being small, but if it is small, then for the attracted species the distribution can be expanded as the first two terms of its Taylor expansion about $v_1 = 0$

as $f_1(v_1) = f_0 + v_1 f'_0$ and one finds

$$\begin{aligned}\dot{P}_p &\simeq m\dot{U} \int_{z_1}^{z_2} -2f_0 v_0 dz, \\ \dot{P}_p + \dot{P}_t &\simeq m\dot{U} \int_{z_1}^{z_2} \int_{-v_0}^{v_0} (f_t - f_0) dv dz.\end{aligned}\quad (28)$$

These expressions agree with those of Dupree. However, this approximation does not work for the repelled species, instead giving a divergent integral. Physically this problem arises because reflected particles are not properly treatable by the short transit time approximation. If there are reflected particles then (as Dupree noted) a net reflection force (momentum transfer rate) independent of any acceleration arises

$$\dot{P}_r = m \int_{z_1}^{z_2} \int_{-\sqrt{2\psi}}^{\sqrt{2\psi}} -2f_1(v_1)|v_1|v_1 dv_1 dz, \quad (29)$$

and dominates the repelled particle effects. However, if the number of reflected particles is negligible, then $\dot{P}_r \rightarrow 0$ and a different small- ϕ approximation of equation 26 applies, giving

$$\dot{P}_p = m\dot{U} \int_{z_1}^{z_2} \int -3 \left(\frac{\phi}{mv_1^2} \right)^2 f_1(v_1) dv_1 dz. \quad (30)$$

This is the important repelled particle force term, second order in ϕ , that Dupree's treatment omitted.

Reference (Hutchinson and Zhou, 2016) shows that if there is a uniform background force accelerating the particles at a rate \dot{v}_b , then in the above expressions one should replace \dot{U} with $\dot{U} - \dot{v}_b$. An electron hole for which ion interaction can be ignored then conserves momentum when $\dot{U} = \dot{v}_b$. That is, it accelerates at the same rate as an electron. This explains the simulation observation of electron holes moving out of a wake along the background electron phase-space trajectory. Situations where both electron and ion forces apply require more extended analysis. One such situation is the observed self-acceleration of initially stationary electron holes by interaction with ions. It is shown theoretically that the ion jetting force (30) becomes small compared with electron (28) when the hole speed relative to ions is greater than approximately $(m_i/m_e)^{1/4} \sqrt{T_e/m_i} = 6.5c_s$ (dimensional units, hydrogen), and that holes initialized gently at zero speed self accelerate to a calculable speed of this order of magnitude, which agrees remarkably well with simulation (Zhou and Hutchinson, 2016).

A more specific simulation using a specially-developed hole-tracking PIC code implemented an artificial background force to accelerate or decelerate controllably the ions (but not the electrons). The process is illustrated in figure 20(a). The hole is initialized with a slight positive velocity and quickly speeds up to just over $6c_s$ as expected from self-acceleration. Then at time 1500 the cold ions are artificially accelerated (blue lines) till 3500

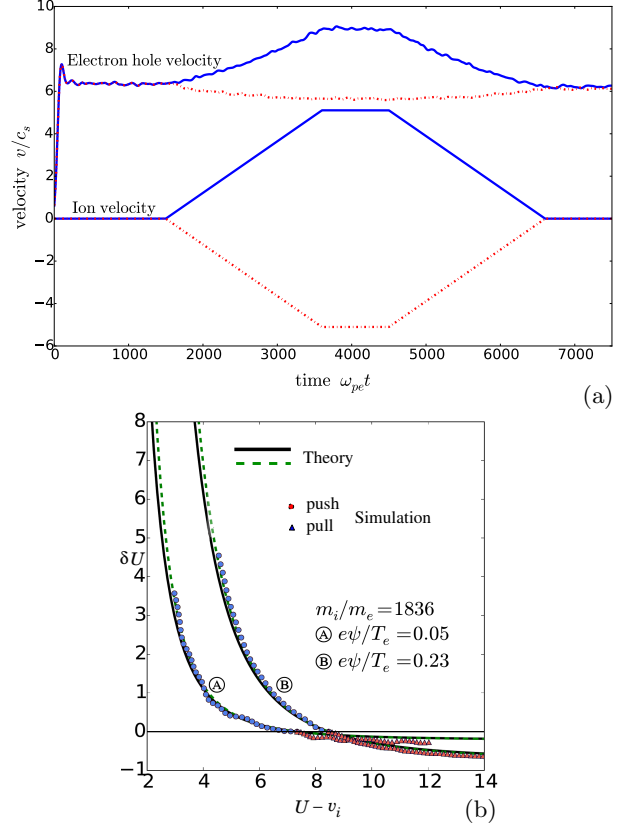


FIG. 20 (a) Artificially pushing ion velocity toward hole velocity (blue), or pulling it away (red) in PIC simulation. (b) Agreement of simulation results with analytic theory. Reprinted from (Zhou and Hutchinson, 2016), with the permission of AIP Publishing.

and then at 4500 decelerated back to zero speed. The hole velocity responds by accelerating by not quite as much, and then decelerating back to its $\sim 6c_s$ value. A second simulation (red dashed lines) instead decelerates and then accelerates the ions. The hole changes its velocity much less, but still reversibly. In figure 20(b) is shown the remarkable quantitative agreement of the analytic theory and simulation, for the hole velocity change during this process δU , versus the closeness of approach of the ion velocity $U - v_i$. Two different hole amplitudes are shown. The theory line is (in c_s velocity units)

$$\delta U = (M_{ie}^4/3) ([U - v_i]^{-3} - [U_0 - v_{i0}]^{-3}), \quad (31)$$

where $U_0 - v_{i0}$ is the initial velocity difference when $\delta U = 0$, and $M_{ie}^4/3 \simeq (m_i/m_e)\psi/T_e$ for shallow holes.

The inverse third power of the velocity difference shows that the strength of the ion interaction becomes great if the ion stream approaches the hole velocity. And it turns out to be easily strong enough in the wake simulations that, when the hole velocity lies between the velocities of two ion streams, it is essentially trapped by them and cannot be accelerated past by background electric field. In general, electron holes cannot smoothly over-

take a narrow ion stream. And this is the explanation for the few holes in the wake simulation that are trapped and remain in the wake long enough to grow to large amplitudes. Their velocity is trapped between two ion streams. The other holes that propagate out along the electron phase space trajectories have untrapped velocities.

All these comparisons show that electron holes do indeed behave like composite entities whose momentum conservation properties we can calculate, giving quantitative predictions of their motion.

C. Oscillatory Instability of Electron Hole Velocity

In the course of the simulations described in the previous section, a new phenomenon was observed: oscillatory instability of the hole speed when the ion stream velocity approaches the hole speed. It was comprehensively analyzed in a follow up paper by Zhou and Hutchinson (2017). Figure 21(a) illustrates the approach of the ion velocity (v_i) toward the hole (U) caused by artificial pushing (time 2000 to ~ 2400) and the subsequent growth of the instability, during which trailing ion density oscillations are visible 21(b).

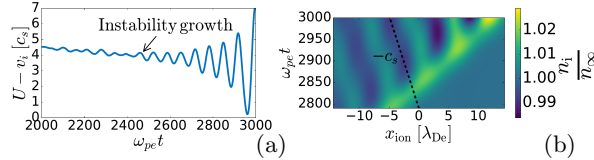


FIG. 21 (a) Threshold and growth of the velocity instability. (b) Ion density contours versus position in the ion frame (x_{ion}) during the instability showing trailing ion acoustic oscillations. From (Zhou and Hutchinson, 2017) reprinted with permission from Cambridge University Press.

The kinematic analysis of this oscillation proceeds as before for electrons, because they remain well approximated by the short-transit-time assumption, giving the same \dot{P}_e . But ions do not satisfy this approximation. Instead, their perturbed response must be approximated as an integral along unperturbed orbits (for small oscillatory perturbation) of the energization $\delta\mathcal{E} = \int \dot{U} v dt$, where now \dot{U} is proportional to $\exp(-i\omega t)$ with ω the complex frequency. After extremely heavy algebra, a long expression is found for \dot{P}_i , which reduces for $\psi \ll U^2$ (shallow holes) and writing the mean (unperturbed) hole velocity U in the ion frame ($v_i = 0$), to yield a form

$$\frac{\dot{P}_i}{\dot{P}_e} = -\frac{F(\omega/U)}{G(U)}, \quad (32)$$

where F is a complex function that depends only on its argument ω/U and spatial integrals over the normalized shape (mostly width) of the hole potential $\tilde{\phi}(z) \equiv$

$\phi(z)/\psi$; while G is a real function that is effectively $(m_e/m_i)(U^2/\psi)^2 \dot{P}_e$, and has dependence only on U and ϕ integrals, not ω . The dispersion relation is momentum conservation: $\dot{P}_i/\dot{P}_e = -1$, and a Nyquist analysis shows that unstable (positive) growth rate $\gamma = \Im(\omega)$ occurs for U less than a critical value U_c , at which the real frequency is ω_c . The critical speed for a small amplitude hole shape $\psi \text{sech}^4(z/4\lambda)$ is $U_c \sim (m_i/m_e)^{1/4} \psi^{1/2}$, but in Figure 22 the calculations are carried out numerically.

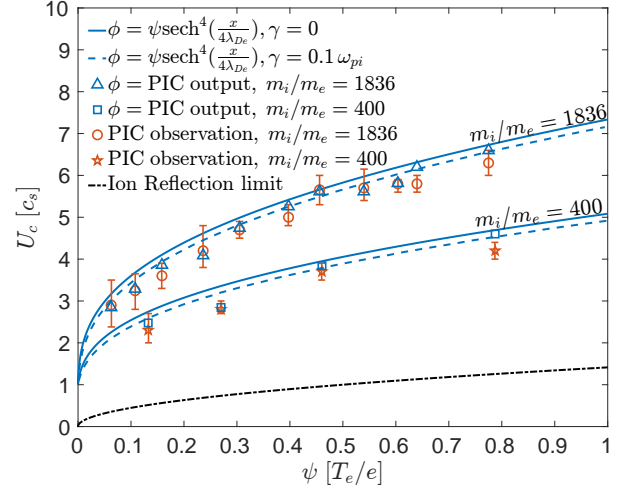


FIG. 22 Critical hole speed at which instability occurs. Lines: theory for sech^4 shape potential. Points: comparison of theory (triangle, square) versus observed onset (circle, star) for the simulation's actual potential shape. From (Zhou and Hutchinson, 2017), reprinted with permission from Cambridge University Press.

The lines show the instability boundary and (dashed) the place just below it where $\gamma = 0.1\omega_{pi}$, for an exact sech^4 shape versus hole amplitude ψ . Two different mass ratios are shown. The points are PIC simulation comparisons, showing in blue the analytic U_c for the actual (slightly variable) hole shape in the simulation, and in red the observed instability onset. The agreement is excellent. The agreement between theoretical and observed real part of the frequency (not shown) is equally good.

D. Hole-Soliton Coupling and Slow Electron Holes

As described earlier, some simulations by Saeki and Genma (1998) generated a solitary structure called a Coupled Hole Soliton (CHS). The way this phenomenon works is essentially through the momentum interaction of electron holes coupling to ions. In an ion acoustic soliton, a positive (electron attracting) potential is generated by densification of streaming repelled ions. This positive potential attracts an electron hole, and can effectively trap it so that it is attached to the soliton through its electric field. In Zhou and Hutchinson (2018) a series of controlled one-dimensional numerical experiments

were conducted to explore the behavior of CHS states. A CHS is launched by a carefully prepared initial state of the code, in which the ions local to the structure are given a velocity offset and the local electron distribution is given a Gaussian dimple (a local depression of $f_e(v)$) at an appropriate velocity. Without the dimple, a simple ion acoustic soliton tends to be launched; but with it, a CHS results. The soliton moves away in a direction determined by the local ion velocity offset, leaving behind a train of ion-acoustic oscillations, but carrying with it an electron hole that is clearly visible in the electron phase space and density.

The hole's presence is observed to assist the formation of the soliton, and once formed somewhat enhances its speed relative to the standard soliton dispersion relation (equation 20). A frequently cited aspect of KdV soliton behavior is that colliding solitons appear to pass through one another retaining their amplitude and speed. In contrast, two colliding electron holes, if their speeds are not greatly different, have long been observed to combine with one another to form a deeper electron hole (see e.g. Figure 9). In this study, colliding CHSs display a kind of hybrid behavior. During the collision, while the ion density perturbations of the holes overlap, the electron holes combine with one another within the potential peak, moving at electron orbit speeds, much faster than the ions. However, the ion compressions appear to continue with almost their original velocities, and as they begin to separate, they appear to tear apart the large combined electron hole so that one still sees two CHSs propagating away from the collision, although not with exactly the same amplitudes as before.

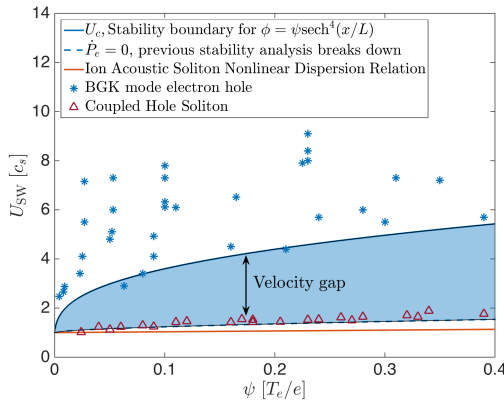


FIG. 23 The theoretical unstable gap (shaded region) between (simulated) free electron holes (blue points) and Coupled Hole-Solitons (red points). Reprinted from (Zhou and Hutchinson, 2018) with the permission of AIP publishing.

Extensive exploration of CHS existence in the simulations (Figure 23) showed that there is a speed gap between the CHS state, which is a little above the ion acoustic soliton speed, and the free electron hole state, which is several times c_s . This is attributable to the oscil-

latory instability which occurs in the gap and generally causes the electron hole either to accelerate out of the gap, becoming a free BGK electron hole with little ion interaction, or to be captured into a CHS state. Discussion is given of transition out of the CHS state by what the paper calls “Ion Landau Damping”. I now believe that the amplitude decay is mislabeled by this name, for the reasons given in section V.A. But in any case, whatever the decay mechanism, it is observed that if a CHS decays in amplitude, thereby moving into the speed gap, its position begins to oscillate within the potential well created by the ion density perturbation of the soliton. And the oscillation can grow sufficiently large that the hole escapes the soliton influence and moves off at speed above the gap.

The opposite process of transition from a free electron hole to a CHS was also demonstrated, using two symmetric, oppositely propagating ion streams ($v_i = \pm 4c_s$), and causing the hole amplitude to grow by growing the plasma density. The open $100\lambda_D$ long domain was injected with increasing fluxes of electrons and ions, which forms an increasing, somewhat concave, density profile. The initially stationary small hole $\psi \simeq 0.1$ in unity density grows in potential as the background density grows until, at time 1200 (ω_{pe}^{-1}), the increase is stopped and the density flattens at 3.2, with (by time 1800) a local ion density enhancement and ion acoustic waves being generated by the hole. The hole settles, the waves disappear, and by time 3330 a CHS persists with $\psi \simeq 3$, and a local density peak of ~ 4 : well above the 3.2 background, showing the strong ion response. This sequence occurs only when the density growth rate is sufficiently fast, otherwise the oscillatory instability occurring during the transition across the unstable gap disrupts the hole and parts of it are accelerated to high speed by ion interaction and lost.

A final reported set of numerical experiments in this paper concerned the Buneman instability, arising from strong relative ion-electron drift. The wave train that it generates in the nonlinear stage, when the ions are cold $T_e = 20T_i$, $\bar{v}_e = 45c_s$, consists of CHS-like ion density enhancements coupled with electron phase-space holes. By contrast, with equal temperatures $T_e = T_i$, $\bar{v}_e = 70c_s$ the instability generates waves that appear to consist of trains of pure electron holes, traveling at $4-5c_s$ (relative to the ions) above the oscillatory velocity instability gap.

In an attempt to detect the instability gap in nature, Zhou and Hutchinson plotted satellite data from Graham *et al.* (2016) on a figure like 23. The comparison was unfortunately inconclusive, mostly because the hole amplitudes were so small that the gap was as narrow as the apparent uncertainty in hole speed. Further observational analysis of MMS magnetopause data by Steinvall *et al.* (2019) did reveal some velocities along the red region of 23 that might have been coupled hole-solitons, and a few holes of high amplitude above the velocity gap,

that was suggestive of fast holes, as well as many of low amplitude around and below $U = 1$.

A later major statistical study of hole speeds in MMS data, Lotekar *et al.* (2020), analyzed (during fast-flow events in the magnetotail) more than 8000 holes, of which 2400 were observed on at least three spacecraft. Such

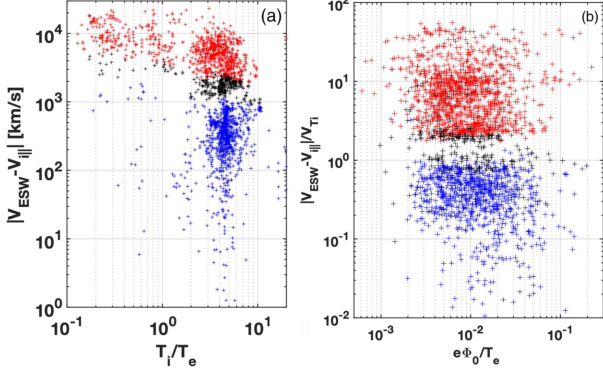


FIG. 24 Hole speeds observed by MMS (a) versus background temperature ratio, (b) normalized to ion thermal speed versus hole amplitude, showing a suggestive gap just above the ion thermal speed. From Lotekar *et al.* (2020).

observations allow much more precise determination of hole speed. The parallel separation of the craft was a few up to about 10km, and by careful cross-correlation events were selected that were holes propagating from one craft to others. Velocities relative to the craft down to 100km/s could be determined. These were all electron holes, having positive potential polarity (only about 20 were excluded from analysis because of being negative). Distributions of hole length, amplitude, duration, and occurrence provide important evidence concerning their generation and stability, that will be mentioned in other contexts, but here we focus on the velocity statistics shown in Figure 24.

The colors separate slow holes (blue) with speed (relative to ions) $v_h < 0.05$ of the electron thermal speed, fast $v_h > 0.1$ (red), and intermediate (black). We observe that when $T_i < T_e$ almost all holes are fast, but there are many holes in plasmas with $T_i \sim 3T_e$ that are slow, having speeds that are less than v_{ti} . There appears to be an almost empty gap in the intermediate speed range, which is suggestive of the theoretical forbidden range where the oscillatory instability occurs. However, there is no sign of a restriction of the slow hole velocities to the soliton velocity, as observed in the CHS simulations. So probably these slow holes (with $T_i > T_e$ unlike the simulations) are not coupled hole soliton structures.

The question then arises as to what permits them to be so slow. As we have noted earlier, holes simulated starting at slow speeds, within the ion distribution, are usually observed to self-accelerate by interactions with the ions, ending up at speeds generally significantly exceeding the ion acoustic speed. Yet the slow holes of

Lotekar *et al.* (2020) have not experienced this effect. How do they exist? The theoretical answer is given by Hutchinson (2021b). One way to explain it intuitively is in terms of the ion density change that accumulates in the hole. For a single-humped background ion distribution such as a Maxwellian, in the interior of which the hole velocity resides, the density perturbation caused by a positive potential structure (electron hole) is negative: ion charge density is decreased. However, in the opposite extreme, if the ion distribution is composed of the sum of (say two) Maxwellians with different mean velocities, then if they are sufficiently spaced apart, a hole between them will instead cause an increase of the ion charge. In this second situation, the electron hole controlling the potential experiences an *attraction* to the ion density perturbation, rather than a repulsion. This can prevent self-acceleration. The alternative intuitive explanation, which forms the basis of a more thorough calculation of the velocity stability threshold, is to recognize that slow holes by definition cause ion reflection. And, although the reflection force averages to zero in equilibrium, including for example a symmetric ion distribution, if a hole accelerates away from that equilibrium, then the ion force becomes non-zero. The sign of the force and its resulting acceleration is such as to amplify the velocity perturbation, yielding unstable growth of the motion, unless the background ion velocity distribution is double humped and the equilibrium lies near its local minimum. Thus the theoretical answer to how slow electron holes can exist is that they require a local minimum in the ion velocity distribution to avoid unstable acceleration. A range of different model ion distributions for which electron holes are theoretically marginally stable against the self-acceleration instability is shown in Figure 25(a). The equilibrium hole velocity is marked on each curve with a cross.

Almost simultaneously with this theory, Kamaletdinov *et al.* (2021) performed an in-depth study of the measured ion distribution functions during which slow electron holes were observed by MMS. An example is shown in Figure 25(b). The observed hole velocity lies right in the local minimum of the double-humped ion distribution, as the theory says is necessary for a stable equilibrium. Moreover, the authors obtained the ion distributions for all the approximately 1000 slow electron holes identified by Lotekar *et al.*, and found that the ion velocity distributions essentially all had this sort of double-humped character, and the hole velocity lay in the distribution's local minimum. Thus these well-characterized slow electron holes show remarkable agreement with the theoretical requirements for slow holes, and the statistics of this comparison are very extensive.

Some simulations of slow electron holes in double-humped ion distributions that the quasi-static theory of (Hutchinson, 2021b) indicates should be stable, showed a different phenomenon of “overstability” treated the-

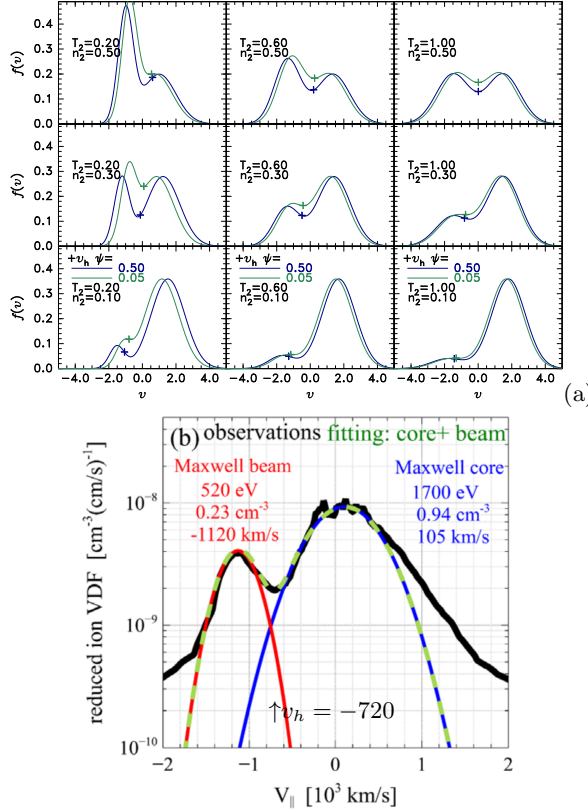


FIG. 25 (a) Various two-Maxwellian ion distribution shapes that permit electron holes marginally stable against self-acceleration. Reprinted with permission from (Hutchinson, 2021b) copyright the American Physical Society (2021). (b) Example measured parallel distribution function (black line) with the hole velocity indicated by the arrow. Reprinted with permission from (Kamaletdinov *et al.*, 2021) copyright the American Physical Society (2021).

oretically by Hutchinson (2022). That is, they exhibited growing velocity and position *oscillations*. When the oscillation grows to sufficient amplitude in the simulations, the electron hole escapes the local influence of the attractive ion density rise, no longer a slow hole. This phenomenon is not represented within the quasi-static theory, and instability calculations require a full scale numerical solution of the linearized Vlasov equation for the ions, whose transit time is comparable to the oscillation period, and which therefore introduce a phase-shift dependent on ω into the response equations. More details will be discussed of the solution techniques employed when we come to treat transverse stability. But the comprehensive one-dimensional slow hole instability theory results are summarized in Figure 26. When the shifts $\pm v_s$ (in ion thermal units $\sqrt{T_i/m_i}$, $T_i = T_e$) of the two symmetric Maxwellian ion distribution components is small, there is pure growth of the hole velocity given by a purely imaginary ω . It is approximately $\Im(\omega) = 0.3\psi^{1/2}$. As v_s is increased, giving rise to flattening of the distribution and eventually a local minimum,

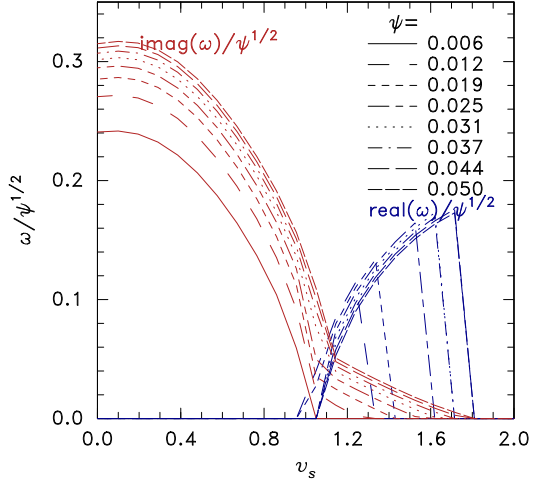


FIG. 26 Real and imaginary parts of the frequency versus the velocity shifts ($\pm v_s$) of two equal Maxwellian ion components, for a range of electron hole amplitudes ψ . From (Hutchinson, 2022).

the growth rate decreases, and for small $\psi \lesssim 0.01$ just stabilizes at $v_s \simeq 1.05$. However, holes of greater amplitude instead become overstable, with finite real frequency, whose magnitude grows during deepening of the local f_i minimum. The growth rate for a specific amplitude continues to decrease until the instability eventually ceases. Thus the quasi-static analysis needs to be complemented by this fuller eigenfrequency determination to give a complete picture of the theoretical one-dimensional stability of slow electron holes. They need a rather deeper local minimum for stability than is indicated by the quasi-static approximation, or else they must have a very small potential amplitude ψ .

VI. ASYMMETRIC ELECTRON AND ION HOLES

A. Theory of hole asymmetry and acceleration

In the previous section we have described how the kinematics of holes governs their behavior as composite entities capable of free motion and acceleration. The observed quantitative agreement between simulation and analytic calculation justifies the approximation that any hole shape variation, internal vibrations or distortions, is a small effect on the overall momentum balance.

A further assumption implicit in almost all the treatments discussed is that the hole potential profile is symmetric in space about the hole center. When the charge density is indeed a function only of potential, this symmetry is inherent in the governing equations, because trapped densities are themselves symmetric (in equilibrium at least), and so even asymmetric passing velocity distributions do not immediately induce any spatial asymmetry.

However, asymmetric kinetic potential structures do exist. Double layers are the best known example, where the potential difference across the structure is the dominant factor, and is often assumed to be monotonic. Asymmetries in electron and ion holes can also arise from the same mechanism as in double layers: particle reflection. In the context of holes, when the potential variation is dominated by a local positive or negative peak, and the potential difference between the two sides of the hole is small, the dominant reflection effects arise from the repelled species: ions at an electron hole, or electrons at an ion hole. Such reflections break the symmetry when the background velocity distribution of the reflected particles is asymmetric in the hole frame, making the charge density a function of *both* the potential and the sign of the position (z) relative to the potential peak ($z = 0$). Reflected particles contribute only to the density on the side of the peak from which they approach the hole. Obviously this is a dominant effect for a double layer, but it may be a more moderate factor for an electron or ion hole. Figure 1(ii) illustrates schematically the sort of situation we have in mind, where the ion hole asymmetry is presumed to arise from a small shift of the electron distribution's velocity center. Figure 27 illustrates actual

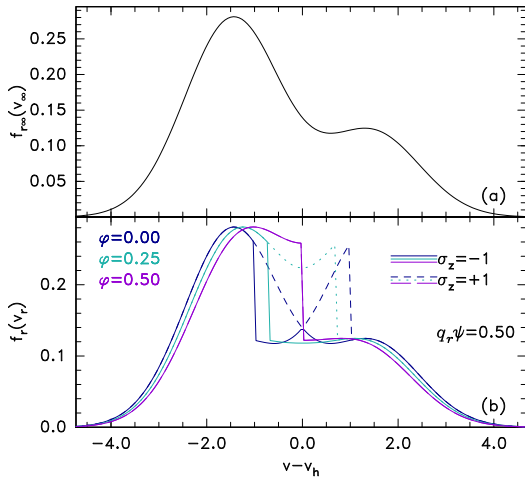


FIG. 27 Example of asymmetric repelled species velocity distributions in the presence of reflection. (a) Background (incoming) distribution. (b) Distributions at three different potentials on either side (σ_z) of the peak.

repelled species velocity distributions at different potentials (b) when the background distribution (a) is asymmetric. Discontinuities arise at velocity corresponding to marginally reflected particles, and the densities are different on the different sides (σ_z) of the hole.

Finding a theoretical solitary structure equilibrium in this situation requires a considerably more elaborate process that we now outline. The original papers(Hutchinson, 2021b, 2023b) give much more detail. Determining whether a particle velocity is reflected requires knowing the height ψ of the potential peak. It

is therefore easiest to use a variant of the BGK (integral equation) approach. Knowing ψ and the specified repelled species background distribution $f_r(v)$ provides the repelled density $n_r(\phi, \sigma_z)$. Since the repelled density is different at $z \rightarrow \pm\infty$, the attracted species must also have asymmetric distant density to satisfy neutrality. This n_a asymmetry can only be induced by a potential difference $\Delta\phi = \phi(+\infty) - \phi(-\infty)$. (The zero of potential is taken at $[\phi(+\infty) + \phi(-\infty)]/2$.) Whatever the attracted species distribution is, its distant density is a function only of potential. Thus, $\Delta\phi$ can be found by solving the equations $n_a(\pm\Delta\phi/2) = n_r(\pm\Delta\phi/2, \sigma_z = \pm 1)$. For example, if the attracted species is Maxwellian of reference temperature, then $n_a = n_0 \exp(-q_a \phi)$, which, given n_r , yields $q_a \phi = -\ln(n_r/n_0)$.

For any arbitrary electron hole velocity v_h relative to (say) the ion frame, there will then generally be a net ion reflection force on the hole. The hole force balance can then only be satisfied by a net transfer of momentum to the attracted species, and in the general case when attracted species reflection does not exactly balance it, hole acceleration will occur. In other words, the hole will in fact not be in equilibrium in respect of hole motion. Only at a set of discrete hole velocities, and corresponding $\Delta\phi$, will the ion reflection force be exactly balanced by attracted species reflection from the potential difference $\Delta\phi$ across the hole. Those discrete true equilibrium hole velocities can be found by iterative search. They generally lie close to any local maxima or minima in $f_r(v)$. The stability of those equilibria with respect to slow perturbations of the hole velocity is then determined by the sign of the derivative with respect to v_h of the total force.

It is helpful to distinguish between what is called the “extrinsic” force or momentum transfer, which arises purely because of $\Delta\phi$, and the “intrinsic” force, which is present regardless of $\Delta\phi$ (Hutchinson, 2023b). The intrinsic momentum transfer to the attracted species is attributable purely to acceleration,

$$\dot{P}_{aint} = M_a \dot{v}_h \quad \text{where} \quad M_a = \int \tilde{n} dz. \quad (33)$$

Here \tilde{n} is the hole attracted density arising just from the depression of its phase-space density relative to the flat plateau, and is therefore negative. M_a is the effective hole mass, also negative. The intrinsic reflection force on the repelled species is the electric field force times its charge density integrated over the hole

$$\dot{P}_{rint} = F_{rint} = \int_{q_r \phi > |\Delta\phi|/2} -n_r q_r \frac{d\phi}{dz} dz. \quad (34)$$

The extrinsic force, combined for both species, can be expressed as the Maxwell stress difference across the potential range $-|\Delta\phi|/2 < q_r \phi < +|\Delta\phi|/2$ on the lower-potential wing of the hole. This can immediately be

found from the distant asymptotic form $\phi \propto \exp(-|z|/\lambda)$, where λ is the generalized Debye shielding length, giving

$$\dot{P}_{ext} = F_{ext} = \Delta\phi|\Delta\phi|/2\lambda^2. \quad (35)$$

We then have a kind of Newton's Second/Third law: $-F_{rint} - F_{ext} = M_a \dot{v}_h$, in which the hole's mass M_a is negative. Equilibria lie at velocities such that $F = F_{rint} + F_{ext}$ is zero. But those equilibria for which dF/dv_h is positive are unstable, because any small difference of v_h from the equilibrium causes acceleration that increases the difference. The general result is that equilibria near a local maximum of $f_r(v)$ are unstable and those near a local minimum are stable. Figure 28 shows the force vari-

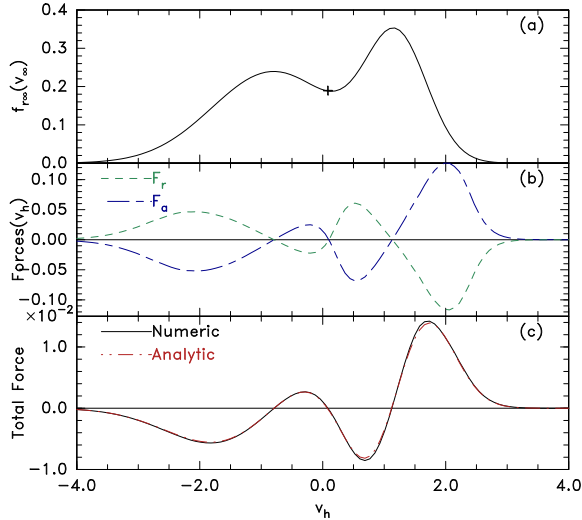


FIG. 28 Repelled and attracted species force balance as a function of hole velocity when $\psi = 0.1$. Only the velocity with total force ($F = F_r + F_a$) zero and negative slope, marked with a cross, is a stable equilibrium. Reprinted with permission from (Hutchinson, 2023b), copyright AIP publishing (2023).

ation with v_h and the fact that force-zeroes near peaks on the repelled species distribution are unstable, and near (local) valley bottoms are stable to slow acceleration.

It proves possible (Hutchinson, 2023b) by Taylor expanding the repelled distribution about the hole velocity, for moderate or small ψ , to derive an analytic approximation to the total force

$$F = F_{rint} + F_{ext} = -4\psi^2 f'_r - \frac{8}{9}\psi^3 f''_r \quad (36)$$

where primes denote velocity derivatives. The resulting analytic line in Figure 28(c) is in excellent agreement with the numerical calculation. The corresponding analytic approximation for the potential drop across the hole is

$$\Delta\phi = \frac{-4\psi^2 f'_r - \frac{2}{3}\psi^3 f'''_r}{1/\lambda^2 - f' + \psi f'''_r/12} = \frac{\frac{2}{9}\psi^3 f'''_r}{1/\lambda^2 - f' + \psi f'''_r/12}, \quad (37)$$

where the second form sets F (equation 36) to zero so it applies only at equilibrium. In view of the ψ^3 factor, we see that $\Delta\phi$ is thus very small unless the hole amplitude is big $\psi \sim 1$. In equilibrium, small amplitude holes are thus predicted to have potentials very close to symmetric. However, holes that are accelerating, for which equation 36 is not zero, can have more substantial asymmetries.

Holes with velocities near an equilibrium that is unstable because of particle reflection experience exponential growth of their velocity Δv_h relative to the equilibrium velocity. The simplest example is a hole with velocity at the peak of the repelled particle distribution. In figure 28 that would be the zero-crossings of F at $v_h = -0.8$ and 1.2 . The growth rate γ of Δv_h there depends on the second derivative f''_r . A single Maxwellian peak has $f''_r = -(T_a/T_r)^{3/2}/\sqrt{2\pi}$ and gives a growth rate $\gamma = -(4/\sqrt{2\pi})\psi^2\theta^{-3/2}/M_a$ in attracted species units (ion units for an ion hole), where $\theta = T_r/T_a$. The hole mass for a sech^4 shaped hole is to leading order $M_a \simeq -(16/3)\psi\sqrt{1+1/\theta}$ which gives

$$\gamma \simeq \frac{3}{4\sqrt{2\pi}} \frac{\psi}{\theta\sqrt{\theta+1}}. \quad (38)$$

A large repelled species temperature (large θ) thus decreases the acceleration growth rate. But in the case of an ion hole it is really the curvature of the electron distribution very close to its peak that determines stability and growth. A perfectly flat f_r ($f''_r = 0$) there zeroes the growth rate, but would be very difficult to measure. In any case, this growth rate, and the associated acceleration rate for finite f'_r are slow enough that treating an ion hole as a composite entity lasting many bounce periods of its trapped ions is a consistent approximation. In other words, equation 38 which represents a quasi-static treatment of the particle dynamics, is accurate only if the timescale of growth is long compared with particle transit or bounce times. That is certainly true of electrons in an ion hole, since the growth rate is then in absolute units of ω_{pi} ; and when ψ is not large it is valid for ions too. However, for an electron hole it is a poor approximation for ion dynamics since the characteristic ion timescale is $\sqrt{m_i/m_e}$ longer than electron. Electron hole unstable acceleration needs a more elaborate treatment and can give a growing velocity oscillation in some cases (see Hutchinson (2022), 2022, and figure 26 in Section V.D).

All of the mathematical discussion so far applies to electron or ion holes, when we use the different normalizations, with the caveat just mentioned about different timescale approximations. In addition, the different *velocity* scales make the practical importance of reflection greater for ion holes than electron holes. Electron holes can easily have velocities relative to ions that make the ion response and especially the ion reflection negligible, whereas ion holes, whose velocities are generally limited to a few times $\sqrt{T_i/m_i}$, almost never travel fast enough for electron reflection to be negligible. Using the design-

nation “slow” to indicate a structure whose velocity lies within the repelled distribution, we can say that electron holes are often not slow, whereas ion holes are almost always slow. This velocity scale difference also means that electron holes accelerated by ion reflection can remain intact once their speed is raised beyond the ion thermal spread; while ion holes, if they are accelerated, disengage from the attracted *ion* distribution long before disengaging from the electron distribution. The result is most plausibly collapse of the ion hole, since at $v_h \gg v_{ti}$ there is no ion phase space density in which a depletion could occur.⁵ Nevertheless, ion holes are unambiguously observed in space as is discussed in Section VI.B.

Before that, though, we should note that when an electron hole is accelerating it can develop potential asymmetry, even when there is negligible ion response. Two possible mechanisms for causing this acceleration and potential asymmetry are (i) mirror force arising from a parallel gradient of magnetic field strength, which is the topic of the analysis of Kuzichev *et al.* (2017); Vasko *et al.* (2016); and (ii) background conservative (e.g. gravitational or background electrostatic) force with resulting density gradients, which are the subject of simulations by Vasko *et al.* (2017c). These papers are motivated in part by the possibility of particle energization by adiabatic heating of trapped electrons, and by the possibility that substantial total potential drop, sometimes inferred in space, can accumulate from a sequence of small drops across successive electron holes.

The theory of Vasko *et al.* (2016) concentrates on an adiabatic mechanism of particle energization. The conservation of magnetic moment μ for a particle moving up a slow positive magnetic field strength gradient increases its perpendicular energy ($\propto |B|$). In the absence of any other forces, its total energy is conserved and the parallel kinetic energy decreases by an equal amount until the orbit is reflected when $v_{\parallel} = 0$. However, an electron trapped in the electric field of a moving electron hole is constrained to move at an average speed equal to that of the hole. It then bounces somewhat asymmetrically in the electric potential well, in such a way that any loss of average parallel kinetic energy is made up by the average of the hole electric field force. Therefore it is possible for its perpendicular and total kinetic energy to increase without limit as long as $|B|$ increases (and μ is conserved). This energization might then give rise to particles with energy much larger than thermal, without requiring a large electron hole potential. This paper calculates that some of the perpendicular energy given trapped particles comes from parallel energy lost by untrapped particles. It supposes that the difference

between these two transfers is small, and then addresses the evolution of the hole potential amplitude, assuming that the hole velocity is fixed and given. (Invoking the “given field” approximation O’Neil (1965).) A weakness of this approach is that it is likely that (the ignored) hole acceleration or deceleration is a more important effect than hole growth, and neither are properly treated in the “given field” approximation. Kuzichev *et al.* (2017) reports continuum Vlasov simulations of the process in a specified magnetic field gradient. They do indeed show hole deceleration when moving into an increasing $|B|$. It proves to be considerably faster than would be predicted by the average mirror-force acceleration of trapped particles. Further simulation results with similar setup are described in Shustov *et al.* (2021) where braking (deceleration) of holes in reconnection layers with increasing $|B|$ is modelled. Varying the hole amplitude shows that smaller ψ gives slower deceleration, and smaller $\Delta\phi$, but the mirror force is the predominant mechanism for all amplitudes.

The simulations of (Vasko *et al.*, 2017c), video examples of which can be viewed at https://www.youtube.com/playlist?list=PLVd7b9xQL_fP6wqp84NJf5gPmiHmpYrRA, are similar except that they apply a force arising from general potential U (independent of perpendicular energy). The background density is taken to vary spatially in accordance with a Boltzmann factor. These also show hole acceleration noticeably faster than would occur for single electrons in this potential. Its cause is not explained, just said to be unsurprising in view of energy exchange with passing electrons. A feature of all these simulations is that the starting hole velocity is quite large $1.3(v_{te})$, so these holes are out on the wing of the electron distribution, approaching the unusual type of Turikov (1984) (see figure 10).

Electron reflection from the potential drop that is observed to be developed is one important possible cause of deviation of the observed effective charge to mass ratio from unity. Another, perhaps more important, is that in the non-uniform density, hole growth is expected, which also gives rise to acceleration, and this mechanism, derived in (Hutchinson and Zhou, 2016) is ignored in the comparison by (Vasko *et al.*, 2017c). The observed amplitude variation in the simulations is rather small. So a complete explanation is still somewhat elusive.

B. Recent ion hole observations

The Earth’s bow shock is a region displaying large amplitude, often electrostatic, fluctuations. In it the incoming ions moving at near the solar wind speed are slowed and densified over a relatively short distance in which the magnetic field strength is also enhanced by a factor of a few. It is known that a substantial fraction of the

⁵ An alternative speculation is that conceivably a hole of the “Turikov” type (Turikov (1984)), figure 10, might persist.

inflowing ions are actually reflected within the shock and return back upstream with approximately their incoming speed. This phenomenon can easily give rise to a kind of two-stream instability of the ions (actually ion acoustic instability), theoretically analyzed long ago by Stringer (1964). Therefore ion instabilities have long been proposed as a major cause of bow shock electrostatic fluctuations (see e.g. Akimoto and Winske (1985)). Until recently it has been extremely difficult to detect the velocity and hence potential polarity of the observed solitary bipolar-field electrostatic structures in the bow shock. The assumption that they were electron holes, made for Wind satellite measurements by (Bale *et al.*, 2002), was called into question by analysis of the Cluster data (e.g. Hobara *et al.* (2008)) showing negative potential polarity. But Cluster did not have electric field measurements along its spin axis; so full three-dimensional field diagnosis was not available.

From approximately 2018 onward, however, careful interferometric analysis by Kamaletdinov *et al.* (2022); Vasko *et al.* (2018b, 2020); Wang *et al.* (2020, 2021) have shown the solitary structures observed by MMS, with full 3D field measurements during several bow shock crossings, to be predominantly *negative* potentials. That is, they are (most probably) ion holes. Wang *et al.* (2021) present the most comprehensive data analysis, including more than 2000 bipolar field structures of negative polarity (setting aside the ~ 100 observed positive ones). Because the solitary structures had lengths comparable to the antenna separations, corrections to the time dependence of the voltage-differences were essential to determining the spatial shape of the field \mathbf{E} and the structure's propagation velocity v_h and direction \mathbf{k} . After applying these corrections the directions of \mathbf{E} and \mathbf{k} were found from single-craft signal correlations to coincide within 20 degrees, and the uncertainty in v_h was $< 30\%$ at 90% confidence level. The statistical distribution of hole velocities (in the \mathbf{E} direction) relative to the mean plasma ion velocity peaked close to zero and extended up to approximately 2 times $\sqrt{(T_e + 3T_i)/m_i}$, where temperatures are measured in the upstream plasma flow. Figure

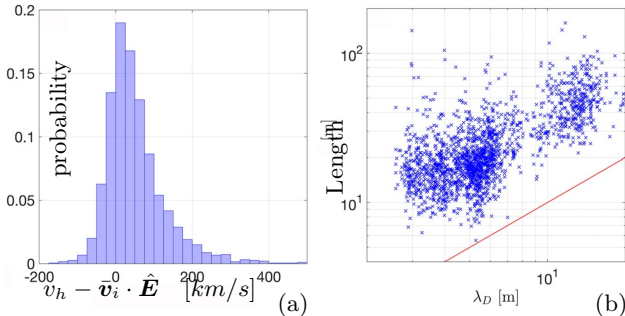


FIG. 29 Ion holes in the Earth's bow shock. (a) Histogram of observed ion hole velocities in the ion frame. (b) Hole lengths compared with Debye length λ_D . From (Wang *et al.*, 2021)

29(a) shows the absolute velocity distribution. The hole length distribution peaks at approximately $3.5\lambda_D$ with a range from ~ 2 to ~ 8 . Moreover the correlation of length with λ_D was unequivocal over nearly a factor of 10, as illustrated in figure 29(b). Amplitudes were mostly $\psi \lesssim 0.1T_e$ but with a small proportion up to ~ 0.3 . Significantly, the principal direction \mathbf{k} of hole electric field and (hence) apparent propagation velocity \mathbf{v} , is mostly nearly perpendicular to the shock normal, with little statistical difference in the sign of the small normal velocity component. The magnetic field is a somewhat preferred direction for hole propagation, though with little difference in the sign of $\mathbf{B} \cdot \mathbf{v}$, but there is also a substantial fraction of the hole velocities spread almost uniformly across all possible angles with respect to the magnetic field.

The interpretation offered by Wang *et al.* (2021) is based on the reasonable assumption that forming ion holes requires at least several bounce periods, with the bounce frequency (for intermediate trapping depth) estimated as $\omega_b = \sqrt{\psi}\lambda_D/L \simeq \sqrt{\psi}/3$, yielding $\omega_b \sim \omega_{pi}/10$. The range 1 to 10 bounce periods in typical bow shock plasmas then corresponds roughly to 10 to 100 ms as the minimal hole lifetime and of order 1 to 10 km propagation distance. Arguing on theoretical grounds that growth of an ion-ion instability saturates when the bounce frequency is comparable to the initial growth rate, and estimating the maximum growth rate theoretically for cold ion components, yields a maximum saturation amplitude (taken as ψ) proportional to $n_e L^2$. It is somewhat greater than the observed hole amplitudes and has comparable slope with respect to length L ; so amplitude observations are at least consistent with ion-ion instabilities being the underlying generation mechanism. Moreover oblique propagation with respect to the relative velocity is another theoretical characteristic of ion-ion instabilities when the beam velocities are more than approximately $2c_s$ apart, consistent with observations showing predominantly tangential orientation of \mathbf{k} , assuming the ion beam velocity separation is approximately in the shock normal direction.

Elsewhere, Wang *et al.* (2022) have analyzed solitary structures of negative potential polarity in the Earth's Plasma Sheet, including the handful set aside by Kamaletdinov *et al.* in their electron hole study because of their negative polarity. The structures, 153 in total, are simultaneously observed on all four MMS spacecraft, providing accurate velocity diagnosis by inter-craft correlation even though single-craft interferometry was not usable because of spacecraft potential variations. They show evidence of being strongly oblate (an order of magnitude wider than they are long) since the single principal normal \mathbf{k} is the same for all spacecraft and the perpendicular electric fields are small. The angle between \mathbf{k} and the magnetic field is distributed approximately uniformly over its entire range, 0 to 90 degrees. This ob-

served non-alignment is attributed to the unmagnetized ion parameters $\omega_{pi} \gg \Omega_i$ of this plasma region. The background ion velocity distributions in which the ion holes occur are highly non-Maxwellian, but their second moment corresponds to a temperature of approximately 5 keV, which should be compared with the electron temperature of ~ 2 keV. This temperature ratio provides experimental demonstration that there is really no requirement $T_e/T_i \gtrsim 3.5$ for ion hole existence, as mentioned in section II.D. The hole speeds lie between 0.2 and approximately 3 times $\sqrt{T_e/m_i}$; this places them within the ion distribution and disappearing as they move beyond its extent. Hole amplitudes $|\psi|$ are from $\sim 10^{-3}$ up to $\sim 0.2T_e$; and there appear to be potential drops across them up to $\sim \frac{1}{4}|\psi|$, which might suggest, based on the asymmetry theory, that they are in the process of accelerating.

VII. TRANSVERSE INSTABILITY THEORY

The predominant theoretical development of electron and ion holes discussed so far is of their one-dimensional equilibrium and momentum balance. However, these phenomena occur in multidimensional space, and there is plenty of observational evidence in the historical review that holes are often multidimensional, of limited transverse extent. Simulations of two stream instabilities in multiple dimensions between approximately 1998 and 2001 (Goldman *et al.*, 1999; Lu *et al.*, 2008; Miyake *et al.*, 1998; Mottez *et al.*, 1997; Muschietti *et al.*, 2000; Oppenheim *et al.*, 1999, 2001; Singh *et al.*, 2001) observed instabilities breaking up the transverse extent of electron holes. And two-dimensional simulations established that electron holes that start as quiescent one-dimensional entities (uniform in the transverse direction) when the bounce frequency exceeds the cyclotron frequency (Muschietti *et al.*, 2000, 1999; Wu *et al.*, 2010) $\omega_b \gtrsim \Omega$ are unstable to kinks with finite transverse wavenumber k . Even when the magnetic field strength exceeds this threshold, a much slower growing instability is observed in some simulations, associated with long wavelength striations aligned with the magnetic field that are identified as whistler waves. Despite various theoretical ideas and analyses attempting to explain the threshold (Jovanović and Schamel, 2002; Vettouli and Oppenheim, 2001) and the whistler-related instability (Berthomier *et al.*, 2002; Newman *et al.*, 2001a; Roth *et al.*, 2002), none were really persuasive about the underlying mechanisms. The original speculative “electron focussing” mechanism of Muschietti tended to be cited in the context of observations and simulations.

A. Jetting as the instability mechanism

There matters lay until Hutchinson (2017) briefly reported simulations that contradicted the focussing mechanism, and emphasized that the transverse instability mechanism and threshold were still open questions. This was a clearly unsatisfactory theoretical situation, since the transverse instability is implicated in determining the multidimensional structure of observed electron holes. The transverse stability of pure electron holes (fast enough that ion response is negligible) was therefore addressed.

In Hutchinson (2018a) the simulation evidence was reported in detail together with a simple analytic explanation of the mechanism, based on the kinematic momentum conservation, explained in one dimension in the present paper’s section V. The PIC simulations approximately confirm the long-standing criterion to stabilize the fast growing instability, except for providing a slightly higher numerical coefficient $\Omega \gtrsim 1.5\omega_b$. However, the electron focussing mechanism formerly proposed to provide the mechanism was discredited since the electron density enhancement was usually on the convex side of the kinked hole not the concave. Instead this work proposed that the transverse instability for negligible magnetic field strength is explained by considering the constant transverse velocity v_y of particles in the presence of a kinked hole whose parallel displacement is $z_h(y, t) = \xi \exp[i(ky - \omega t)] = \xi \exp[(ikv_y - \omega_i)t]$, when v_y is constant so $y = v_y t$, and $\omega = i\omega_i$ is pure imaginary. An electron with this transverse velocity therefore experiences a hole whose acceleration (at the electron position) is $\ddot{z}_h = -(kv_y - i\omega_i)^2 z_h$. Averaging this acceleration over all v_y gives $\langle \ddot{z}_h \rangle = (-\langle k^2 v_y^2 \rangle + \omega_i^2) z_h = (-k^2 T_y/m_e + \omega_i^2) z_h$. In general, the momentum transfer to electrons by jetting, \dot{P}_e , is proportional to the acceleration $\langle \ddot{z}_h \rangle$. But since the momentum balance ignoring ion response is $\dot{P}_e = 0$, it does not much matter what the coefficient of proportionality is, provided it does not significantly vary with v_y . The instability growth rate must then satisfy $\langle \ddot{z}_h \rangle = 0$, yielding

$$\gamma = \omega_i = \pm k \sqrt{T_y/m_e}. \quad (39)$$

This treatment is valid for small enough k , but when kv_y approaches the bounce or parallel transit frequency of electrons in the hole, the coefficient of proportionality reverses its sign and cancellation of the acceleration of different velocity particles suppresses the instability, eventually reversing the velocity average $\langle \dot{P}_e \rangle$. Because the transit time of the particles responsible for jetting is roughly $L/\sqrt{\psi}$, where L is the hole length (typically ~ 4), the critical wavenumber at which the instability is suppressed is approximately $k_c \simeq \sqrt{\psi}/L$ (using a thermal $v_y \simeq 1$). The maximum growth rate occurs somewhere below k_c : let us suppose half ($k_{max} \sim \sqrt{\psi}/8$); and the

growth rate there will be perhaps half of equation 39 because of the incipient stabilization. That yields the estimate $\gamma_{max} \simeq k_c/4 \simeq \sqrt{\psi}/4L \simeq \sqrt{\psi}/16$. Figure 30

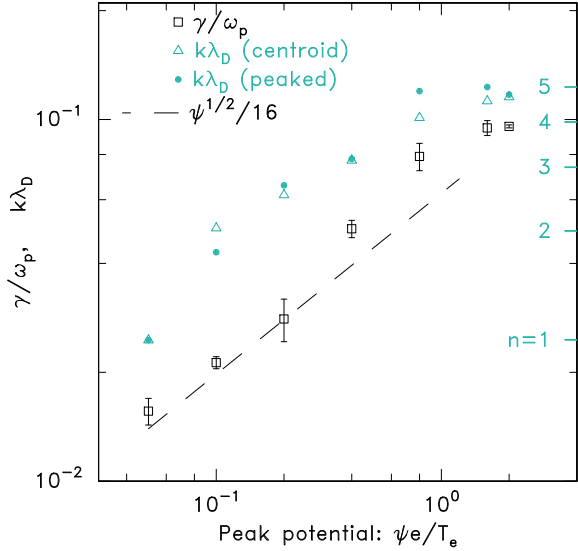


FIG. 30 Comparison of growth rate and wave number observed in simulations with their theoretical estimates. Reprinted with permission from (Hutchinson, 2018a), copyright the American Physical Society (2018), showing agreement within uncertainties.

shows a comparison of these estimates with the observed growth rate and wavenumber of the dominant transverse instability observed in simulations. The agreement is better than approximately 50% (up to a hole amplitude of $\psi \sim 1$), which is within the probable uncertainty of the estimates and observations. Thus, jetting is the mechanism of the transverse instability when magnetic field is negligible. The effect of finite Ω is certainly to weaken the instability, but a rigorous quantitative calculation requires much more detailed mathematical treatment, to be described next.

B. Instability calculation including magnetic field

A full mathematical calculation of the transverse instability based on the jetting approach was undertaken by Hutchinson (2018b), of which a summary description will be given here, omitting many mathematical details. It is a treatment of the time-dependent Vlasov-Poisson system linearized for small potential perturbations relative to a steady one-dimensional nonuniform hole equilibrium. The Vlasov solution for the electrons, which provides the perturbation to the distribution f_1 , is written as an integral over all prior time of the first order acceleration term $\nabla\phi_1 \cdot \nabla_v f_0$, where $\phi_1 = \hat{\phi}(z) \exp(ky - \omega t)$ is the potential perturbation and f_0 is the unperturbed velocity distribution. Linearization implies that the integration path can be approximated as being along the *unperturbed* orbit in

phase space, and the result is

$$f_1(t) = q\phi_1(t) \frac{\partial f_0}{\partial \mathcal{E}_{\parallel}} + q \int_{-\infty}^t \left(i(\omega - kv_y) \frac{\partial f_0}{\partial \mathcal{E}_{\parallel}} + ikv_y \frac{\partial f_0}{\partial \mathcal{E}_{\perp}} \right) \hat{\phi} e^{i(ky - \omega\tau)} d\tau. \quad (40)$$

Here τ is the time prior to the instant under consideration t , and the value of $\hat{\phi}$ in the integral is at the prior orbit position and time $y(\tau), z(\tau)$. The parallel and perpendicular energies are $\mathcal{E}_{\parallel} = q\phi + v_{\parallel}^2/2$ and $\mathcal{E}_{\perp} = v_{\perp}^2/2$ in normalized units. The leading term is called (somewhat misleadingly, but for historic reasons) “adiabatic”, meaning that it is the perturbation that would occur for an infinitesimally slow perturbation. No jetting is contributed by this term. Jetting all comes from the integral term which is the “non-adiabatic” perturbation, and can be written

$$\tilde{f} = iq_e \left((\omega - kv_y) \frac{\partial f_0}{\partial \mathcal{E}_{\parallel}} + kv_y \frac{\partial f_0}{\partial \mathcal{E}_{\perp}} \right) \Phi e^{i(ky - \omega t)}, \quad (41)$$

where

$$\Phi(z_t) \equiv \int_{-\infty}^t \hat{\phi}(z(\tau)) e^{-i\omega'(\tau-t)} d\tau, \text{ and } \omega' = \omega - kv_y. \quad (42)$$

When the magnetic field is ignorable, v_y is simply a constant. This Vlasov solution must in addition satisfy the Poisson equation

$$\frac{d^2 \hat{\phi}}{dz^2} - k^2 \hat{\phi} = -\frac{q_e}{\epsilon_0} \int f_{\parallel 1} dv_z = -\frac{q_e}{\epsilon_0} \left(\hat{\phi} \frac{dn_0}{d\phi_0} + \int \tilde{f}_{\parallel} dv_z \right). \quad (43)$$

In order to proceed, one needs to know the spatial form or forms of $\hat{\phi}(z)$, that is, the eigenmode shape. Unlike the standard wave treatments in a uniform background plasma, the eigenmodes for a solitary hole equilibrium are not Fourier modes ($\exp(ik_z z)$), and if one chose to express the eigenmode shapes in Fourier space they would consist of an infinite sum of coupled Fourier contributions. In principle (Lewis and Symon, 1979) the linearized Vlasov-Poisson problem for a solitary equilibrium is an integro-differential eigensystem for which two sets of basis functions for the potential and for the distribution perturbations ($\hat{\phi}$ and \tilde{f}) are combined by vectors of amplitude coefficients. The system becomes an infinite matrix equation of which the eigenmodes are the required perturbations whose corresponding eigenvalues ω need to be assessed for stability. To form the matrix in its entirety would require a complete set of evaluations of the prior Vlasov integral for the whole basis, which would be overwhelming. Instead, we proceed by realizing that the dominant eigenmode is a parallel shift of the original hole, whose linearized form is $\hat{\phi} = -\xi d\phi_0/dz$, where ξ is the displacement. Although this might be only an approximation to the precise perturbation structure,

the eigenvalue can be found to second order accuracy in any deviation from the shift mode approximation by using the “Rayleigh Quotient” treatment (see e.g. (Parlett, 1974)). A more familiar plasma example of such an approach is the use of the energy principle together with an assumed approximate displacement to estimate MHD instability growth rate for a magnetic confinement configuration. The present application proceeds by substituting the shift mode into the full Poisson equation, multiplying by $\hat{\phi}$, and integrating over all space arriving at

$$F_E \equiv \xi k^2 \int \epsilon_0 \left(\frac{d\phi_0}{dz} \right)^2 dz = - \int \frac{d\phi_0}{dz} q_e \int \tilde{f}_\parallel dv_z dz \equiv F_p + F_t. \quad (44)$$

The value of ω that satisfies this equation is the approximation to the eigenfrequency of the mode. Physically, the left hand side is the net Maxwell stress force on the kinked hole while the right hand side is the jetting force of passing and trapped particles. So the equation is the momentum balance of the hole as a composite entity.

The paper shows that when $k = 0$ then, in the approximation of short transit time such that $e^{-i\omega(\tau-t)}$ in equation 42 can be taken as unity, exactly the same expressions are obtained for the jetting as were derived by the more elementary treatment (eqs 26, 27 in section V.B). And in this approximation the growth rate of the transverse instability with $k \neq 0$ is essentially as given in equation 39, though with minor ($< 50\%$) coefficient corrections at large amplitude $\psi \sim 1$.

The past time integral needed to evaluate the forces *without* short transit time approximation can (after integration by parts) be written

$$\tilde{L}(\omega') \equiv \int_{-\infty}^t (v_z - v_\infty) i e^{-i\omega'(\tau-t)} d\tau, \quad (45)$$

where $\omega' = \omega - kv_y$. For passing orbits v_∞ is the distant velocity, and for trapped orbits it is zero. Then the contribution to the passing and trapped jetting forces per unit perpendicular velocity per unit parallel velocity (which must be integrated $d^2v_\perp dv_\parallel$ over the velocity distribution at $z \rightarrow \infty$ for passing and at $z = 0$ for trapped orbits to give the total) is

$$\frac{dF_{p,t}}{d^2v_\perp dv_\parallel} = i\xi \left(\omega' \frac{\partial f_0}{\partial W_\parallel} + (\omega - \omega') \frac{\partial f_0}{\partial W_\perp} \right) \times \int_{p,t} -q \frac{d\phi}{dz} \omega' \tilde{L}_{p,t}(z, \omega') \frac{dz}{v_z} v_\parallel. \quad (46)$$

All the integrals are carried out numerically and the dispersion relation $F_p + F_t = F_E$ solved to give the growth rate γ as a function of k . The Maxwell stress F_E is mostly ignorable, and the result is in remarkably good agreement with the heuristic estimates explained in section VII.A.

When a uniform magnetic field is present, it is shown that after considerable algebra one can extend the treatment, accounting for the helical orbits (so v_y is sinusoidal in time), using the same function Φ but expanding in integer cyclotron harmonics m with $\omega' = \omega + m\Omega$ instead of $\omega + kv_y$. The harmonics’ coefficients for Maxwellian perpendicular distribution are proportional to $I_m(\zeta_t)$, where I_m is the modified Bessel function and $\zeta_t = k\sqrt{T_\perp}/\Omega = kr_L$ is the finite thermal gyro radius parameter. Thus

$$\tilde{f}_\parallel = \sum_{m=-\infty}^{\infty} i \left[(m\Omega + \omega) \frac{\partial f_{\parallel 0}}{\partial W_\parallel} + m\Omega \frac{f_{\parallel 0}}{T_\perp} \right] \times q_e \Phi_m e^{-\zeta_t^2} I_m(\zeta_t^2), \quad (47)$$

where $\Phi_m(z) \equiv \int_{-\infty}^t \hat{\phi}(z(\tau)) e^{-i(m\Omega + \omega)(\tau-t)} d\tau$. Evaluat-

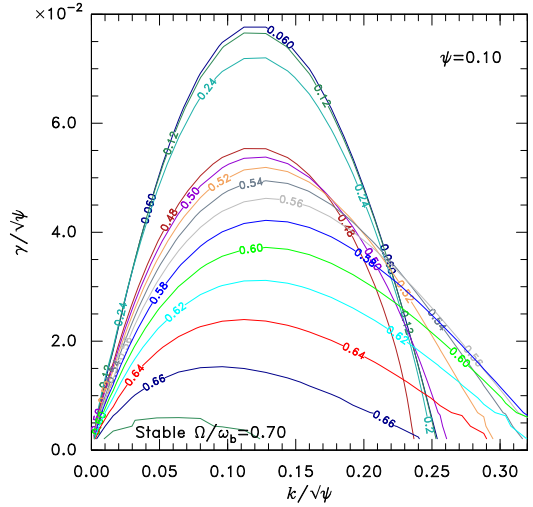


FIG. 31 Growth rate γ of the transverse instability versus wavenumber k , for a range of magnetic field strengths Ω/ω_b (labeling the lines). Reprinted with permission from (Hutchinson, 2018b) copyright Cambridge University Press.

ing \tilde{f}_\parallel , then substituting into $F = F_p + F_t - F_E$ whose zeroes give equation 44 and plotting the zero contour corresponding to equality on the plane (k, γ) , for imaginary frequency $\omega = i\gamma$, gives the results of figure 31. The growth rate and perpendicular wave number are both proportional to $\sqrt{\psi}$ except when ψ is large, ~ 1 . So they are plotted normalized to $\sqrt{\psi}$ giving approximately a universal curve regardless of amplitude ψ .

When the magnetic field is weak $\Omega/\omega_b \lesssim 0.1$ it may be ignored and one gets the unmagnetized result with $k_c = \sqrt{\psi}/4$, $k_{max} = \sqrt{\psi}/4$, and γ_{max} a little larger than $\sqrt{\psi}/16$. As the magnetic field is increased it systematically decreases the peak γ_{max} , and the (pure growth) instability disappears at $\Omega/\omega_b = 0.70$. The reason for the growth suppression is shown quantitatively to be caused by the progressive sign reversal of particle force contributions from orbits more deeply trapped. (All of the

quantitative results are for a sech^4 potential, and ignore ion response.)

This magnetic field threshold $\Omega/\omega_b = 0.70$ for stability is approximately half that observed in simulations. This discrepancy was shown, in Hutchinson (2019b), to be because there is an additional type of instability, not considered in (Hutchinson, 2018b), that has finite real part of frequency as well as imaginary part. It is an oscillating instability, and occurs slightly above this magnetic field strength threshold for purely growing modes. The new results for this mode were obtained using the same analysis but removing the restriction to zero real part of the frequency ω_r . They are also accompanied by detailed comparisons with PIC simulation. Figure 32 shows calcu-

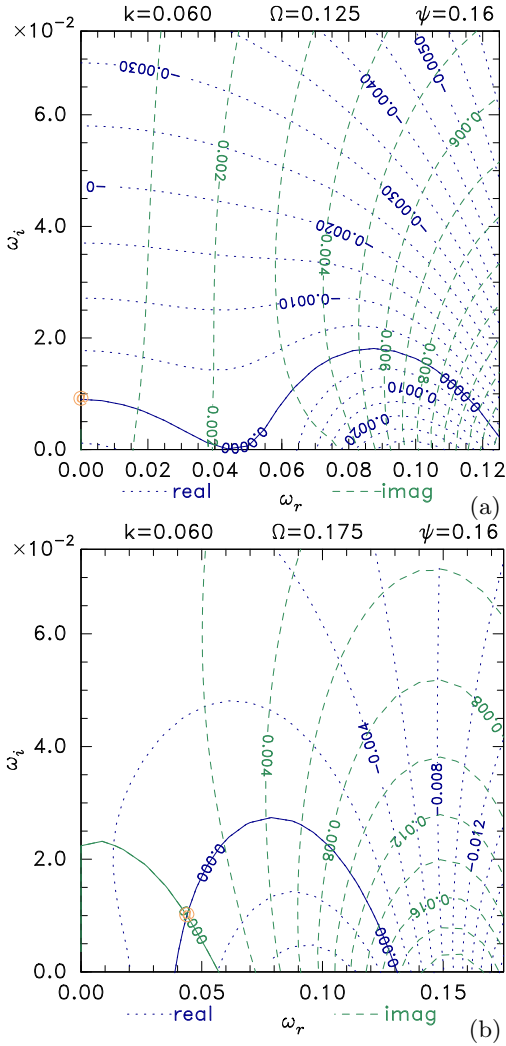


FIG. 32 Contours of the real and imaginary part of the total force F , which are both zero at the eigenfrequency marked $@$. Reprinted with permission from (Hutchinson, 2019b), copyright the American Physical Society.

lated contours of the real and imaginary parts of the total force F that must both be zero at the eigenfrequency, on the complex ω plane, for two cases. (a) has magnetic field

strength $\Omega = 0.125$: below the pure-growth stabilization threshold $\Omega = 0.7\omega_b = 0.7\sqrt{\psi}/2 = 0.14$ (for sech^4 hole amplitude $\psi = 0.16$). It shows an intersection of the real F zero contour (solid blue) with the imaginary F zero contour along the vertical axis, at a purely growing ($\omega_r = 0$) frequency $\omega_i \simeq 0.01$ (marked with $@$). By contrast, in (b) at $\Omega = 0.175$ above the 0.14 threshold, the real F contour no longer intersects the $\omega_r = 0$ axis: no pure-growing instability is present. But it does intersect a branch of the (solid green) imaginary F zero contour at position $\omega = (0.043, 0.01)$ indicating oscillatory growth.

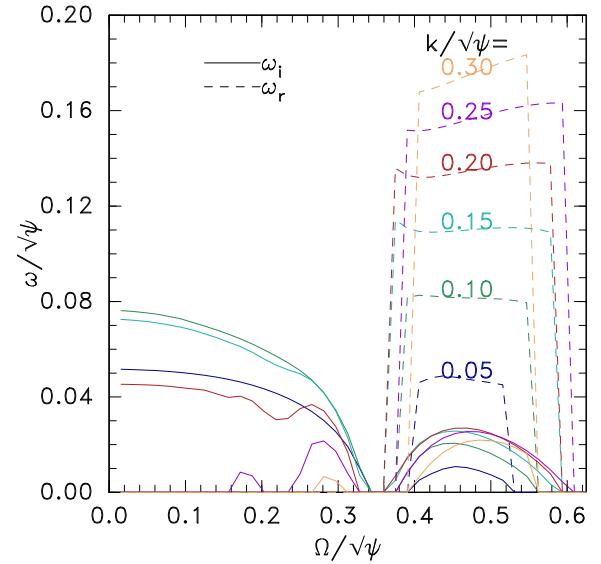


FIG. 33 Real and imaginary parts of the eigenfrequency versus magnetic field strength for a range of wave numbers. Reprinted with permission from (Hutchinson, 2019b), copyright the American Physical Society.

Extensive numerical investigation of unstable eigenfrequencies is summarized in figure 33. As noted previously, for small and moderate ψ , normalizing the frequency and wavenumber by $\sqrt{\psi}$ yields essentially universal curves. Then the real (ω_r dashed line) and imaginary (ω_i solid line) parts of the frequency are plotted versus Ω for the relevant range of wavenumber k . When $\Omega/\sqrt{\psi} < 0.35$ (equivalent to $\Omega < 0.7\omega_b$), pure growing instability occurs ($\omega_r = 0$ and $\omega_i > 0$) for k in the middle of its range. That is the prior result. However for $0.35 < \Omega/\sqrt{\psi} \lesssim 0.6$ a range of oscillatory instabilities occurs whose ω_r is essentially independent of Ω but determined by k . This is responsible theoretically for the extended unstable range of Ω .

The results of PIC simulations of initially one-dimensional sech^4 holes are directly compared with these analytic results over a full range of corresponding parameters.

Figure 34 displays the perturbation mode structure evolution for three magnetic fields. The color contours indicate the PIC's perturbation $\tilde{\phi}$; time is along the hor-

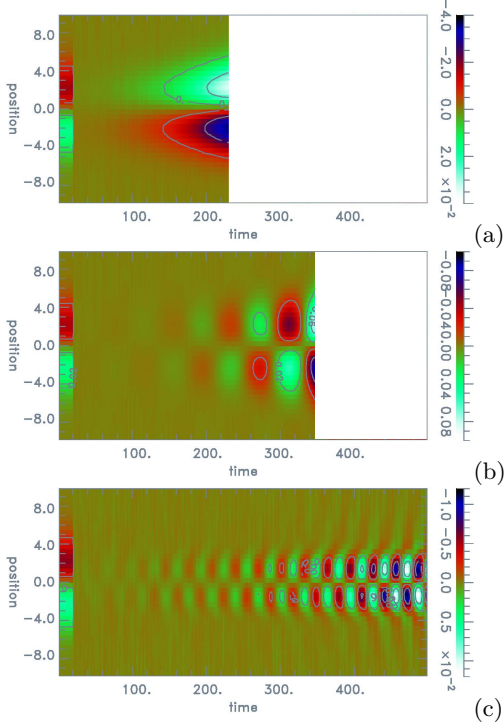


FIG. 34 Simulation instability perturbation parallel structure as a function of time and parallel position, as contours of $\hat{\phi}$. Hole amplitude is $\psi = 0.49$. The three magnetic field strength cases are: (a) $\Omega = 0.2$ (b) $\Omega = 0.25$ (c) $\Omega = 0.45$. Reprinted with permission from (Hutchinson, 2019b), copyright the American Physical Society.

izontal axis; and parallel position z relative to the hole center is on the vertical axis. (Only a local fraction of the total simulated z -length is displayed). At the left ($t = 0 - 20$) is shown an arbitrarily scaled contour of $d\phi_0/dz$, the theoretical shift mode, for comparison with the later growing simulated perturbation. The first case 34(a) has $\Omega/\omega_b = 0.57$ below the threshold (0.7) for pure growth stabilization. It shows pure growth with mode structure highly similar to the shift mode. In figure 34(b), $\Omega/\omega_b = 0.71$ just above the threshold for oscillatory instability, the oscillations are clear, and have comparable mode structure. Figure 34(c), $\Omega/\omega_b = 1.29$ ($\Omega/\sqrt{\psi} = 0.64$) is at the upper end of the observed overstable region, and slightly above the analytic limit of instability ($\Omega/\sqrt{\psi} = 0.6$) shown in figure 33. Its mode structure is narrower than the shift mode, showing that there is some deviation from the analytic mode approximations, which explains the slightly extended unstable range.

With the exception of this extension and a more gradual cut off of the simulations' growth to near zero at high Ω , the detailed comparison of 25 simulations shows very good agreement with analysis of the real frequency (better than $\sim 20\%$, despite some limitations attributable to discrete k enforced by limited y simulation length); excel-

lent agreement ($\lesssim 5\%$) with the Ω -thresholds for mode oscillation and growth; and good agreement with growth rates.

C. Strong magnetic field approximation

The remarkable agreement with simulation of the analysis of magnetic field stabilization of the transverse instability confirmed the identification of the instability mechanism; but it left open some important indications that, at even higher magnetic field, a new type of instability with much longer transverse wave-length and much lower frequencies persists. This strong-field region instability probably corresponds to what was observed in the earlier high-field simulations of (Goldman *et al.*, 1999; Lu *et al.*, 2008; Newman *et al.*, 2001b; Oppenheim *et al.*, 1999, 2001; Umeda *et al.*, 2006; Wu *et al.*, 2010), usually in association with coupled long-parallel-wavelength potential waves, identified as belonging to the “whistler” wave branch. In figure 34(c) (which is actually not in the high field regime) one can see similar coupled streaks, but with higher frequency, extending up and down to distances far beyond the localized oscillating mode.

In Hutchinson (2019a) the high-field limit was addressed. It can be analyzed in the approximation of purely one-dimensional motion of the electrons, which corresponds to the general magnetized analysis when only the $m = 0$ cyclotron harmonic needs to be retained. Using the general numerical Vlasov solution, the contours of force obtained are shown in figure 35(a). The real and imaginary parts of the mode frequency ω_r and ω_i are observed to scale such that if they are normalized as $\hat{\omega}_r = \omega_r/\psi^{3/4}$ and $\hat{\omega}_i = \omega_i/\psi^{3/2}$ (not the same factor as before, or as each other), then contours that are essentially universal are obtained at small ψ . Contours of the real part of F are to an excellent approximation vertical lines. The horizontal positions of those lines are determined by the value of k through the real part of equation 44, i.e. the real part balance between jetting and the transverse Maxwell stress ($\propto \xi k^2 \psi^2$). The imaginary part zero contour is approximately triangular in shape and independent of k . For this particular k , the real part zero contour intersects it at its peak. This k is the mode with the greatest ω_i , the fastest growing.

A fully analytic linearized treatment of the stability of a sech^4 potential shape hole is given in this work, which treats the shift mode in the one-dimensional motion limit. It identifies three main force terms contributing to the imaginary F . These are (i) the imaginary trapped electron force arising from resonance between the bounce frequency and the mode real frequency: F_R , (ii) the intrinsically imaginary part of the passing particle force F_p , and (iii) the non-resonant part of the electron force: F (mostly trapped) whose imaginary part arises only because of the imaginary part of ω and the

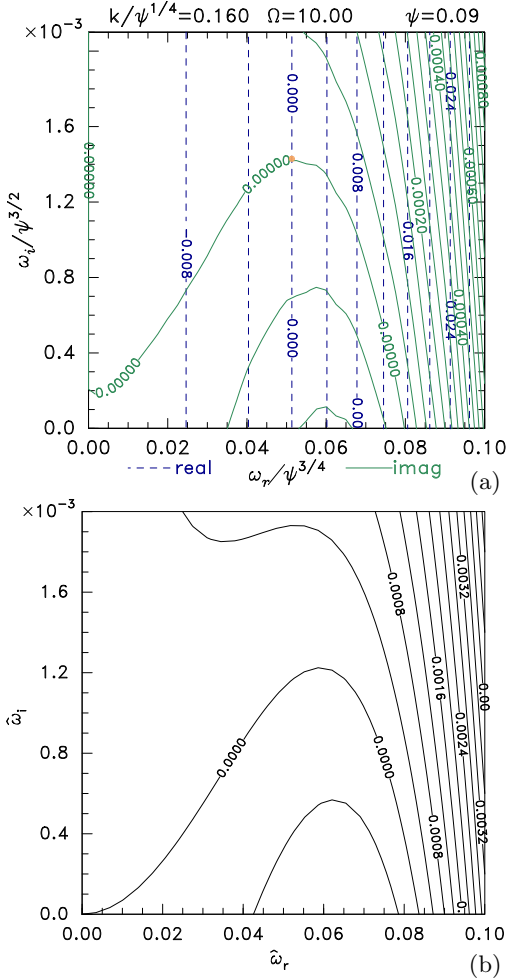


FIG. 35 Comparison of (a) the numerically calculated force contours, with (b) the imaginary part contours of the analytic approximation, showing good agreement. Reprinted with permission from (Hutchinson, 2019a) copyright Cambridge University Press.

fact that $F \propto \omega^2$. These are evaluated analytically using square-wave approximations of the trapped position $z(t)$ (because the orbits dwell much of the time near their turning points), and of the positional advance of the passing particles $z - v_\infty(t - t_0)$ (because this advance mostly occurs near the potential peak $z = 0$). The total for small ω_i is

$$\Im(F) = \Im[F_R + F_p + 2i \frac{\omega_i}{\omega_r} F(\omega_r)] = \xi[C_t \omega_r^5 / \psi^{1/2} + C_p \omega_r^2 \psi + C_i \omega_i \omega_r \psi], \quad (48)$$

where the coefficients are obtained by the integration approximations as $C_t \simeq 1000$, $C_p \simeq -7$, and $C_i \simeq 10$. The scaling relations $\hat{\omega}_r = \omega_r / \psi^{3/4}$ and $\hat{\omega}_i = \omega_i / \psi^{3/2}$ render the scaled expression

$$0 = \Im(F) = \xi \psi^{13/4} \hat{\omega}_r [C_t \hat{\omega}_r^4 + C_p \hat{\omega}_r^2 + C_i \hat{\omega}_i], \quad (49)$$

showing why the frequency scalings have the form they

do (and that the scaling for force is $\hat{F} = F / \psi^{13/4} \hat{\omega}_r$ though this scaling is not applied in the figure). Figure 35(b) shows the analytic contours of $\Im(F)$. The comparison with the numerical figure 35(a) is very satisfactory. It should be noted how extremely small the growth rate ω_i is even for $\psi \sim 1$ and that it quickly becomes much smaller ($\propto \psi^{3/2}$) for smaller ψ . The absolute relationship between k and ω_r for this shaped hole is $k^2 = (315/256) C_i \omega_r^2 / \psi$, which is $k / \psi^{1/4} = 3.5 \hat{\omega}_r$.

The overall agreement between numerical evaluations and analytic approximations is strong confirmation of the correct identification of the key components of the force that need to be balanced. The identification shows that the resonant force has a *stabilizing* contribution, not, as has often been assumed in prior theories, a destabilizing one. This counter-intuitive situation results from the fact that the hole mass is negative, and the instability is a negative energy mode (Lashmore-Davies, 2005) (which grows as its energy becomes more negative).

The same paper (Hutchinson, 2019a) reports comparisons of the theory with new PIC simulations. These prove to be in good agreement with the theory on the ratio k / ω_r of the unstable modes, but only qualitative (of order factor of 2) agreement in growth rates, with the simulations showing larger growth rates when instability occurs. This is attributed to the fact that the maximum growth rate is determined by the stabilizing resonant force at very low frequencies corresponding to trapped particle orbits very close to $\mathcal{E} = 0$, at which there is (in theory) a discontinuity in the distribution slope. Any stochastic orbit wandering or numerical effective collisionality in the simulation there is liable to reduce df/dv , and hence reduce the resonant stabilization (i.e. make the hole more unstable).

It is observed, as in prior simulations, that small changes in the computational domain size can suppress or enhance instability. This implicates resonant whistler wave effects in finite domains as influential in simulations (but not necessarily in nature), but it does not show that coupling to whistler waves is the mechanism of instability, as has sometimes been proposed. In contrast, what is shown is that there is an instability for which coupling to whistler waves, though sometimes relevant in simulations, is unnecessary to its mechanism.

Umeda *et al.* (2006) observed no instabilities in their high field simulations with hole potential below $\psi = 0.8$. Somewhat similarly, in the present simulations no instabilities that grew to substantial amplitude were observed even up to time 10,000 for initial hole heights $\psi < 0.4$. There was some evidence of competition between different transverse modes at quite low amplitude.

Summarizing the high magnetic field (one-dimensional motion) transverse instability: there is theoretically a very slowly growing oscillatory instability $\omega_i \sim 10^{-3} \psi^{3/2}$, that has been observed in simulations only for deep holes $\psi > 0.4$. Its mechanism does not depend on coupling

to whistler waves, but it is observed to excite them (as do other oscillatory hole instabilities). Its destabilization is by the imaginary component of the passing particle jetting (F_p); the resonant trapped particle force F_R is a counterbalancing stabilizing effect. The real frequency of the fastest growing mode (of transverse wavenumber k) is $\omega_r \simeq 0.3k\sqrt{\psi} \simeq 0.05\psi^{3/4}$.

D. Ion response effect on transverse instability

All the preceding discussion of this section is of electron holes in which ion response is ignored, justified by supposing the holes fast compared with the ion velocity distribution. However, in Hutchinson (2022) the transverse instability theory of slow electron holes including ion response, was presented. It also addressed the one-dimensional consequences for the dynamics of the slow holes summarized for this review in subsection V.D.

The many degrees of freedom of this more complicated situation have not all been explored but the paper presents two representative figures of the dependence of the complex frequency on ion distribution shape, transverse wavenumber, and magnetic field strength. Broadly speaking, ion distributions that are double humped with the hole velocity lying in their local minimum, represented by two equal Maxwellians shifted by $v_s = 1.3$ (compare figure 26) show the least effect of ion response on the transverse instability, and indeed when amplitude is small ($\psi = 0.01$) the results are little changed by ion response. At moderate amplitude ($\psi = 0.09$), however, the effect is to increase the growth rate of the intermediate regime ($0.35 < \Omega/\sqrt{\psi} < 0.6$) oscillatory instability by perhaps a factor of two, and to cause the high field ($0.6 < \Omega/\sqrt{\psi} < 1$) regime to have a growth rate $\omega_i/\sqrt{\psi} \sim 0.03$, comparable to the intermediate, and much higher than the strong magnetic field approximation for electron-only response.

For a single-humped ion distribution ($v_s = 1$), the destabilization of the high field regime is present even for low amplitude ($\psi = 0.01$). Moreover the intermediate and high field regime instabilities become purely growing ($\omega_r = 0$) for some longer transverse wavelengths, showing that the ion reflection force hole acceleration mechanism, which for a single-humped distribution gives pure growth, has begun to be more important than the electron jetting. At $\psi = 0.09$ these single-humped ion interactions dominate all but the shortest transverse wavelengths, and the growth rates are several times higher than when ion interactions are absent. Thus, ion reflection forces for slow electron holes of moderate depth in single-humped ion distributions strongly enhance the transverse instability and make the fastest growing modes of longer transverse wavelength. There is doubtless scope for further theoretical and computational exploration of the transverse instability of slow electron holes.

E. Generalized multi-mode transverse instability

Although the mechanisms of transverse hole instability are comprehensively identified in the prior subsections, there remain some quantitative discrepancies in the comparisons with simulation that are thought to arise from the fact that the actual linearized perturbation potential structure is not exactly the shift mode that has been assumed. An appropriate challenge is then to establish a theory that predicts the modification of the eigenmode by deviations from the shift mode, and how much that changes the instability eigenvalue (ω). In effect, this is the challenge that the early work of Lewis and Symon (1979) analyzed and set forth an outline mathematical program to solve. For non-linear wave states Schwarzmeier *et al.* (1979) used this technique to solve for the unstable merging of adjacent peaks of a periodic wave. Much later Siminos *et al.* (2011) used a Fourier method to construct the predominant eigenmode for this one-dimensional problem.

However, the very few previous attempts to implement such a program for the electron hole transverse instability were unsuccessful either because of incorrect identification of the predominant form of the instability (e.g. addressing symmetric perturbations instead of antisymmetric) or because their method of integrating the Vlasov equation was inappropriate. Theoretical coupling to whistler waves was previously investigated based on ad hoc assumptions about the coupling strength that were not well justified. Calculating this coupling rigorously is formally part of the same mathematical program. The recent work of Chen and Hutchinson (2023) successfully carried out a rigorous analysis of this problem for sech^4 shaped electron hole equilibria, as will now be explained.

The unstable linearized eigenmode $\hat{\phi}(z)$ of a solitary potential structure is not exactly the shiftmode when ω is finite. In principle it can be represented exactly by a weighted sum of any complete (infinite) set of functions. The prescription of (Lewis and Seyler, 1982; Lewis and Symon, 1979) is that the most convenient functions are the eigenfunctions of the adiabatic Poisson operator. For an equilibrium of the form $\phi_0(z) = \psi \text{sech}^4(z/4)$, the adiabatic operator is

$$V_a = \left[\frac{d^2}{dz^2} - \frac{\phi_0'''}{\phi_0'} \right] = \left[\frac{d^2}{dz^2} + \frac{30}{16} \text{sech}^2(z/4) - 1 \right], \quad (50)$$

It can be shown that the eigenmodes of this operator that satisfy $V_a|u\rangle = \lambda|u\rangle$ (using bra-ket notation) consist of just 5 discrete eigenmodes of limited z -extent, plus a continuum of eigenmodes that extend to $|z| = \infty$ with sinusoidal behavior far from the hole. Figure 36 illustrates these eigenmodes. Of the discrete modes numbered 1-5, three are symmetric (1,3,5), and two are antisymmetric (2,4). Mode 4 is the shift mode, which, normalized to

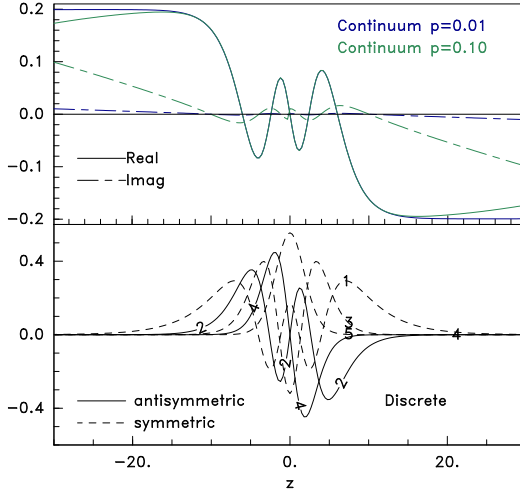


FIG. 36 The eigenmodes of the adiabatic Poisson operator. Reprinted with permission from (Chen and Hutchinson, 2023) copyright Cambridge University Press.

make $\langle u|u \rangle = \int u^* u dz = 1$, is

$$|4\rangle = -3 \tanh(z/4) \operatorname{sech}^4(z/4) \sqrt{70}/16, \quad (51)$$

proportional to $d\phi_0/dz$. The other modes, including the continuum, similarly have analytic forms helpful for evaluation. They will not be given explicitly here. The eigenvalues can be written

$$\lambda_u = u^2/16 - 1, \quad (52)$$

where u is the integer mode number for the discrete modes and for the relevant antisymmetric continuum modes u is equal to $4i\sigma_z k_z = i\sigma_z p$, where k_z is the positive parallel wavenumber of the mode in the external sinusoidal region, and σ_z is the sign of z . The shift mode $|4\rangle$ eigenvalue λ_4 is zero. That is why it is the dominant mode, and is exactly the relevant mode in the limit of low frequency.

For an infinitesimally small ω these eigenmodes are exactly the eigenmodes of the linearized Vlasov-Poisson problem, and are uncoupled from one another. However, when ω is finite, the Vlasov-Poisson problem acquires a non-zero non-adiabatic contribution that is written as a non-adiabatic operator \tilde{V} , such that Poisson's equation becomes

$$(-k_\perp^2 + V_a + \tilde{V})|\hat{\phi}\rangle = 0, \quad (53)$$

where the squared transverse wavenumber $k_\perp^2 \equiv \lambda_\perp$ can be considered the full eigenvalue. The operator \tilde{V} couples the adiabatic eigenmodes together, but since they are a complete set, any perturbation mode can be written as a weighted sum and integral of eigenmodes: $|\hat{\phi}\rangle = \sum_{j,\text{discrete}} a_u |u\rangle + \int_{p,\text{continuum}} a(p) dp$, where $p = u/i\sigma_z$ is real and positive. The sums and integrals are limited to the antisymmetric forms when considering the dominant

transverse instability. No coupling arises between symmetric and antisymmetric modes. Substituting into Poisson's equation, left-multiplying by any adiabatic eigenmode $\langle s|$, and using the orthogonality of the eigenmodes, we get

$$0 = (\lambda_s - \lambda_\perp) \langle s|s \rangle a_s + \sum_j \langle s|\tilde{V}|j\rangle a_j + \int \langle s|\tilde{V}|p\rangle a(p) dp. \quad (54)$$

This is a matrix equation $\mathbf{Ma} = 0$ in which the off-diagonal matrix elements arise from the non-adiabatic couplings $\langle s|\tilde{V}|j,p\rangle$, and which, if ω and hence \tilde{V} is specified, requires a specific value of λ_\perp to make $|\mathbf{M}| = 0$ and permit a solution for the coupled mode amplitudes \mathbf{a} . Actually it is more convenient in practice to take λ_\perp as fixed and find iteratively the ω that then makes $|\mathbf{M}| = 0$.

As it stands, the continuum integral makes this an infinite dimension matrix. Moreover the inner products $\langle s|\tilde{V}|p\rangle$ for the continuum involve an infinite domain z -integral over which the continuum adiabatic eigenfunctions remain finite. However, the paper shows that the continuum contributions for any frequency are concentrated about a specific parallel wavenumber (i.e. p -value) that satisfies the sinusoidal wave dispersion relations (for kinetic electrostatic whistler waves) in the external region. The p -integral over that small range can be carried out analytically. It is therefore possible to approximate all the continuum contributions into a single amplitude $a_q = \int a(p) dp$ and the entire coefficient vector as $\mathbf{a} = (a_2, a_4, a_q)$ representing the two antisymmetric discrete adiabatic eigenmodes plus the continuum, and approximate the matrix \mathbf{M} as 3×3 . The infinite z -integrals can be handled by subtracting a purely multiplicative sinusoidal wave operator V_w . Calculating the matrix elements still requires numerical evaluation for the electron hole region, but the external region integrals can be obtained analytically. Thus, the initially overwhelming dimensionality of the eigenmode problem is reduced to finding the zero of the determinant of the complex 3×3 matrix \mathbf{M} . When $|\mathbf{M}| = 0$, it has just two independent rows, and solving $\mathbf{Ma} = 0$ determines the direction of the vector \mathbf{a} , in the form of two values a_2/a_4 and a_q/a_4 : the coupling coefficients of the subdominant modes to $|4\rangle$. Incidentally, the upper right matrix diagonal coefficient is simply the shiftmode $|4\rangle$ force, assumed in the previous work to be the total to be zeroed. The multimode analysis generalizes the calculation.

Completing this analysis thus provides both the corrections to the perturbation eigenmode shape, and the coupling between the hole shift-mode and the external "whistler" waves. Figure 37 summarizes extensive numerical calculations. The upper part of (a) shows shift-mode (pure $|4\rangle$ eigenmode) frequencies ω as a function of Ω for four values of k_\perp , and the lower part shows the difference $\delta\omega$ that must be added to ω to obtain the calculated multimode value. Those differences are of order

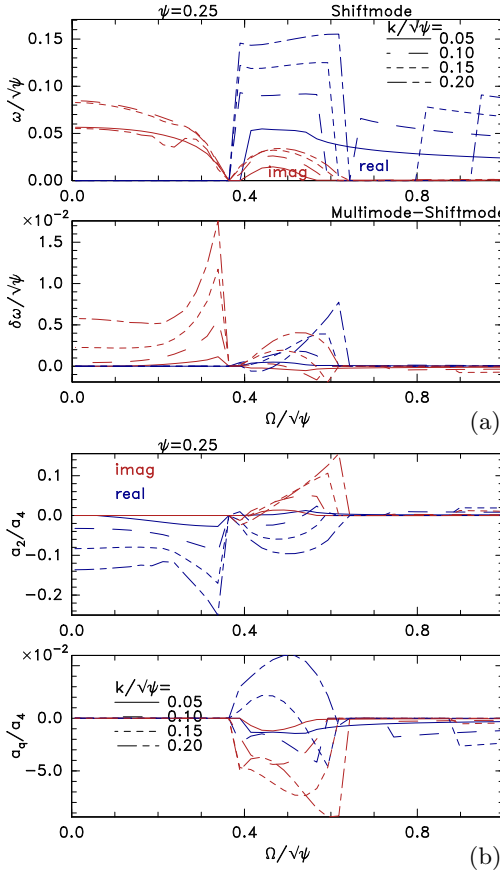


FIG. 37 (a) Shiftmode frequency, and the difference multimode - shiftmode frequency, real (red) and imaginary (blue) parts. (b) Relative amplitude of the secondary discrete mode (a_2) and the continuum mode a_q . Reprinted with permission from (Chen and Hutchinson, 2023) copyright Cambridge University Press.

< 10% growth rate increase for the low- Ω purely growing instability (except near its upper threshold); and similar for the intermediate oscillatory regime. In the high field regime the differences are very small and stabilizing. Figure 37(b) shows the corresponding secondary mode relative amplitudes. The value of a_q/a_4 is the coupling to the continuum mode, which is substantial only in the oscillatory regimes, in accordance with simulation observations.

The contribution of the secondary discrete mode is illustrated more intuitively in figure 38, which shows the parallel shape of the unstable shiftmode and multimode calculations, together with a corresponding observed mode structure in a PIC simulation. The parameters of this case are close to the upper end of the intermediate (oscillatory) Ω -range. Concentrating on the real part, it is clear that the addition of the $|4\rangle$ discrete mode component *narrow*s the mode structure, making it much closer to the observed PIC shape than the shiftmode alone.

In summary, the multimode analysis demonstrates mathematically that using the shiftmode slightly under-

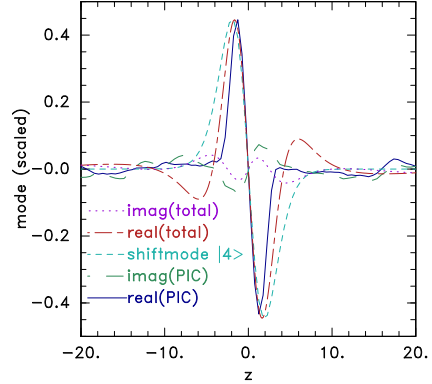


FIG. 38 Real and imaginary parts of the unstable mode spatial structure, for shiftmode and total multimode, compared with observed mode structure in a PIC simulation. Reprinted with permission from (Chen and Hutchinson, 2023) copyright Cambridge University Press.

estimates the growth rate of the transverse instability near its upper threshold. In part at least, this is because the true unstable perturbation structure is narrower than the shiftmode, which emphasizes the unstable contribution of deeper trapped orbits over the stabilizing contribution of marginally trapped orbits, in accordance with prior qualitative considerations.

VIII. MULTI-DIMENSIONAL HOLES

This section addresses some important phenomena that are inherent to holes of limited transverse extent.

A. Equilibria

It is of course only an approximation to treat electron holes as purely one-dimensional in space. Multi-dimensional equilibria have in addition been explored for a long time in the literature. Higher dimensionality introduces several different new effects. The first and perhaps most obvious is that for a hole of finite transverse dimensions Poisson's equation must be written $\nabla^2\phi = -\rho$, and the transverse derivatives provide a new contribution. References (Chen and Parks, 2002; Schamel, 1979) take the form of the hole to be separable and the transverse contribution to arise from the radial derivative. Since the particle motion is taken still to conserve parallel energy, the main effect is to require more charge deficit to support a particular peak potential $\psi(z = 0, r = 0)$. The one-dimensional motion limit is also assumed in (Chen *et al.*, 2004; Krasovsky *et al.*, 2004b) but with Gaussian radial variation, and (Muschietti *et al.*, 2002) used transverse Gaussian but $\text{sech}(z)$ parallel shape with variably flattened top. The work of Krasovsky *et al.* (2004b) proceeded instead from a prescribed trapped particle dis-

tribution that varied linearly with $-\mathcal{E}$ for $\mathcal{E} < \mathcal{E}_j$ but was constant for $\mathcal{E}_j < \mathcal{E} < 0$. The mathematical convenience of this choice is that the Poisson equation takes the Helmholtz form $(\nabla^2 + k^2)\phi = \text{const}$.

Although assuming separable potential form is mathematically convenient, it is never in fact accurate in the distant regions of a multidimensional hole. The reason is that when the potential is small, Debye shielding is the dominant effect, it gives a modified Helmholtz equation (i.e. with negative constant $k^2 = -1/\lambda_D^2$). Thus, in an axisymmetric hole at $z = 0$ and large transverse distance r , $\frac{d\phi}{dr} \simeq \phi/\lambda_D$ and $\frac{d\phi}{dz} = 0$, while at $r = 0$ and large $|z|$, $\frac{d\phi}{dz} \simeq \phi/\lambda_D$ and $\frac{d\phi}{dr} = 0$. These limits are incompatible with a separable form.

Aiming to discover how serious these inconsistencies are for multidimensional holes, Hutchinson (2021d) developed a more general approach to synthesizing such holes based on a general prescription of the trapped parallel velocity distribution $f_t(\mathcal{E})$ allowing various parallel (z) hole shapes, and a desired radial peak potential variation $\psi(r)$. The parallel distribution chosen allows an analytic solution of the one-dimensional parallel differential equation incorporating an approximation of the transverse field divergence. This solution finds the approximate $f_t(\mathcal{E}, r)$ parameters to yield the desired $\psi(r)$. The scheme then iteratively solves the unapproximated multidimensional Poisson equation to find the entire two-dimensional (r, z) variation of the potential self-consistently with the prescribed $f_t(\mathcal{E}, r)$.

Figure 39 shows an example. The color contours in (a) indicate the the trapped electron density deficit \tilde{n} relative to a flat plateau distribution. The passing density is set by the background velocity distribution (and orbit energy conservation). The lines are logarithmic potential contours. The radial and parallel positions are on identical scales. Notice the equal spacing of the contour lines all the way round, for distances beyond the colored region. It arises from the predominantly passing particle Debye shielding giving effectively a modified Helmholtz equation there with constant $\nabla^2\phi/\phi = 1/\lambda_d^2$. In the inner regions, the line contours do not follow the color contours, because the trapped density is a function of r as well as of ϕ . This was found to be a general property of axisymmetric holes of limited transverse size. Velocity distributions that depend only on ϕ are self-consistent only when exactly spherical, even when limited to purely parallel motion, demonstrating that the proposed equilibria of (Krasovsky *et al.*, 2004b) are unphysical.

Satellite observations of electron holes generally consist of measurements of the electric field components along a passage through the hole in approximately the parallel direction at constant r , because of the hole's high parallel velocity. Frequently the ratio of the peak electric field in the perpendicular and parallel directions is taken as indicative of the ratio of the hole extents in the parallel and perpendicular directions; in other words it

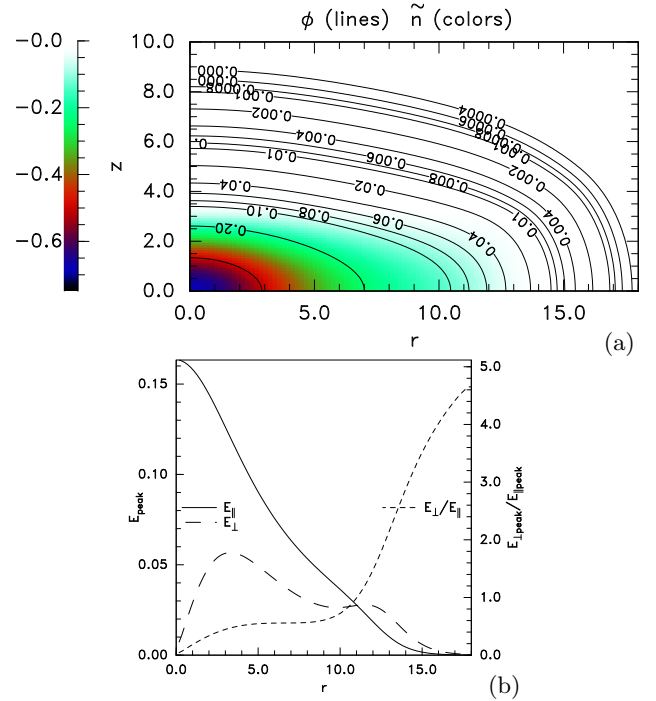


FIG. 39 A fully consistent axisymmetric electron hole. (a) Potential and density-deficit contours. (b) Peak electric field variation with track radius. From Hutchinson (2021d).

is assumed $L_{\parallel}/L_{\perp} \simeq E_{\perp}/E_{\parallel}$. Although this measure is heuristically plausible, the actual observed peak field ratio depends on the radius of the satellite track. Figure 39(b) documents the observational variation for the oblate hole of 39(a), of the peak E_{\perp} and E_{\parallel} , and their ratio, as a function of track radius. The typical contour aspect ratio, L_{\parallel}/L_{\perp} is approximately $\frac{1}{3}$, but the corresponding observed field ratio varies between zero and approximately 0.6 in the strong field region and rises to values substantially greater than 1 in the radial wings. This disappointingly wide range of uncertainty in the relationship between peak E ratio and hole potential shape shows that caution is required in interpreting the field ratio; and it re-emphasizes the importance of multi-satellite simultaneous observations of holes in order to determine their shape.

Tong *et al.* (2018) report such simultaneous measurements in MMS data from the PSBL, where all four satellites encounter the hole. Assuming the gradients of electric field are constant over the satellite tetrahedron, they can be obtained from the electric field measurements, and provide an estimate of the divergence $\nabla \cdot \mathbf{E}$, which is the charge density. The observed charge densities are either tri-polar (-+-), or purely negative, consistent with passing respectively through either the central or wing regions of an electron hole. The hole shape is estimated by fitting a theoretical potential profile of the form

$$\phi = \psi \exp([z - z_0]^2 / 2d_{\parallel}^2) \mathcal{H}(\mathcal{R}) \quad (55)$$

where $z_0 = v_h t$ is the moving parallel potential peak, and $\mathcal{R}^2 = (x - x_0)^2/d_{min}^2 + (y - y_0)^2/d_{max}^2$, is constant on ellipses with a single center x_0, y_0 , in the transverse plane, whose minor and major axes x and y have been rotated to minimize the difference between the predicted and observed field variation at the four satellites. The most successful of the radial dependencies explored was found to be $\mathcal{H} = \exp(-\mathcal{R}^2/2)$. Of the dozens of holes examined, four were able to be adequately fitted in this way, and many others were not, for reasons not entirely explained. Two of the fits were close to axisymmetry: $d_{max}/d_{min} \lesssim 1.3$; but two were not: $d_{max}/d_{min} \simeq 2$ and 3. The oblateness of the fitted holes, d_{min}/d_{\parallel} was in the range 1 - 2, which is consistent with the empirical scaling of Franz *et al.* (2000), eq. (25).

The study of Steinvall *et al.* (2019) instead fitted an axisymmetric model $\phi = \psi \exp(-z^2/2l_{\parallel}^2 - r^2/2l_{\perp}^2)$ of hole potential to 4-satellite MMS observations of 236 slow electron holes at the magnetopause. The E_{\perp}/E_{\parallel} is small, predominantly between 0.1 and 0.5, which is consistent with the ratio Ω/ω_p (~ 0.1 to 0.2) being small. But the scaling of eq. (25) is not reproduced within the data. The model implies $l_{\perp} = \sqrt{\psi r/E_{\perp}}$, which can be used to deduce values of l_{\perp} if the hole center (and satellite position) is known giving r . But only for 10 holes was a consistent hole center identified, and the deduced l_{\perp}/l_{\parallel} for them varied from < 2 to ~ 6 without identified cause. Several instrumental and noise factors were cited as possible reasons for the inconsistency of the model in the rest of the cases, as well as the possibility of non-axisymmetric hole shapes.

The observational evidence concerning hole shapes seems therefore to indicate holes have considerable variety. Weak magnetic field strength favors oblate electron holes, and strong field seems to permit spherical or even prolate holes. But in nature electron holes often seem not to be axisymmetric, and it is unclear what determines how close they are to axisymmetry.

B. Gyro orbit effects and Scattering

Finite electron gyro-radius implies that electrons in holes do not move purely along the magnetic field. In a spatially one-dimensional situation (uniform in the x and y directions) no new effects enter into the *equilibrium*, though translational symmetry can be broken by transverse instabilities. There are, however, two indubitable effects of finite gyro-radius on hole equilibria of limited transverse size. One is an effective transverse averaging over the gyro-radius of the parallel potential gradient, which impedes electron trapping when the transverse hole size is small. The other is that resonant coupling between the electron bounce frequency and the gyro-frequency in the presence of perpendicular electric field causes energy transfer between parallel and perpendicu-

lar electron energy (even though the total kinetic plus potential energy is exactly conserved). This transfer makes the parallel energy increase or decrease, and can thereby detrap particles with negative parallel energy near zero, and trap passing particles with small positive parallel energy. A third proposed mechanism is sometimes attributed to a supposed gyrokinetic modification of the effective perpendicular plasma dielectric response; this last mechanism does not actually apply to phase-space holes, and references to it are misleading.

The errors involved in invoking a supposed “gyrokinetic” dielectric response are explained in Hutchinson (2021c). The original speculation by Franz *et al.* (2000) (often cited thereafter (Berthomier *et al.*, 2003; Fu *et al.*, 2020; Holmes *et al.*, 2018; Jovanović *et al.*, 2002; Tong *et al.*, 2018; Vasko *et al.*, 2017a, 2018a; Wu *et al.*, 2010)) was that their observations fitted by equation 25 could be explained by a modified Poisson equation of the form

$$\left[\nabla_{\parallel}^2 + \left(1 + \frac{\omega_{pe}^2}{\Omega^2} \right) \nabla_{\perp}^2 \right] \phi = (n_e - n_0), \quad (56)$$

which they attributed to gyrokinetic theory. However, the extra term ω_{pe}^2/Ω^2 arises in the equations which they cite in a more complicated way than a simple polarization drift. The actual gyrokinetic expression for transverse permittivity is $\epsilon_{\perp} = 1 + [1 - \Gamma_0(\zeta_t^2)]/(k_{\perp}^2 \lambda_{De}^2)$, where the finite gyro-radius parameter is $\zeta_t = k_{\perp} \sqrt{T_{\perp}}/\Omega = k_{\perp} r_L$, and $\Gamma_0(\zeta_t^2) = e^{-\zeta_t^2} I_0(\zeta_t^2)$. It reduces to approximately $\epsilon_{\perp} = 1 + \omega_{pe}^2/\Omega^2$ only in the limit that both $\zeta_t^2 \ll 1$ and $k_{\parallel}/k_{\perp} \ll 1$. But neither of these parameters is small in an electron hole for which ω_{pe}^2/Ω^2 is not small. So adopting equation 56 for electron holes is erroneous when ϵ_{\perp} is significantly different from unity; it is an abuse of gyrokinetic equations. Quite apart from that, the effect of a steady electrostatic structure on the density of the attracted charge species is a long-studied plasma problem related to probe theory (Al'pert *et al.*, 1965; Hutchinson and Patacchini, 2007; Laframboise, 1966; Laframboise and Sonmor, 1993; Lampe *et al.*, 2001) in which no such anisotropic shielding is introduced. The only difference with an electron hole is the absence of particle absorption, which is a simplification. The paper (Hutchinson, 2021c) reports a collisionless PIC simulation of a spherical potential structure with a wide range of applied magnetic fields, demonstrating that there is no anisotropy in the shielding that would be implied by equation 56. Equation 25 may be empirically useful, but the gyrokinetic shielding explanation of it is incorrect.

The resonant trapping/detrapping phenomenon is explored in Hutchinson (2020), by numerical orbit integration and by analytic calculation of the resonant island widths in an axisymmetric ($\phi = \phi(r, z)$) electron hole. These two approaches are found to agree remarkably well. Figure 40 shows a so-called Poincaré plot of numerical orbits. Many orbits having different starting parallel en-

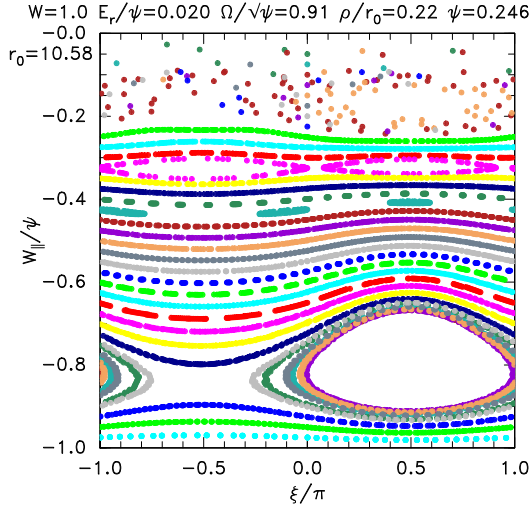


FIG. 40 Poincaré plot in the space of parallel energy versus gyro-phase of electron orbit evolution in a transverse electric field. From Hutchinson (2020).

ergy are followed. Each is a specific color, and a point is plotted on this graph each time the orbit passes $z = 0$, corresponding to its parallel energy $W_{\parallel} = \mathcal{E}_{\parallel} = v_{\parallel}^2/2 + q\phi$ and the phase of the gyro-motion $\xi = \tan^{-1}(v_r/v_{\perp})$ as it does so. This example has starting radius $r_0 = 10.58$, at which the hole equilibrium has a chosen radial electric field $E_r = -d\phi/dr = 0.02\psi$. The potential peak at this radius is $\psi = \phi(r_0, 0) = 0.246$, and the magnetic field strength is $\Omega = 0.91\psi$. The total particle energy, which is perfectly conserved, is $W = 1$ and mostly consists of perpendicular kinetic energy $v_{\perp}^2/2$. The resulting gyro radius is $\rho = 0.22r_0$. Orbit at the more negative W_{\parallel}/ψ , from about -0.23 downward to the most negative possible value -1, are observed to follow stable tracks. The open tracks correspond to non-resonant orbits, moderately perturbed in W_{\parallel} by transfer to and from W_{\perp} , but never reversing their direction of phase advance. The closed tracks surround resonances where the gyro frequency equals an even harmonic of the bounce frequency. The resonance is sufficiently strong to produce an island in the Poincaré plot on the tracks of which the phases of bounce and gyration remain within a limited region. At some discrete parallel starting energy there is a separatrix between the open and closed tracks (for example the upper pink track at $W_{\parallel}/\psi \simeq -0.35$) with one or more x-points. The large island centered about $W_{\parallel}/\psi = -0.81$ is the second harmonic ($m = 2$) resonance, and the one at -0.35 is the fourth ($m = 4$). There are many other higher harmonic resonances, but all those above $m = 4$ are not traced out by the plot, because overlap of successively more closely spaced islands for $m \geq 6$ causes the orbits to become stochastic above about -0.23. They wander quasi-randomly in W_{\parallel} until they become untrapped when it becomes greater than zero. There are other orbits that

start untrapped but wander in to become trapped for a time. They can be considered to be the illustrated by the same stochastic orbits only followed backwards in time (by time reversal symmetry).

Thus, for a hole that is limited in transverse extent, and therefore experiences a perpendicular field E_r like this, only fairly deeply trapped orbits are permanently trapped. The stochastic orbits stay trapped only for a limited number of bounces before escaping the hole as passing orbits. The anticipated consequence is that the stochastic region has approximately constant phase space density, equal to the phase space density of the low-energy background orbits. This observation motivates the flat edge distribution functions of figures 4 and 5. In summary, there is theoretically always a stochastic region of only temporarily trapped orbits near the trapping energy boundary $\mathcal{E} = 0$, but when $\Omega/\sqrt{\psi} > 2$ a large fraction of orbits are permanently trapped. In contrast if $\Omega/\sqrt{\psi} < 1$ a large fraction are not permanent unless the transverse scale length ψ/E_{\perp} is rather large. The paper (Hutchinson, 2020) gives more quantitative description of the trapping and detrapping criteria. Unfortunately there seems to be, as yet, no published experimental evidence supporting these conclusions.

Setting aside the erroneous direct invocation of a supposed gyrokinetic permittivity explained above, the two valid multidimensional effects discussed so far are (1) transverse field divergence, and (2) resonant parallel energy changes leading to stochastic orbits. There is a third, namely (3) (non-resonant) gyro-averaging over transverse orbit. This effect is treated for self-consistent axisymmetric holes in Hutchinson (2021a). It involves orbits that cannot be treated as localized in the transverse direction because their gyro-radius is comparable to the transverse length scale of the potential variation. This is where some of the techniques of gyrokinetics become relevant. Of course the resonant orbit stochasticization occurs simultaneously and its effects need to be combined with gyro-averaging. The theory shows that gyro-averaging and perpendicular velocity integration over a Gaussian perpendicular velocity distribution, are together equivalent to convolving the quantity of interest with a 2-dimensional Gaussian of width equal to the thermal gyro-radius $r_{gt} = v_t/\Omega$ in the perpendicular plane. The transverse orbit-averaged quantity is therefore

$$\bar{\phi}(\mathbf{x}_c) = \int \phi(\mathbf{x}_c + \mathbf{r}_g) e^{-(\mathbf{r}_g/r_{gt})^2/2} \frac{d^2 r_g}{2\pi r_{gt}^2}, \quad (57)$$

where \mathbf{x}_c is the guiding center, \mathbf{r}_g is the (2-D) gyro-radius vector from it to the particle position $\mathbf{x}_c + \mathbf{r}_g$, and overbar denotes the gyro-average of whatever quantity is under discussion (ϕ here). Then, because a further transverse gyro-averaging occurs in the transformation from guiding-center density to particle density (which determines charge density), the effective potential $\bar{\phi}(r, z)$ ac-

counting for finite gyro-radius is smoothed by two equal Gaussian transverse convolutions relative to what would be obtained for the same trapped particle deficit without accounting for gyro-radius (i.e. at high magnetic field). (Two Gaussian convolutions are the same as one with width $\sqrt{2}r_{gt}$.)

Direct numerical orbit integration validates the intuitive idea that parallel trapping is determined mostly by the gyro-averaged parallel energy $\bar{W}_{\parallel} = v_{\parallel}^2/2 + \bar{\phi}$ except that resonant orbit stochasticization can detrap the orbits near $W_{\parallel} = 0$.

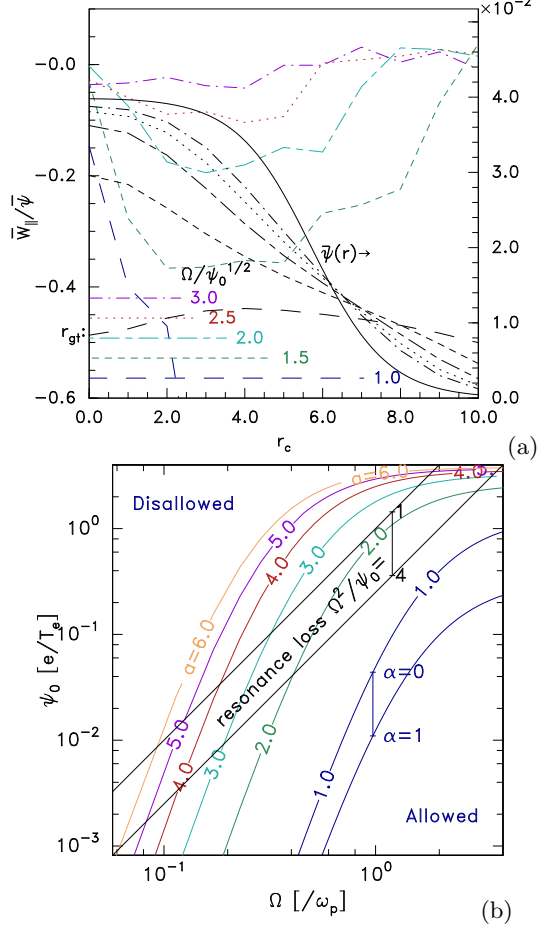


FIG. 41 (a) Gyro-averaged potential $\bar{\psi}$ and lowest permanently trapped orbit $\bar{W}_{\parallel}/\bar{\psi}$ versus guiding center radius for a range of Ω . (b) Maximum allowable hole amplitude ψ_0 permitted by distribution non-negativity (colors) and resonant detrapping (black). From Hutchinson (2021a).

Figure 41(a) shows in black on the right-hand scale the gyroaveraged peak potential profile $\bar{\psi}(r) = \bar{\phi}(0, r)$ for a particular $\psi(r)$ profile having $\psi_0 = 0.04$. Different line styles are for different magnetic field strengths $\Omega/\psi_0^{1/2}$ and hence gyro-radii; the solid line is unaveraged $\psi(r)$. The gyro-averaging effect is always to lower the $\bar{\psi}(r)$ peaks and raise the wings, although the effect is relatively small for $\Omega/\psi_0^{1/2} > 2$. The colored lines instead

show the maximum value of $\bar{W}/\bar{\psi}$ for which the orbits are permanently trapped, using the same line style notation. At the highest Ω s all orbits are permanent except for those close to $W = 0$, but at the lowest field, orbits are almost entirely detrapped.

Figure 41(b) gathers these observations to plot lines above which axisymmetric holes are disallowed either because they violate the requirement of non-negative $f(v)$ (colored) or because they are seriously depleted by resonant detrapping (black). The non-negativity constraint is made more stringent by gyro-averaging because of the smoothing of the effective (gyro-averaged) potential. Quantitatively that depends on the hole's effective transverse size a , defined as $2a^2 = \langle r^2 \rangle = \int_0^\infty r^2 \psi(r) r dr / \int_0^\infty \psi(r) r dr$, and the lines are labelled with the value of a . There is some dependence also on the form assumed for the parallel distribution deficit, which is controlled by the parameter α . The most forgiving value, $\alpha = 0$, corresponds to a waterbag shaped \bar{f} deficit and all lines use this except the lowest: $a = 1$, $\alpha = 1$, which illustrates the approximate uncertainty introduced by parallel hole shape. Resonant orbit detrapping is represented by the straight diagonal lines for low and high values of Ω^2/ψ_0 . The upper bound lies somewhere between them. We observe that at low values of Ω (in units of ω_p) only very shallow ($\psi_0 < 10^{-2}$) holes are permitted, and cannot have too small a transverse size a . For $\Omega \sim 0.5$ though, resonant detrapping is by far the more limiting factor unless $a \lesssim 2$. For $\Omega \gtrsim 1$ transverse size is hardly limited and prolate holes are permitted by the criteria investigated.

A different consequence of finite transverse size of electron or ion holes is that they can scatter passing electrons in velocity space. Viewed in the frame of the steady hole, this process does not change the total particle energy, but it transfers the kinetic energy between parallel and perpendicular velocities when there is a perpendicular component of the hole electric field (transverse potential inhomogeneity). This transfer can be calculated by finding the total perpendicular work done on the particle, like the corresponding calculation for trapped particles, except considering a single hole transit, rather than periodic bouncing. The transfer is largest when the gyration of the transverse velocity is by approximately half a period during the transit. That is, $\Omega\tau_t \sim \pi$, where $\tau_t \sim L_{\parallel}/v_{\parallel}$ is the (parallel) transit time. Depending on the gyrophase of the encounter, the transfer to \mathcal{E}_{\perp} is either positive or negative. In contrast, if $\Omega\tau_t \gg \pi$, then the $\mathbf{v}_{\perp}(\mathbf{E}_{\perp})$ power oscillations during transit average to a small total; while conversely $\Omega\tau_t \ll \pi$ implies the encounter is very brief because $v_{\parallel} \gg L_{\parallel}/\Omega$; so the total transfer is small. Vasko *et al.* (2017b) calculate the mean square energy transfer in a single encounter with an axisymmetric Gaussian hole of parallel and perpendicular scales L_{\parallel} and L_{\perp} , and deduce the velocity diffusion coefficient as a function of particle energy and pitch

angle (i.e. of position in velocity space), when encountering a randomly positioned assembly of equal holes. For their application to understanding particle precipitation by scattering into the loss-cone of a magnetic mirror trapping region, they also average over mirror bounce motion and spatial variation. They conclude that pitch angle scattering by electron holes can be comparable to that of “chorus waves” (another leading mechanism) in the outer radiation belt. In a follow-up paper, Vasko *et al.* (2018a) show that their calculation of scattering from holes is consistent with the classic quasi-linear rates of Kennel and Engelmann (1966). And in a more recent calculation Shen *et al.* (2021) show how allowing a broad range of hole amplitudes broadens the extent in phase-space of the diffusivity. They give diffusion rate expressions in terms of the spatially averaged spectrum $\mathbf{E}(\mathbf{k}, \omega)$ of the electric field fluctuations, which satellite observations may be able to determine more easily than trying to determine the density, size, and shape of electron holes.

C. Magnetic field perturbations

Ideal electron holes, viewed in the frame in which they are stationary, are static electromagnetic structures. A guiding assumption of the present review is that the electric field is predominantly responsible for localizing them (at least in the direction of any background magnetic field). In other words they are predominantly electrostatic and the background magnetic field can be considered uniform. Although such an electrostatic treatment is a good starting approximation for virtually all holes that have been observed, holes also in fact cause local perturbations to the magnetic field, which are sometimes observable.

As has been mentioned in subsection IV.D, the earliest observations of magnetic perturbations caused by electron holes were attributed to a simple Lorentz transformation of the hole’s electric field from the hole frame to the frame of the satellite measuring the electric and magnetic fields (Ergun *et al.*, 1998a,b, 1999). And only later (Andersson *et al.*, 2009) did it become clear that there are parallel magnetic field perturbations, which cannot be attributed to Lorentz transform, and must therefore exist in the hole frame. The mechanism proposed for enhancement of the magnetic field strength within the hole was electric current attributable to $\mathbf{E} \wedge \mathbf{B}$ drift of electrons, and this was given good theoretical grounding in (Tao *et al.*, 2011). Related ideas were proposed in (Treumann and Baumjohann, 2012). Vasko *et al.* (2015) observed in data from the Van Allen probes the unusual effect instead of reduction of $|B|$ within some holes in the outer radiation belt, and interpreted the cause as being diamagnetic currents from energetic anisotropic trapped electron distributions. A recent additional theoretical development is the inclusion of the

polarization drift of electrons (Yang *et al.*, 2023), which changes mostly the perpendicular magnetic perturbation. In this subsection a summary of magnetic perturbation theory for an axisymmetric electron hole in a uniform magnetic background field is given, working in the hole frame in dimensional (SI) units.

First, one should note that a purely one-dimensional potential structure, in which $\mathbf{E} = -\hat{\mathbf{z}}d\phi/dz$ is parallel to \mathbf{B} , gives zero magnetic field perturbation because it possesses no transverse electric field or current. A finite electron hole transverse radius, however, implies an \mathbf{E}_\perp ($= \mathbf{E}_r$ positive) and an electron drift electric current density $\mathbf{j}_{E \wedge B} = q_e n_e \mathbf{E}_r \wedge \mathbf{B} / B^2$ ($= -q_e n_e \frac{\partial \phi}{\partial r} \hat{\mathbf{r}} \wedge \mathbf{B} / B^2$) in the $+\hat{\theta}$ direction (for right-handed r, θ, z coordinates). Diamagnetic current arises from electron pressure gradient, contributing an additional current density $\mathbf{j}_{\nabla p} = \nabla_{\perp} p_{e\perp} / B$. If the hole is much longer than its radial extent (highly prolate) so we can approximate it as an infinite length cylinder, then, by Ampere’s law, the azimuthal current density generates a local magnetic field gradient $\partial B_z / \partial r = -\mu_0 j_{e\theta}$, implying that B_z increases toward the hole center, that is, the current *increases* the central values of $|B_z|$. Applying these expressions to a radial path we get

$$\frac{\partial}{\partial r} \frac{B_z^2}{2\mu_0} = en_e \frac{\partial \phi}{\partial r} - \nabla p_{e\perp} \quad (58)$$

Integration ignoring any n_e variation in the first term on the right then yields $\delta B_z B / \mu_0 \simeq [B(r)^2 - B(\infty)^2] / 2\mu_0 = en_e \phi(r) - [p_{e\perp}(r) - p_{e\perp}(\infty)] = en_e \phi - \delta p_\perp$, which can be recognized as radial force balance between magnetic pressure, electric field and kinetic pressure. Inclusion of diamagnetic current (arising from δp_\perp) in subsequent expressions where it is omitted simply requires ϕ to be replaced with $\phi - \delta p_\perp / en_e$.

The ion response is also neglected, which is justified by ions’ heavier mass when the hole is moving sufficiently faster than the ion velocity distribution. Tao *et al.* (2011) demonstrate by numerical orbit integration that ignoring ion’s $\mathbf{E} \wedge \mathbf{B}$ drift current is well justified. And they observe that for a separable Gaussian hole shape $[\phi(r, z) = \psi \exp(-r^2/2l_\perp^2 - z^2/2l_\parallel^2)]$, the (linearized) parallel magnetic field perturbation at the origin ignoring diamagnetic current can be written

$$\begin{aligned} \delta B_z(r = 0, z = 0) &= (\mu_0 n_e e \psi / B) g(l_\perp / l_\parallel) \\ &= B(\hat{\psi} / \hat{\Omega}) (T / m_e c^2) g(l_\perp / l_\parallel) \end{aligned} \quad (59)$$

where $(\hat{\psi} / \hat{\Omega})$ are in our normalized hole units. The effects of finite aspect ratio l_\perp / l_\parallel are expressed by the function

$$g(s) = \Re \left\{ [1 - s^2 + s^2 \cos^{-1}(1/s) \sqrt{s^2 - 1}] / (1 - s^2)^2 \right\}, \quad (60)$$

which is unity at $s \rightarrow 0$, and which they plot.

Yang *et al.* (2023) calculate the effect of electron polarization drift, arising from the time dependence of E_r

experienced by electrons moving through the hole. It gives rise to an additional B_θ perturbation as follows. A closed contour C at $r = r_c, z = z_c$ (where r_c and z_c are constants) is spanned by the surface S : $z = z_c, r \leq r_c$. Applying Stokes' theorem to the steady Ampere's law, using cylindrical symmetry we have the standard result $B_\theta(r_c) = \mu_0 I(r_c, z_c)/2\pi r_c$ where I is the total electric current crossing S . The electric current density is $\mathbf{j} = q_e(n_e \bar{\mathbf{v}}_e - n_i \bar{\mathbf{v}}_i)$, where $\bar{\mathbf{v}}_e$ and $\bar{\mathbf{v}}_i$ are averages over the respective distribution functions. Remove any background field gradients by supposing that far away from the hole there is no current density $n_{e\infty} \bar{\mathbf{v}}_{e\infty} - n_{i\infty} \bar{\mathbf{v}}_{i\infty} = 0$. And again suppose that ions are sufficiently heavy and fast moving (in the hole frame) that their density and velocity is unperturbed by the hole: $n_i \bar{\mathbf{v}}_i = n_{i\infty} \bar{\mathbf{v}}_{i\infty}$. Then $\mathbf{j} = \mathbf{j}_e - \mathbf{j}_{e\infty} = q_e(n_e \bar{\mathbf{v}}_e - n_{e\infty} \bar{\mathbf{v}}_{e\infty})$. The electron guiding-center polarization drift is cumulative, such that it results in a radial orbit displacement $\delta r = \frac{m_e}{q_e B^2} E_r = q_e E_r / m_e \Omega^2$, which is negative, that is inward. Consequently the radial displacement of the guiding-center is directly proportional to the radial electric field (and zero at infinity, since $E_r = 0$ there). Inclusion of just the polarization drift therefore causes all the orbits that at infinity have guiding-centers inside the radius $r_c - \delta r$ to pass through the surface S of radius r_c at z_c , giving rise at lowest order in $\delta r/r_c$ to a change in parallel current $\delta I_{v_p}(r_c) = -2\pi r_c \delta r j_{e\infty} = -2\pi r_c (m_e E_r / q_e B^2) j_{e\infty}$ (δr is negative). And hence

$$\delta B_{\theta v_p}(r_c) = \frac{\partial \phi}{\partial r} \frac{\mu_0}{B^2} m_e n_e \bar{v}_{e\infty}. \quad (61)$$

In addition to the polarization drift, however, radial motion occurs because of a magnetic field $B_r \neq 0$, arising from $\partial B_z / \partial z$ via the drift-current mechanism equation 58 and $\nabla \cdot \mathbf{B} = 0$. Parallel guiding-center motion therefore gives an additional parallel current change δI_{B_r} crossing S proportional to the change of the magnetic flux linked by the contour of radius r_c . That is

$$\delta I_{B_r}(r_c) = j_{e\infty} \int_0^{r_c} (\delta B_z / B) 2\pi r dr, \quad (62)$$

and to lowest order in prolate holes

$$\delta I_{B_r}(r_c) = \int_0^{r_c} \frac{2\mu_0}{B^2} e n_e \phi r dr q_e n_e \bar{v}_{e\infty}. \quad (63)$$

In the prolate approximation one quickly finds

$$\frac{\delta I_{B_r}}{\delta I_{v_p}} \simeq \frac{\omega_{pe}^2}{c^2} \frac{\int_0^{r_c} \phi r dr}{r_c \partial \phi / \partial r|_{r_c}} \sim \frac{\omega_{pe}^2 r_c^2}{c^2} = \frac{T}{mc^2} \frac{r_c^2}{\lambda_{De}^2}, \quad (64)$$

which is small unless temperatures are relativistic or r_c/λ_{De} is large. So ignoring the B_r effect on δI_z and hence on B_θ is generally a good approximation.

For the above drift analysis to be quantitatively correct, however, holes of typical parallel length λ_{De} require

$\omega_{pe}/\Omega \lesssim 1$; otherwise thermal electrons transit the hole in less than one gyroperiod and more complicated analysis is required. The approximate effect is that the radial displacement is determined by inertial electric acceleration during the transit, and becomes $\delta r \sim \frac{q_e E_r}{m_e \omega_{pe}^2}$ rather than $\frac{q_e E_r}{m_e \Omega^2}$, which might be heuristically approximated as $\delta r \sim q_e E_r / m_e (\Omega^2 + \omega_{pe}^2)$. In any case, evaluating the field perturbations everywhere for arbitrary aspect ratio requires a full numerical calculation, even for separable Gaussian potential shapes.

What is observed by the satellite in its rest frame is given by the Lorentz transform of the hole-frame \mathbf{E} and \mathbf{B} . In the linearized approximation, it simply gives an additional azimuthal field $\delta \mathbf{B}_{Lorentz} = \hat{\theta} \delta B_{\theta Lorentz} = \hat{\theta} v_h E_r / c^2$, where v_h is the parallel velocity of the hole in the satellite frame. This azimuthal field proportional to E_r is the same shape as that of the polarization drift and their relationship for small $\delta r/r$ ignoring diamagnetic current can be written

$$\delta B_{\theta v_p} \simeq \frac{\omega_{pe}^2}{\Omega^2} \delta B_{\theta Lorentz}, \quad (65)$$

(with $\Omega^2 \rightarrow \sim (\Omega^2 + \omega_{pe}^2)$ at low Ω/ω_{pe}). Estimates of hole speed obtained by assuming B_θ arises purely from Lorentz transformation, may therefore be misleading when ω_{pe}/Ω is not small.

Steinvalld *et al.* (2019) analyzed MMS data accounting for the electron $\mathbf{E} \wedge \mathbf{B}$ drift and Lorentz transform effects but not polarization drift, using all four spacecraft to give a 3-dimensional picture. They measured a discrepancy in the magnetic field relative to their Gaussian model, for high speed and amplitude holes. It consisted of an oscillatory perpendicular component with right-handed polarization, which they interpret as a damped whistler wave excited by the hole through a Cerenkov mechanism previously analyzed and observed in reconnection simulations by Goldman *et al.* (2014).

There is now growing observational evidence of the local excitation of electron holes and related electron vorticity in space plasma magnetic reconnection (see e.g. Ahmadi *et al.* (2022)), and in reconnection simulations (see e.g. Chang *et al.* (2022)). So magnetic field influence on holes and hole influence on magnetic fields seems to be a topic of increasing relevance.

IX. PROSPECTS

As this review has sought to convey, solitary potential structures are a major nonlinear, coherent, constituent of many dynamic plasma systems. They are not naturally analyzed by spatial Fourier decomposition, and in that sense are more like the individual water waves on a beach than the spatially periodic electromagnetic waves used for communications or plasma heating. Our

understanding of them has developed somewhat episodically over the past sixty years, as theory, observation, experiment, and computer simulation have all made essential contributions. Recent progress has been remarkable, enabled and motivated by increasingly sophisticated satellite measurements, powerful high-performance simulation, new insights, and rigorous analysis. Many opportunities for progress still remain, and some brief speculative closing remarks about them are perhaps appropriate.

Electron and ion holes are anticipated to occur in situations with kinetically unstable velocity distributions. That usually means, for predominantly electrostatic phenomena, distributions with multiple peaks. However, we so far have very little systematic understanding of just how the distribution shapes relate to the parameters of generated phase-space holes and to their long term fate. There might be much to be learned from systematic simulation studies (going beyond the individual examples that tend to dominate the literature) to explore how initializing background distribution details influence the coherent outcome, and how the velocity distributions subsequent to instability relate to hole formation and merging processes. It is already clear that holes can have a wide range of parallel lengths. Therefore the extensive recent transverse stability calculations assuming $\text{sech}^4(z/4\lambda)$ potential shape are just a particular choice. It would be of considerable interest to know how hole length influences transverse stability.

Multisatellite observations have only begun to measure the three-dimensional shapes of electron and ion holes. There is undoubtedly already archived data that might bring additional clarity to the situations where holes are or are not approximately axisymmetric, and what determines their aspect ratio (oblateness). Future missions involving larger teams of satellites would likely give much more comprehensive information on holes' spatial form, from fast measurements of all three electric field components. But managing and mining that data will require sophisticated automated algorithms to extract it.

What electron and ion holes do to the plasma is still an area of great uncertainty. For example, are electron holes a major player in determining particle scattering, precipitation, reconnection rates, anomalous resistivity, obstacle wake behavior, and so on? Or are they mostly interesting markers, of value for diagnosing the progress of other more dominant controlling factors? We mostly don't know.

Holes have been deliberately generated in laboratory experiments, and observed to accompany reconnection. But how prevalent are they in terrestrial plasmas? The uncertainty about this question arises in large part from the difficulty of Debye-length scale measurements; can new high-resolution diagnostics establish the degree of prevalence of coherent solitary structures, or can basic plasma experiments of longer Debye-length observe and measure them in a controlled way?

In closing, one might ask if there are engineering applications of phase-space holes to accomplish human tasks. To my knowledge, not so far. That fact probably limits the effort likely to be expended in studying them. However, they may substantially impact human activities in space, and they certainly help to explain a lot of what satellites observe in space plasmas. In any case, the intellectual challenge and adventure which lies behind all of natural science remains great in an area of nonlinear physics like this. New knowledge and understanding is to some degree its own reward. Solitary plasma phase-space structures remain a topic open to new discoveries in the challenging area of nonlinear physics.

ACKNOWLEDGMENTS

I am greatly indebted to my students Christian Haakonsen, Chuteng Zou, Xiang Chen, and collaborator David Malaspina for the pleasure of working closely with them over the years to develop a deep understanding of electron holes. Ivan Vasko and his students have been a source of inspiration and world-wide leadership in interpreting current satellite data concerning electron and ion holes. I thank them for sharing their work in progress and welcoming occasional theoretical input from me. Ivan Vasko read the present MS in draft and I thank him very much for this substantial help.

No external financial support was received for the writing of this article, and no data were produced.

REFERENCES

Ahmadi, Narges, Stefan Eriksson, David Newman, Laila Andersson, Robert E. Ergun, and Frederick D. Wilder (2022), "Observations of Electron Vorticity and Phase Space Holes in the Magnetopause Reconnection Separatrix," *Journal of Geophysical Research: Space Physics* **127** (8), e2022JA030702.

Akimoto, K, and D. Winske (1985), "Ion-acoustic-like waves excited by the reflected ions at the Earth's bow shock," *Journal of Geophysical Research: Space Physics* **90** (A12), 12095–12103.

Al'pert, Ya L, A V Gurevich, and L P Pitaevskii (1965), *Space Physics with Artificial Satellites* (Consultants Bureau, New York).

Andersson, L, R E Ergun, J Tao, A Roux, O Lecontel, V Angelopoulos, J Bonnell, J P McFadden, D E Larson, S Eriksson, T Johansson, C M Cully, D N Newman, M V Goldman, K H Glassmeier, and W Baumjohann (2009), "New features of electron phase space holes observed by the THEMIS mission," *Physical Review Letters* **102** (22), 225004.

Andrews, J G, and J E Allen (1971), "Theory of a double sheath between two plasmas," *Proceedings of the Royal Society of London. Series A, Mathematical and Physical Sciences* **320**, 459–472.

Bale, S D, A Hull, D E Larson, R P Lin, L Muschietti, P J Kellogg, K Goetz, and S J Monson (2002), "Electrostatic Turbulence and Debye-Scale Structures Associated with Elec-

tron Thermalization at Collisionless Shocks," *The Astrophysical Journal* **575** (1), L25—L28.

Bale, S D, P J Kellogg, D E Larsen, R P Lin, K Goetz, and R P Lepping (1998), "Bipolar electrostatic structures in the shock transition region: Evidence of electron phase space holes," *Geophysical Research Letters* **25** (15), 2929–2932.

Berk, H L, C E Nielsen, and K V Roberts (1970), "Phase Space Hydrodynamics of Equivalent Nonlinear Systems: Experimental and Computational Observations," *Physics of Fluids* **13** (4), 980.

Berk, H L, and K. V. Roberts (1967), "Nonlinear study of vlasov's equation for a special class of distribution functions," *The Physics of Fluids* **10** (7), 1595–1597.

Berman, R H, D. J. Tetreault, T. H. Dupree, and T. Boutros-Ghali (1982), "Computer Simulation of Nonlinear Ion-Electron Instability," *Physical Review Letters* **48** (18), 1249–1252.

Bernstein, I B, J M Greene, and M D Kruskal (1957), "Exact nonlinear plasma oscillations," *Physical Review* **108** (4), 546–550.

Berthomier, M, G Dubois, and L Muschietti (2008), "Stability of three-dimensional electron holes," *Physics of Plasmas* **15** (11), 10.1063/1.3013452.

Berthomier, M, L Muschietti, J W Bonnell, I Roth, and C W Carlson (2002), "Interaction between electrostatic whistlers and electron holes in the auroral region," *Journal of Geophysical Research: Space Physics* **107** (A12), 1–11.

Berthomier, M, R. Pottelette, L. Muschietti, I. Roth, and C. W. Carlson (2003), "Scaling of 3d solitary waves observed by fast and polar," *Geophysical Research Letters* **30**, SSC 4.1–5.

Bertrand, Pierre, Daniele Del Sarto, and Alain Ghizzo (2019), *The Vlasov Equation 1: History and General Properties* (John Wiley & Sons) google-Books-ID: czqyDwAAQBAJ.

Birch, Paul C, and Sandra C Chapman (2001), "Particle-in-cell simulations of the lunar wake with high phase space resolution," *Geophysical Research Letters* **28** (2), 219–222.

Block, Lars P (1978), "A double layer review," *Astrophysics and Space Science* **55** (1), 59–83.

Boström, Rolf, Georg Gustafsson, Bengt Holback, Gunnar Holmgren, Hannu Koskinen, and Paul Kintner (1988), "Characteristics of Solitary Waves and Weak Double Layers in the Magnetospheric Plasma," *Physical Review Letters* **61** (1), 82–85.

Brunner, S, and E. J. Valeo (2004), "Trapped-Particle Instability Leading to Bursting in Stimulated Raman Scattering Simulations," *Physical Review Letters* **93** (14), 145003.

Buchanan, Mark, and J J Doring (1993), "Nonlinear waves in collisionless plasmas," *Physics Letters A* **179**, 306–310.

Bujarbarua, S, and H Schamel (1981), "Theory of finite-amplitude electron and ion holes," *Journal of Plasma Physics* **25**, 515–529.

Børve, Steinar, Hans L. Pécseli, and Jan Trulsen (2001), "Ion phase-space vortices in 2.5-dimensional simulations," *Journal of Plasma Physics* **65** (2), 107–129.

Cairns, R A, A A Mamum, R Bingham, R Boström, R O Dendy, C M C Nairn, and P K Shukla (1995), "Electrostatic solitary structures in non-thermal plasmas," *Geophysical Research Letters* **22** (20), 2709–2712.

Califano, F, and M Lontano (2005), "Electron hole generation and propagation in an inhomogeneous collisionless plasma," *Physical Review Letters* **95** (24), 1–4.

Carril, Hugo A, Jorge A. Gidi, Roberto E. Navarro, and Jaime A. Araneda (2023), "Formation of multiple BGK-like structures in the time-asymptotic state of collisionless Vlasov-Poisson plasmas," *Physical Review E* **107** (6), 065203.

Cattell, C, J Dombeck, J Wygant, J F Drake, M Swisdak, M L Goldstein, W Keith, A Fazakerley, M André, E Lucek, and A Balogh (2005), "Cluster observations of electron holes in association with magnetotail reconnection and comparison to simulations," *Journal of Geophysical Research* **110** (A1), A01211.

Cattell, C, J. Wygant, J. Dombeck, F. S. Mozer, M. Temerin, and C. T. Russell (1998), "Observations of large amplitude parallel electric field wave packets at the plasma sheet boundary," *Geophysical Research Letters* **25** (6), 857–860.

Chang, Cong, Kai Huang, Quanming Lu, San Lu, Xiancai Yu, Rongsheng Wang, Longlong Sang, and Xinliang Gao (2022), "Electrostatic Solitary Waves and Electron-beam Instabilities in the Separatrix Region of Magnetic Reconnection," *The Astrophysical Journal* **933** (1), 67.

Chen, Li-Jen, and G K Parks (2002), "BGK electron solitary waves in 3D magnetized plasma," *Geophysical Research Letters* **29** (9), 41–45.

Chen, Li Jen, Jolene Pickett, Paul Kintner, Jason Franz, and Donald Gurnett (2005), "On the width-amplitude inequality of electron phase space holes," *Journal of Geophysical Research: Space Physics* **110** (A9), 1–11.

Chen, Li-Jen, David Thouless, and Jian-Ming Tang (2004), "Bernstein–Greene–Kruskal solitary waves in three-dimensional magnetized plasma," *Physical Review E* **69** (5), 55401.

Chen, Xiang, and I.H. Hutchinson (2023), "Multimode theory of electron hole transverse instability," *Journal of Plasma Physics* **89** (1), 10.1017/s0022377822001143.

Collantes, J R, and V. A. Turikov (1988), "Stability of solitary BGK waves," *Physica Scripta* **38** (6), 825.

Davidson, Ronald C (1972), *Methods in Nonlinear Plasma Theory* (Academic Press, New York).

Dodd, R K, J C Eilbeck, J D Gibbon, and H C Morris (1982), *Solitons and Nonlinear Wave Equations* (Academic Press).

Dodin, I Y, and N. J. Fisch (2014), "On the nature of kinetic electrostatic electron nonlinear (KEEN) waves," *Physics of Plasmas* **21** (3), 10.1063/1.4868230.

Dodin, I Y, P. F. Schmit, J. Rocks, and N. J. Fisch (2013), "Negative-Mass Instability in Nonlinear Plasma Waves," *Physical Review Letters* **110** (21), 215006.

Drake, J F, M Swisdak, C Cattell, M A Shay, B N Rogers, and A Zeiler (2003), "Formation of electron holes and particle energization during magnetic reconnection," *Science (New York, N.Y.)* **299** (5608), 873–877.

Drazin, P G, and R. S. Johnson (1989), *Solitons: An Introduction* (Cambridge University Press).

Du, Aimin, Mingyu Wu, Quanming Lu, Can Huang, and Shui Wang (2011), "Transverse instability and magnetic structures associated with electron phase space holes," *Physics of Plasmas* **18** (3), 10.1063/1.3561796.

Dupree, T H (1983), "Growth of phase-space density holes," *Physics of Fluids* **26** (9), 2460.

Dupree, Thomas H (1982), "Theory of phase-space density holes," *Physics of Fluids* **25** (2), 277.

Eliasson, B, and P K Shukla (2004a), "Dynamics of electron holes in an electron-oxygen-ion plasma," *Physical Review Letters* **93** (4), 45001.

Eliasson, B, P K Shukla, and M E Dieckmann (2006), "Theoretical and simulation studies of relativistic ion holes in astrophysical plasmas," *New Journal of Physics* **8** (4), 55–

55.

Eliasson, Bengt, and Padma Kant Shukla (2004b), “Trapping of Langmuir waves in Ion Holes,” *Physica Scripta* **2004** (T107), 192.

Ergun, R E, C. W. Carlson, J. P. McFadden, F. S. Mozer, G. T. Delory, W. Peria, C. C. Chaston, M. Temerin, I. Roth, L. Muschietti, R. Elphic, R. Strangeway, R. Pfaff, C. A. Cattell, D. Klumpar, E. Shelley, W. Peterson, E. Moebius, and L. Kistler (1998a), “FAST satellite observations of large-amplitude solitary structures,” *Geophysical Research Letters* **25** (12), 2041–2044.

Ergun, R E, C W Carlson, J P McFadden, F S Mozer, L Muschietti, I Roth, and R J Strangeway (1998b), “Debye-Scale Plasma Structures Associated with Magnetic-Field-Aligned Electric Fields,” *Physical Review Letters* **81** (4), 826–829.

Ergun, R E, C W Carlson, L Muschietti, I Roth, and J P McFadden (1999), “Properties of fast solitary structures,” *Nonlinear Processes in Geophysics* **6**, 187–194.

Farrell, W M, M L Kaiser, J T Steinberg, and S D Bale (1998), “A simple simulation of a plasma void: Applications to Wind observations of the lunar wake,” *Journal of Geophysical Research: Space Physics* **103** (A10), 23653–23660.

Fox, W, M Porkolab, J Egedal, N Katz, and A Le (2008), “Laboratory Observation of Electron Phase-Space Holes during Magnetic Reconnection,” *Physical Review Letters* **101** (25), 255003.

Fox, W, M Porkolab, J Egedal, N Katz, and A Le (2012), “Observations of electron phase-space holes driven during magnetic reconnection in a laboratory plasma,” *Physics of Plasmas* **19** (3), 32118.

Franz, J R, P M Kintner, J S Pickett, and L J Chen (2005), “Properties of small-amplitude electron phase-space holes observed by Polar,” *Journal of Geophysical Research: Space Physics* **110** (A9), 10.1029/2005JA011095.

Franz, J R, P M Kintner, C E Seyler, J S Pickett, and J D Scudder (2000), “On the perpendicular scale of electron phase-space holes,” *Geophysical Research Letters* **27** (2), 169–172.

Franz, Jason R, Paul M Kintner, and Jolene S Pickett (1998), “POLAR observations of coherent electric field structures,” *Geophysical Research Letters* **25** (8), 1277–1280.

Friedland, L, F Peinetti, W Bertsche, J Fajans, and J Wurtele (2004), “Driven phase space holes and synchronized Bernstein, Greene, and Kruskal modes,” *Physics of Plasmas* **11** (9), 4305–4317.

Fu, H S, F. Chen, Z. Z. Chen, Y. Xu, Z. Wang, Y. Y. Liu, C. M. Liu, Y. V. Khotyaintsev, R. E. Ergun, B. L. Giles, and J. L. Burch (2020), “First Measurements of Electrons and Waves inside an Electrostatic Solitary Wave,” *Physical Review Letters* **124** (9), 095101.

Gary, S Peter, and Robert L Tokar (1985), “The electron-acoustic mode,” *The Physics of Fluids* **28**, 2439–2441.

Ghizzo, A, B. Izrar, P. Bertrand, E. Fijalkow, M. R. Feix, and M. Shoucri (1988), “Stability of Bernstein–Greene–Kruskal plasma equilibria. Numerical experiments over a long time,” *The Physics of Fluids* **31** (1), 72–82.

Goldman, M V, D L Newman, and R E Ergun (2003), “Phase-space holes due to electron and ion beams accelerated by a current-driven potential ramp,” *Nonlinear Processes in Geophysics* **10**, 37–44.

Goldman, M V, D L Newman, G Lapenta, L Andersson, J T Gosling, S Eriksson, S Markidis, J P Eastwood, and R Ergun (2014), “ v Cerenkov Emission of Quasiparallel Whistlers by Fast Electron Phase-Space Holes during Magnetic Reconnection,” *Physical Review Letters* **112** (14), 145002.

Goldman, M V, M M Oppenheim, and D L Newman (1999), “Nonlinear two-stream instabilities as an explanation for auroral bipolar wave structures,” *Geophysical Research Letters* **26** (13), 1821–1824.

Goldman, Martin V, David L Newman, and André Mangeney (2007), “Theory of weak bipolar fields and electron holes with applications to space plasmas,” *Physical Review Letters* **99** (14), 2–5.

Graham, D B, Yu V Khotyaintsev, A Vaivads, and M André (2016), “Electrostatic solitary waves and electrostatic waves at the magnetopause,” *Journal of Geophysical Research: Space Physics* **121**, 3069–3092.

Grießmeier, J-M, and H. Schamel (2002), “Solitary holes of negative energy and their possible role in the nonlinear destabilization of plasmas,” *Physics of Plasmas* **9** (6), 2462–2465.

Gurevich, A V (1968), “Distribution of captured particles in a potential well in the absence of collisions,” *Sov. Phys. JETP* **26**, 575–580.

Gurevich, A V, L P Pitaevskii, and V V Smirnova (1969), “Ionospheric aerodynamics,” *Space Science Reviews* **9**, 805–871.

Gurevich, A V, and L P Pitaevsky (1975), “Non-linear dynamics of a rarefied ionized gas,” *Progress in Aerospace Sciences* **16** (3), 227–272.

Haakonsen, Christian Bernt, Ian H Hutchinson, and Chuteng Zhou (2015), “Kinetic electron and ion instability of the lunar wake simulated at physical mass ratio,” *Physics of Plasmas* **22** (3), 32311.

Hara, Kentaro, Thomas Chapman, Jeffrey W. Banks, Stephan Brunner, Ilon Joseph, Richard L. Berger, and Iain D. Boyd (2015), “Quantitative study of the trapped particle bunching instability in Langmuir waves,” *Physics of Plasmas* **22** (2), 022104.

Hashimoto, K, M. Hashitani, Y. Kasahara, Y. Omura, M. N. Nishino, Y. Saito, S. Yokota, T. Ono, H. Tsunakawa, H. Shibusawa, M. Matsushima, H. Shimizu, and F. Takahashi (2010), “Electrostatic solitary waves associated with magnetic anomalies and wake boundary of the Moon observed by KAGUYA,” *Geophysical Research Letters* **37** (19), 10.1029/2010GL044529.

Hobara, Y, S. N. Walker, M. Balikhin, O. A. Pokhotelov, M. Gedalin, V. Krasnoselskikh, M. Hayakawa, M. André, M. Dunlop, H. Rème, and A. Fazakerley (2008), “Cluster observations of electrostatic solitary waves near the Earth’s bow shock,” *Journal of Geophysical Research: Space Physics* **113** (A5), 10.1029/2007JA012789.

Holloway, James Paul, and J. J. Doring (1991), “Undamped plasma waves,” *Physical Review A* **44** (6), 3856–3868.

Holmes, J C, R. E. Ergun, D. L. Newman, N. Ahmadi, L. Andersson, O. Le Contel, R. B. Torbert, B. L. Giles, R. J. Strangeway, and J. L. Burch (2018), “Electron Phase-Space Holes in Three Dimensions: Multispacecraft Observations by Magnetospheric Multiscale,” *Journal of Geophysical Research: Space Physics* **123** (12), 9963–9978.

Hudson, M K, W. Lotko, I. Roth, and E. Witt (1983), “Solitary waves and double layers on auroral field lines,” *Journal of Geophysical Research: Space Physics* **88** (A2), 916–926.

Hutchinson, I H (2012), “Electron velocity distribution instability in magnetized plasma wakes and artificial electron

mass,” *Journal of Geophysical Research: Space Physics* **117** (3), A03101, arXiv:1108.5579.

Hutchinson, I H (2017), “Electron holes in phase space: What they are and why they matter,” *Physics of Plasmas* **24** (5), 055601.

Hutchinson, I H (2018a), “Kinematic Mechanism of Plasma Electron Hole Transverse Instability,” *Physical Review Letters* **120** (20), 205101.

Hutchinson, I H (2018b), “Transverse instability of electron phase-space holes in multi-dimensional Maxwellian plasmas,” *Journal of Plasma Physics* **84** (4), 905840411.

Hutchinson, I H (2019a), “Electron phase-space hole transverse instability at high magnetic field,” *Journal of Plasma Physics* **85** (5), 905850501, arXiv:1906.04065.

Hutchinson, I H (2019b), “Transverse instability magnetic field thresholds of electron phase-space holes,” *Physical Review E* **99**, 053209.

Hutchinson, I H (2020), “Particle trapping in axisymmetric electron holes,” *Journal of Geophysical Research: Space Physics* **125** (8), e2020JA028093.

Hutchinson, I H (2021a), “Finite gyro-radius multidimensional electron hole equilibria,” *Physics of Plasmas* **28**, 052302.

Hutchinson, I H (2021b), “How can slow plasma electron holes exist?” *Phys. Rev. E* **104**, 015208, <http://arxiv.org/abs/2104.13800>.

Hutchinson, I H (2021c), “Oblate electron holes are not attributable to anisotropic shielding,” *Physics of Plasmas* **28**, 022902.

Hutchinson, I H (2021d), “Synthetic multidimensional plasma electron hole equilibria,” *Physics of Plasmas* **26**, 062036.

Hutchinson, I H (2023a), “Comment on ‘Evolution Equations of Nonlinearly Permissible, Coherent Hole Structures Propagating Persistently in Collisionless Plasmas’,” *Annalen der Physik* **536**, 2300333.

Hutchinson, I H (2023b), “Ion hole equilibrium and dynamics in one dimension,” *Physics of Plasmas* **30** (3), 032107.

Hutchinson, I H, C B Haakonsen, and C Zhou (2015), “Nonlinear plasma wake growth of electron holes,” *Physics of Plasmas* **22** (3), 32312.

Hutchinson, I H, and L Patacchini (2007), “Computation of the effect of neutral collisions on ion current to a floating sphere in a stationary plasma,” *Physics of Plasmas* **14** (1), 13505.

Hutchinson, I H, and C Zhou (2016), “Plasma electron hole kinematics. I. Momentum conservation,” *Physics of Plasmas* **23** (8), 82101.

Hutchinson, Ian H, and David M Malaspina (2018), “Prediction and Observation of Electron Instabilities and Phase Space Holes Concentrated in the Lunar Plasma Wake,” *Geophysical Research Letters* **45**, 3838–3845.

Hutchinson, IH (2022), “Overstability of plasma slow electron holes,” *Journal of Plasma Physics* **88** (1), 555880101.

infeld, Eryk, and George Rowlands (2000), *Nonlinear Waves, Solitons and Chaos*, 2nd ed. (Cambridge University Press, Cambridge).

Johnsen, H, H L Pécseli, and J Trulsen (1987), “Conditional eddies in plasma turbulence,” *Physics of Fluids* **30**, 2239–2254.

Johnston, T W, Y. Tyshetskiy, A. Ghizzo, and P. Bertrand (2009), “Persistent subplasma-frequency kinetic electrostatic electron nonlinear waves,” *Physics of Plasmas* **16** (4), 042105.

Jovanović, D, and Hans Schamel (2002), “The stability of propagating slab electron holes in a magnetized plasma,” *Physics of Plasmas* **9** (12), 5079–5087.

Jovanović, D, P K Shukla, L Stenflo, and F Pegoraro (2002), “Nonlinear model for electron phase-space holes in magnetized space plasmas,” *Journal of Geophysical Research: Space Physics* **107** (A7), 1–6.

Kamaletdinov, S R, I. Y. Vasko, R. Wang, A. V. Artemyev, E. V. Yushkov, and F. S. Mozer (2022), “Slow electron holes in the Earth’s bow shock,” *Physics of Plasmas* **29** (9), 092303.

Kamaletdinov, Sergey R, Ian H. Hutchinson, Ivan Y. Vasko, Anton V. Artemyev, Ajay Lotekar, and Forrest Mozer (2021), “Spacecraft observations and theoretical understanding of slow electron holes,” *Phys. Rev. Lett.* **127**, 165101.

Kennel, C F, and F. Engelmann (1966), “Velocity Space Diffusion from Weak Plasma Turbulence in a Magnetic Field,” *The Physics of Fluids* **9** (12), 2377–2388.

Korn, J, and H Schamel (1996), “Electron holes and their role in the dynamics of current-carrying weakly collisional plasmas. Part 1. Immobile ions,” *Journal of Plasma Physics* **56** (02), 307–337.

Korteweg, D J, and G. de Vries (1895), “On the change of form of long waves advancing in a rectangular canal, and on a new type of long stationary waves,” *The London, Edinburgh, and Dublin Philosophical Magazine and Journal of Science* **39** (240), 422–443.

Koskinen, Hannu E J, Rickard Lundin, and Bengt Holback (1990), “On the plasma environment of solitary waves and weak double layers,” *Journal of Geophysical Research: Space Physics* **95** (A5), 5921–5929.

Krapchev, Vladimir B, and Abhay K. Ram (1980), “Adiabatic theory for a single nonlinear wave in a Vlasov plasma,” *Physical Review A* **22** (3), 1229–1242.

Krasovsky, V L, H Matsumoto, and Y Omura (2003), “Electrostatic solitary waves as collective charges in a magnetospheric plasma: Physical structure and properties of Bernstein-Greene-Kruskal (BGK) solitons,” *Journal of Geophysical Research: Space Physics* **108** (A3), 1117.

Krasovsky, V L, H Matsumoto, and Y Omura (2004a), “Effect of trapped-particle deficit and structure of localized electrostatic perturbations of different dimensionality,” *Journal of Geophysical Research: Space Physics* **109** (A4), A04217.

Krasovsky, V L, H. Matsumoto, and Y. Omura (2004b), “On the three-dimensional configuration of electrostatic solitary waves,” *Nonlinear Processes in Geophysics* **11** (3), 313–318.

Kruer, W L, J. M. Dawson, and R. N. Sudan (1969), “Trapped-Particle Instability,” *Physical Review Letters* **23** (15), 838–841.

Kurth, W S, D. A. Gurnett, A. M. Persoon, A. Roux, S. J. Bolton, and C. J. Alexander (2001), “The plasma wave environment of Europa,” *Planetary and Space Science Magnetospheres of the Outer Planets (Part I)*, **49** (3), 345–363.

Kuzichev, I V, I. Y. Vasko, O. V. Agapitov, F. S. Mozer, and A. V. Artemyev (2017), “Evolution of electron phase space holes in inhomogeneous magnetic fields,” *Geophysical Research Letters* **44** (5), 2105–2112.

Laframboise, J G (1966), *Theory of Spherical and Cylindrical Langmuir Probes in a Collisionless Maxwellian Plasma at Rest*, Tech. Rep. 100 ((Doctoral Dissertation) University of Toronto Institute for Aerospace Studies).

Laframboise, J G, and L J Sonmor (1993), “Current collection by probes and electrodes in space magnetoplasmas: A review,” *Journal of Geophysical Research* **98** (A1), 337–357.

Lakhina, G S, S. V. Singh, R. Rubia, and T. Sreeraj (2018), “A review of nonlinear fluid models for ion-and electron-acoustic solitons and double layers: Application to weak double layers and electrostatic solitary waves in the solar wind and the lunar wake,” *Physics of Plasmas* **25** (8), 080501.

Lakhina, G S, B T Tsurutani, H Kojima, and H Matsumoto (2000), “Broadband” *Plasma Waves in the Boundary Layers*, *Journal of Geophysical Research* **105**, 27791–27831.

Lamb, George L (1980), *Elements of Soliton Theory* (Wiley) google-Books-ID: QVtFQRNv0MkC.

Lampe, Martin, Glenn Joyce, and Gurudas Ganguli (2001), “Analytic and Simulation Studies of Dust Grain Interaction and Structuring,” *Physica Scripta* **T89** (1), 106.

Landau, L (1946), “On the vibration of the electronic plasma,” *Soviet Physics: Journal of Experimental and Theoretical Physics* **16**, 574, reproduced in Collected papers of L.D. Landau, edited and with an introduction by D. ter Haar, Pergamon Press, 1965, pp. 445–460.

Lapenta, G, S Markidis, A Divin, M Goldman, and D Newman (2010), “Scales of guide field reconnection at the hydrogen mass ratio,” *Physics of Plasmas* **17** (8), 82106.

Lapenta, G, S. Markidis, A. Divin, M. V. Goldman, and D. L. Newman (2011), “Bipolar electric field signatures of reconnection separatrices for a hydrogen plasma at realistic guide fields,” *Geophysical Research Letters* **38**, L17104.

Lashmore-Davies, C N (2005), “Negative energy waves,” *Journal of Plasma Physics* **71**, 101–109.

Lefebvre, Bertrand, Li Jen Chen, Walter Gekelman, Paul Kintner, Jolene Pickett, Patrick Pribyl, Stephen Vincena, Franklin Chiang, and Jack Judy (2010), “Laboratory measurements of electrostatic solitary structures generated by beam injection,” *Physical Review Letters* **105** (11), 115001, arXiv:1009.4617.

Lesur, M, P H Diamond, and Y Kosuga (2014), “Nonlinear current-driven ion-acoustic instability driven by phase-space structures,” *Plasma Physics and Controlled Fusion* **56** (7), 75005.

Lewis, H Ralph, and Charles Seyler (1982), “Stability of Vlasov Equilibria. Part 2. One ignorable coordinate,” *J Plasma Phys* **27**, 25–35.

Lewis, H Ralph, and Keith R Symon (1979), “Linearized analysis of inhomogeneous plasma equilibria: General theory,” *Journal of Mathematical Physics* **20** (1979), 413.

Ling, Kuok-Mee, and Barbara Abraham-Shrauner (1981), “Modified Poisson eigenfunctions for electrostatic Bernstein–Greene–Kruskal equilibria,” *The Physics of Fluids* **24** (4), 629–637.

Lotekar, A, I. Y. Vasko, F. S. Mozer, I. Hutchinson, A. V. Artemyev, S. D. Bale, J. W. Bonnell, R. Ergun, B. Giles, Yu. V. Khotyaintsev, P.-A. Lindqvist, C. T. Russell, and R. Strangeway (2020), “Multisatellite mms analysis of electron holes in the earth’s magnetotail: Origin, properties, velocity gap, and transverse instability,” *Journal of Geophysical Research: Space Physics* **125** (9), e2020JA028066.

Lu, Q M, B Lembège, J B Tao, and S Wang (2008), “Perpendicular electric field in two-dimensional electron phase-holes: A parameter study,” *Journal of Geophysical Research* **113** (A11), A11219.

Lynov, J, P Michelsen, H Pcseli, J Rasmussen, K Saeki, and V Turikov (1979), “Observations of solitary structures in a magnetized, plasma loaded waveguide,” *Physica Scripta* **20**, 328–335.

Lynov, J P, P. Michelsen, H. L. Pcseli, and J. Juul Rasmussen (1980), “Interaction between electron holes in a strongly magnetized plasma,” *Physics Letters A* **80** (1), 23–25.

Malaspina, D M, L Andersson, R E Ergun, J R Wygant, J W Bonnell, C Kletzing, G D Reeves, R M Skoug, and B A Larsen (2014), “Nonlinear electric field structures in the inner magnetosphere,” *Geophysical Research Letters* **41**, 5693–5701.

Malaspina, David M, and Ian H. Hutchinson (2019), “Properties of Electron Phase Space Holes in the Lunar Plasma Environment,” *Journal of Geophysical Research: Space Physics* **124** (7), 4994–5008.

Malaspina, David M, David L Newman, Lynn B Willson, Keith Goetz, Paul J Kellogg, and Kris Kerstin (2013), “Electrostatic solitary waves in the solar wind: Evidence for instability at solar wind current sheets,” *Journal of Geophysical Research: Space Physics* **118** (2), 591–599.

Malaspina, David M, John R. Wygant, Robert E. Ergun, Geoff D. Reeves, Ruth M. Skoug, and Brian A. Larsen (2015), “Electric field structures and waves at plasma boundaries in the inner magnetosphere,” *Journal of Geophysical Research: Space Physics* **120** (6), 4246–4263.

Mamun, A A, and P. K. Shukla (2005), “Nonlinear waves and structures in dusty plasmas,” *Plasma Physics and Controlled Fusion* **47** (5A), A1.

Mangeney, A, C Salem, C Lacombe, J.-L. Bougeret, C Perche, R Manning, P J Kellogg, K Goetz, S J Monson, and J.-M. Bosqued (1999), “WIND observations of coherent electrostatic waves in the solar wind,” *Annales Geophysicae* **17** (3), 307–320.

Matsumoto, H, H. Kojima, Y. Kasaba, T. Miyake, R. R. Anderson, and T. Mukai (1997), “Plasma waves in the upstream and bow shock regions observed by GEOTAIL,” *Advances in Space Research Results of the IASTP Program*, **20** (4), 683–693.

Matsumoto, H, H Kojima, T Miyatake, Y Omura, M Okada, I Nagano, and M Tsutsui (1994a), “Electrostatic solitary waves (ESW) in the magnetotail: BEN wave forms observed by GEOTAIL,” *Geophysical Research Letters* **21** (25), 2915–2918.

Matsumoto, H, I. Nagano, R. R. Anderson, H. Kojima, K. Hashimoto, M. Tsutsui, T. Okada, I. Kimura, Y. Omura, and M. Okada (1994b), “Plasma Wave Observations with GEOTAIL Spacecraft,” *Journal of geomagnetism and geoelectricity* **46** (1), 59–95.

Miyake, T, Y. Omura, and H. Matsumoto (2000), “Electrostatic particle simulations of solitary waves in the auroral region,” *Journal of Geophysical Research: Space Physics* **105** (A10), 23239–23249.

Miyake, T, Y Omura, H Matsumoto, and H Kojima (1998), “Two-dimensional computer simulations of electrostatic solitary waves observed by Geotail spacecraft,” *Journal of Geophysical Research* **103** (A6), 11841.

Montgomery, D, and G Joyce (1969), “Shock-like solutions of the electrostatic vlasov equation,” *Journal of Plasma Physics* **3**, 1–11.

Montgomery, D S, R. J. Focia, H. A. Rose, D. A. Russell, J. A. Cobble, J. C. Fernández, and R. P. Johnson (2001), “Observation of Stimulated Electron-Acoustic-Wave Scattering,” *Physical Review Letters* **87** (15), 155001.

Morse, R L, and C W Nielson (1969), “One-, two-, and three-dimensional numerical simulation of two-Beam plasmas,” *Physical Review Letters* **23** (19), 1087–1090.

Mottez, F, S Perraut, A Roux, and P Louarn (1997), “Coherent structures in the magnetotail triggered by coun-

terstreaming electron beams," *Journal of Geophysical Research* **102** (A6), 11399.

Mozer, F S, O V Agapitov, A Artemyev, J F Drake, V Krasnoselskikh, S Lejosne, and I Vasko (2015), "Time domain structures: What and where they are, what they do, and how they are made," *Geophysical Research Letters* **42** (10), 3627–3638.

Mozer, F S, O. V. Agapitov, B. Giles, and I. Vasko (2018), "Direct Observation of Electron Distributions inside Millisecond Duration Electron Holes," *Physical Review Letters* **121** (13), 135102.

Muschietti, L, I. Roth, C. W. Carlson, and M. Berthomier (2002), "Modeling stretched solitary waves along magnetic field lines," *Nonlinear Processes in Geophysics* **9** (2), 101–109.

Muschietti, L, I Roth, C W Carlson, and R E Ergun (2000), "Transverse instability of magnetized electron holes," *Physical Review Letters* **85** (1), 94–97.

Muschietti, L, I Roth, R E Ergun, and C W Carlson (1999), "Analysis and simulation of BGK electron holes," *Nonlinear Processes in Geophysics* **6** (3/4), 211–219.

Newman, D L, M V Goldman, R E Ergun, and A Mangeney (2001a), "Formation of double layers and electron holes in a current-driven space plasma," *Physical Review Letters* **87** (25), 255001.

Newman, D L, M V Goldman, M Spector, and F Perez (2001b), "Dynamics and instability of electron phase-space tubes," *Physical Review Letters* **86** (7), 1239–1242.

Newman, D L, N. Sen, and M. V. Goldman (2007), "Reduced" multidimensional Vlasov simulations, with applications to electrostatic structures in space plasmas," *Physics of Plasmas* **14** (5), 055907.

Ng, C S, and A Bhattacharjee (2005), "Bernstein-green-kruskal modes in a three-dimensional plasma," *Physical Review Letters* **95** (24), 245004.

Norgren, C, M André, D B Graham, Yu V Khotyaintsev, and A Vaivads (2015a), "Slow electron holes in multicomponent plasmas," *Geophysical Research Letters* **42** (18), 7264–7272.

Norgren, C, M André, A Vaivads, and Y V Khotyaintsev (2015b), "Slow electron phase space holes: Magnetotail observations," *Geophysical Research Letters* **42** (6), 1654–1661.

Norgren, C, D. B. Graham, M. R. Argall, K. Steinvall, M. Hesse, Yu. V. Khotyaintsev, A. Vaivads, P. Tenufjord, D. J. Gershman, P.-A. Lindqvist, J. L. Burch, and F. Plaschke (2022), "Millisecond observations of nonlinear wave–electron interaction in electron phase space holes," *Physics of Plasmas* **29** (1), 012309.

Omura, Y, H. Kojima, and H. Matsumoto (1994), "Computer simulation of electrostatic solitary waves: A nonlinear model of broadband electrostatic noise," *Geophysical Research Letters* **21** (25), 2923–2926.

Omura, Y, H Matsumoto, T Miyake, and H Kojima (1996), "Electron beam instabilities as generation mechanism of electrostatic solitary waves in the magnetotail," *Journal of Geophysical Research* **101** (A2), 2685.

O'Neil, Thomas (1965), "Collisionless Damping of Nonlinear Plasma Oscillations," *The Physics of Fluids* **8** (12), 2255–2262.

Oppenheim, M, D L Newman, and M V Goldman (1999), "Evolution of Electron Phase-Space Holes in a 2D Magnetized Plasma," *Physical Review Letters* **83** (12), 2344–2347.

Oppenheim, M M, G Vetoulis, D L Newman, and M V Goldman (2001), "Evolution of electron phase-space holes in 3D," *Geophysical Research Letters* **28** (9), 1891–1894.

Parlett, B N (1974), "The Rayleigh Quotient Iteration and Some Generalizations for Nonnormal Matrices," *Mathematics of Computation* **28** (127), 679–693.

Pickett, J, S Kahler, L. J Chen, R Huff, O Santolík, Y Khotyaintsev, P Décréau, D Winningham, R Frahm, M Goldstein, G Lakhina, B Tsurutani, B Lavraud, D Gurnett, M André, A Fazakerley, A Balogh, and H Rème (2004), "Solitary waves observed in the auroral zone: the cluster multi-spacecraft perspective," *Nonlinear Processes in Geophysics* **11**, 183–196.

Pickett, J S (2021), "A Review of Electrostatic Solitary Wave Research From the Cluster Mission," *Journal of Geophysical Research: Space Physics* **126** (9), e2021JA029548.

Pickett, J S, L Chen, S W Kahler, O Santolík, M K Goldstein, P Lavraud, P M E Decreau, R Kessel, E Lucek, G S Lakhina, Tsurutani B T, D A Gurnett, N Cornilleau-Wehrlin, A Fazakerley, H Rème, and A Balogh (2005), "On the generation of solitary waves observed by cluster in the near-earth magnetosheath," *Nonlinear Processes in Geophysics* **12**, 181–193.

Pickett, J S, L.-J. Chen, R L Mutel, I W Christopher, O Santolík, G S Lakhina, S V Singh, R V Reddy, D A Gurnett, B T Tsurutani, E Lucek, and B Lavraud (2008), "Furthering our understanding of electrostatic solitary waves through Cluster multispacecraft observations and theory," *Advances in Space Research* **41** (10), 1666–1676.

Pickett, J S, W. S. Kurth, D. A. Gurnett, R. L. Huff, J. B. Faden, T. F. Averkamp, D. Pisa, and G. H. Jones (2015), "Electrostatic solitary waves observed at Saturn by Cassini inside 10 Rs and near Enceladus," *Journal of Geophysical Research: Space Physics* **120** (8), 6569–6580.

Pécseli, H L, R. J. Armstrong, and J. Trulsen (1981), "Experimental observations of ion phase-space vortices," *Physics Letters A* **81** (7), 386–390.

Pécseli, H L, J. Trulsen, and R. J. Armstrong (1984), "Formation of Ion Phase-Space Vortexes," *Physica Scripta* **29** (3), 241.

Raadu, M A (1989), "The physics of double layers and their role in astrophysics," *Physics reports* **178** (2), 25–97.

Raadu, Michael A, and J Juul Rasmussen (1988), "Dynamical aspects of electrostatic double layers," *Astrophysics and Space Science* **144**, 43.

Roberts, K V, and H. L. Berk (1967), "Nonlinear evolution of a two-stream instability," *Phys. Rev. Letters* **19**, 297–300.

Roth, I, L Muschietti, C W Carlson, F S Mozer, and R E Ergun (2002), "Stability and interaction of fast auroral solitary structures in three-dimensional plasma," *Journal of Geophysical Research: Space Physics* **107** (A9), 1239.

Saeki, K, P Michelsen, H L Pcseli, and J Juul Rasmussen (1979), "Formation and Coalescence of Electron Solitary Holes," *Physical Review Letters* **42** (8), 501–504.

Saeki, Koichi, and Hitoshi Genma (1998), "Electron-Hole Disruption due to Ion Motion and Formation of Coupled Electron Hole and Ion-Acoustic Soliton in a Plasma," *Physical Review Letters* **80** (6), 1224–1227.

Sagdeev, R Z (1966), "Cooperative Phenomena and Shock Waves in Collisionless Plasmas," *Reviews of Plasma Physics* **4**, 23, aDS Bibcode: 1966RvPP....4...23S.

Sakanaka, P H (1972), "Beam-generated collisionless ion-acoustic shocks," *Physics of Fluids* **15**, 1323–1327.

Schamel, H (1972), "Stationary solitary, sinusoidal and sinusoidal ion acoustic waves," *Plasma Physics* **14**, 905–924.

Schamel, H (1973), "A modified Korteweg-de Vries equation for ion acoustic waves due to resonant electrons," *Journal of Plasma Physics* **9**, 377–387.

Schamel, H (1979), "Theory of Electron Holes," *Physica Scripta* **20** (3-4), 336–342.

Schamel, H (1982a), "Kinetic Theory of Phase Space Vortices and Double Layers," *Physica Scripta* **1982** (T2A), 228.

Schamel, H (1982b), "Stability of Electron Vortex Structures in Phase Space," *Physical Review Letters* **48** (7), 481–483.

Schamel, H (2000), "Hole equilibria in Vlasov–Poisson systems: A challenge to wave theories of ideal plasmas," *Physics of Plasmas* **7** (12), 4831.

Schamel, H, and S Bujarbarua (1980), "Solitary plasma hole via ion-vortex distribution," *Physics of Fluids* **23**, 2498–2499.

Schamel, Hans (1986), "Electron holes, ion holes and double layers. Electrostatic Phase Space Structures in Theory and Experiment," *Physics Reports* **140** (3), 161–191.

Schamel, Hans (2013), "Comment on ‘Undamped electrostatic plasma waves’ [Phys. Plasmas 19, 092103 (2012)]," *Physics of Plasmas* **20** (3), 034701.

Schamel, Hans (2015), "Particle trapping: A key requisite of structure formation and stability of Vlasov–Poisson plasmas," *Physics of Plasmas* **22** (4), 042301.

Schamel, Hans, and Nikhil Chakrabarti (2023), "Response to Comment on ‘On the Evolution Equations of Nonlinearly Permissible, Coherent Hole Structures Propagating Persistently in Collisionless Plasmas’ [Ann. Phys. (Berlin) 2023, 2300102]," *Annalen der Physik* **n/a** (n/a), 2300441.

Schamel, Hans, Nilakshi Das, and Prathana Borah (2018), "The privileged spectrum of cnoidal ion holes and its extension by imperfect ion trapping," *Physics Letters A* **382** (4), 168–174.

Schamel, Hans, Debraj Mandal, and Devendra Sharma (2020), "Diversity of solitary electron holes operating with non-perturbative trapping," *Physics of Plasmas* **27** (6), 062302.

Schwarzmeier, J L, H R Lewis, B Abraham-Shrauner, and K R Symon (1979), "Stability of Bernstein–Greene–Kruskal equilibria," *Physics of Fluids* **22** (9), 1747.

Shen, Yangyang, Ivan Y. Vasko, Anton Artemyev, David M. Malaspina, Xiangning Chu, Vassilis Angelopoulos, and Xiao-Jia Zhang (2021), "Realistic Electron Diffusion Rates and Lifetimes Due to Scattering by Electron Holes," *Journal of Geophysical Research: Space Physics* **126** (9), e2021JA029380.

Shustov, Pavel I, Ilya V. Kuzichev, Ivan Y. Vasko, Anton V. Artemyev, and Andrew J. Gerrard (2021), "The dynamics of electron holes in current sheets," *Physics of Plasmas* **28** (1), 012902.

Siminos, Evangelos, Didier Bénisti, and Laurent Gremillet (2011), "Stability of nonlinear Vlasov–Poisson equilibria through spectral deformation and Fourier–Hermite expansion," *Physical Review E* **83** (5), 056402.

Singh, N (2003), "Space-time evolution of electron-beam driven electron holes and their effects on the plasma," *Non-linear Processes in Geophysics* **10**, 53–63.

Singh, Nagendra, Sin M Loo, and B Earl Wells (2001), "Electron hole structure and its stability depending on plasma magnetization," *Journal of Geophysical Research* **106** (A10), 21183–21198.

Steinval, K, Yu. V. Khotyaintsev, D. B. Graham, A. Vaivads, P.-A. Lindqvist, C. T. Russell, and J. L. Burch (2019), "Multispacecraft analysis of electron holes," *Geophysical Research Letters* **46** (1), 55–63.

Stix, Thomas Howard (1962), *The theory of plasma Waves* (McGraw-Hill, New York).

Stringer, T E (1964), "Electrostatic instabilities in current-carrying and counterstreaming plasmas," *Journal of Nuclear Energy. Part C, Plasma Physics* **6**, 267–279.

Swanson, D G (1989), *Plasma Waves* (Academic Press).

Tao, J B, R. E. Ergun, L. Andersson, J. W. Bonnell, A. Roux, O. LeContel, V. Angelopoulos, J. P. McFadden, D. E. Larson, C. M. Cully, H.-U. Auster, K.-H. Glassmeier, W. Baumjohann, D. L. Newman, and M. V. Goldman (2011), "A model of electromagnetic electron phase-space holes and its application," *Journal of Geophysical Research: Space Physics* **116**, A11213.

Temerin, M, K Cerny, W Lotko, and F S Mozer (1982), "Observations of double layers and solitary waves in the auroral plasma," *Physical Review Letters* **48**, 1175–1179.

Tong, Y, I. Vasko, F. S. Mozer, S. D. Bale, I. Roth, A. V. Artemyev, R. Ergun, B. Giles, P. A. Lindqvist, C. T. Russell, R. Strangeway, and R. B. Torbert (2018), "Simultaneous Multispacecraft Probing of Electron Phase Space Holes," *Geophysical Research Letters* **45** (21), 11,513–11,519.

Treumann, R A, and W. Baumjohann (2012), "Magnetic field amplification in electron phase-space holes and related effects," *Annales Geophysicae* **30** (4), 711–724.

Turikov, V A (1984), "Electron Phase Space Holes as Localized BGK Solutions," *Physica Scripta* **30** (1), 73.

Umeda, Takayuki (2008), "Generation of low-frequency electrostatic and electromagnetic waves as nonlinear consequences of beam – plasma interactions," *Physics of Plasmas* **15**, 064502.

Umeda, Takayuki, Yoshiharu Omura, Taketoshi Miyake, Hiroshi Matsumoto, and Maha Ashour-Abdalla (2006), "Nonlinear evolution of the electron two-stream instability: Two-dimensional particle simulations," *Journal of Geophysical Research: Space Physics* **111** (10), 1–9.

Valentini, F, D. Perrone, F. Califano, F. Pegoraro, P. Veltri, P. J. Morrison, and T. M. O’Neil (2012), "Undamped electrostatic plasma waves," *Physics of Plasmas* **19** (9), 092103.

Vasko, I Y, O V Agapitov, F Mozer, A V Artemyev, and D Jovanovic (2015), "Magnetic field depression within electron holes," *Geophysical Research Letters* **42** (7), 2123–2129.

Vasko, I Y, O V Agapitov, F S Mozer, A V Artemyev, and J F Drake (2016), "Electron holes in inhomogeneous magnetic field: Electron heating and electron hole evolution," *Physics of Plasmas* **23** (5), 52306.

Vasko, I Y, O. V. Agapitov, F. S. Mozer, A. V. Artemyev, J. F. Drake, and I. V. Kuzichev (2017a), "Electron holes in the outer radiation belt: Characteristics and their role in electron energization," *Journal of Geophysical Research: Space Physics* **122** (1), 120–135.

Vasko, I Y, O. V. Agapitov, F. S. Mozer, A. V. Artemyev, V. V. Krasnoselskikh, and J. W. Bonnell (2017b), "Difusive scattering of electrons by electron holes around injection fronts," *Journal of Geophysical Research: Space Physics* **122** (3), 3163–3182.

Vasko, I Y, V. V. Krasnoselskikh, F. S. Mozer, and A. V. Artemyev (2018a), "Scattering by the broadband electrostatic turbulence in the space plasma," *Physics of Plasmas* **25** (7), 072903.

Vasko, I Y, I. V. Kuzichev, O. V. Agapitov, F. S. Mozer, A. V. Artemyev, and I. Roth (2017c), "Evolution of electron phase space holes in inhomogeneous plasmas," *Physics of Plasmas* **24** (6), 062311.

Vasko, I Y, F. S. Mozer, V. V. Krasnoselskikh, A. V. Artemyev, O. V. Agapitov, S. D. Bale, L. Avanov, R. Ergun, B. Giles, P.-A. Lindqvist, C. T. Russell, R. Strangeway, and R. Torbert (2018b), “Solitary Waves Across Supercritical Quasi-Perpendicular Shocks,” *Geophysical Research Letters* **45** (12), 5809–5817.

Vasko, Ivan Y, Rachel Wang, Forrest S. Mozer, Stuart D. Bale, and Anton V. Artemyev (2020), “On the Nature and Origin of Bipolar Electrostatic Structures in the Earth’s Bow Shock,” *Frontiers in Physics* **8**.

Vedenov, A A, E. P. Velikhov, and R. Z. Sagdeev (1961), “Nonlinear oscillations of rarified plasma,” *Nuclear Fusion* **1** (2), 82.

Vetoulis, Georgios, and Meers Oppenheim (2001), “Electrostatic mode excitation in electron holes due to wave bounce resonances,” *Physical Review Letters* **86** (7), 1235–1238.

Viberg, H, Yu.V. Khotyaintsev, A. Vaivads, M. André, and J.s. Pickett (2013), “Mapping HF waves in the reconnection diffusion region,” *Geophysical Research Letters* **40** (6), 1032–1037.

Villani, Cédric (2014), “Particle systems and nonlinear landau damping,” *Physics of Plasmas* **21** (3), 030901.

Wang, R, I. Y. Vasko, A. V. Artemyev, L. C. Holley, S. R. Kamaletdinov, A. Lotekar, and F. S. Mozer (2022), “Multisatellite observations of ion holes in the earth’s plasma sheet,” *Geophysical Research Letters* **49** (8), e2022GL097919.

Wang, R, I. Y. Vasko, F. S. Mozer, S. D. Bale, A. V. Artemyev, J. W. Bonnell, R. Ergun, B. Giles, P.-A. Lindqvist, C. T. Russell, and R. Strangeway (2020), “Electrostatic Turbulence and Debye-scale Structures in Collisionless Shocks,” *The Astrophysical Journal Letters* **889** (1), L9.

Wang, R, I. Y. Vasko, F. S. Mozer, S. D. Bale, I. V. Kuzichev, A. V. Artemyev, K. Steinvall, R. Ergun, B. Giles, Y. Khotyaintsev, P.-A. Lindqvist, C. T. Russell, and R. Strangeway (2021), “Electrostatic solitary waves in the earth’s bow shock: Nature, properties, lifetimes, and origin,” *Journal of Geophysical Research: Space Physics* **126** (7), e2021JA029357.

Wu, Mingyu, Quanming Lu, Can Huang, and Shui Wang (2010), “Transverse instability and perpendicular electric field in two-dimensional electron phase-space holes,” *Journal of Geophysical Research: Space Physics* **115** (10), A10245.

Yang, Fan, Xu-Zhi Zhou, Yan Zhuang, Chao Yue, Qiu-Gang Zong, Zhi-Yang Liu, and Anton V. Artemyev (2023), “Magnetic Perturbations in Electron Phase-Space Holes: Contribution of Electron Polarization Drift,” *Journal of Geophysical Research: Space Physics* **128** (4), e2022JA031172.

Zhou, C, and I H Hutchinson (2016), “Plasma electron hole kinematics. II. Hole tracking Particle-In-Cell simulation,” *Physics of Plasmas* **23** (8), 82102.

Zhou, Chuteng, and Ian H Hutchinson (2017), “Plasma electron hole ion-acoustic instability,” *J. Plasma Phys.* **83**, 90580501, arXiv:arXiv:1701.03140v1.

Zhou, Chuteng, and Ian H. Hutchinson (2018), “Dynamics of a slow electron hole coupled to an ion-acoustic soliton,” *Physics of Plasmas* **25** (8), 082303.